October 28, 2002 BNL-69395

Report of the BNL Neutrino Working Group: Very Long Baseline Neutrino Oscillation Experiment for Precise Determination of Oscillation Parameters and Search for $\nu_\mu \to \nu_e$ Appearance and CP Violation.

Coordinators: M. Diwan, W. Marciano, W. Weng

Contributors and Participants

D. Beavis, M. Brennan, Mu-Chu Chen, R. Fernow, J. Gallardo, R. Hahn, S. Kahn, H. Kirk, D. Lowenstein, H. Ludewig, W. Morse, R. Palmer, Z. Parsa, D. Raparia, T. Roser, A. Ruggiero, J. Sandberg, N.P. Samios, C. Scarlett, Y. Semertzidis, N. Simos, N. Tsoupas, B. Viren, P. Yamin, M. Yeh
Brookhaven National Laboratory Box 5000, Upton, NY 11973-5000

W. Frati, J. R. Klein, K. Lande, A. K. Mann, R. Van Berg and P. Wildenhain
University of Pennsylvania Philadelphia, PA 19104-6396

R. Corey
South Dakota School of Mines and Technology Rapid City, S.D. 57701

D. B. Cline, K. Lee, B. Lisowski, P. F. Smith
Department of Physics and Astronomy, University of California, Los Angeles, CA 90095 USA

I. Mocioiu, R. Shrock
C.N. Yang Institute for Theoretical Physics, State University of New York, Stony Brook, NY 11974 USA

C. Lu, K.T. McDonald
Joseph Henry Laboratories, Princeton University, Princeton, NJ 08544 USA

Renato Potenza
Istituto Nazionale di Fisica Nucleare, Dipartimento de Fisica e Astronomia, Universita di Catania, 64, Via S. Sofia, I-95123 Catania, Italy

This document contains figures in color. The figures should be viewed in color.

This work was performed under the auspices of the U.S. Department of Energy, Contract No. DE-ACO2-98CH10886.

Contents

1 Executive Summary

On Dec. 1, 2001, Associate Laboratory Director Tom Kirk appointed a BNL based neutrino physics study group. Its charge was to examine future forefront neutrino oscillation experiments that could be carried out using traditional $\nu_\mu(\bar{\nu}_\mu)$ beams of exceptional intensity (super beams) from an upgraded AGS. The study, as reported in this document, addressed detector distances, sizes and technologies as well as novel ideas for cost effective beam lines and AGS upgrade paths. Most important, it focused on the physics discovery and study potential in its assessment of various options.

Given the success of solar and atmospheric neutrino studies in discovering neutrino oscillations and measuring some mixing and mass parameters, it became clear that the next generation accelerator based neutrino oscillation program must be very ambitious. In addition to improving measurements of already approximately known $\Delta m^2_{ij} = m^2_i - m^2_j$ and the large mixing angles θ_{23} and θ_{12}, the next major effort should be capable of determining the as yet unknown mixing angle θ_{13}, the mass hierarchy of neutrinos and the phase δ_{CP}. Together these will provide a measure of CP violation in the lepton sector via the Jarlskog invariant

$$J_{CP} = \frac{1}{8} \sin 2\theta_{12} \sin 2\theta_{23} \sin 2\theta_{13} \cos\theta_{13} \sin\delta$$

Indeed, CP violation is properly viewed as the Holy Grail of neutrino oscillations, since it may be closely connected with the matter-antimatter asymmetry of the universe.

In order to cover a significant region of the allowed θ_{13} parameter space ($\sin^2 2\theta_{13} \leq 0.2$, $0 \leq \delta \leq 2\pi$), to allow for the determination of the mass ordering to the three neutrinos and the possible observation of CP violation a very large detector of approximately 500 kton, a long baseline ($\geq$2000 km) and an intense proton source of 1 megawatt are necessary. For that reason, our studies concentrated primarily on a water Cherenkov detector where the required technology is mature and capable of achieving the required large tonnage. The technical performance of the water detectors has also been fully demonstrated in the relevant event energy ranges. Similarly, a relatively simple cost effective AGS upgrade that primarily increases the repetition rate was examined. Such a large water Cherenkov detector could also be used to search for proton decay, supernova neutrinos, $n\bar{n}$ oscillations, etc. It could also be used to significantly improve measurements of atmospheric neutrino oscillations. Indeed, an extremely attractive picture that emerged from our studies was a very large multi-physics water Cherenkov detector with outstanding discovery potential in many frontier areas of

physics as well as a robust guaranteed program of detailed studies and precise measurements.

In this report, we describe our vision of the very long baseline neutrino oscillation experimental component of that program. It assumes that a 500 kton or larger water Cherenkov detector will be built somewhere in the USA perhaps as a major component of a National Underground Lab and its distance from BNL will be considerable, e.g.. BNL-Homestake (2540 km) or BNL-WIPP (2900 km). To have a sufficient number of detected neutrino events at that distance, a 1 MW AGS proton source (currently the AGS has 0.14 MW of power) is envisioned with targetry focusing and a decay tunnel capable of providing an intense wide band neutrino beam (at 0 degree production) with good support in the $0.5 \leq E_\nu \leq 7$ GeV energy range.

The experimental specifications described above were originally chosen with the idea of measuring the CP violating parameter δ via $\nu_\mu \rightarrow \nu_e$ oscillations. However, during the course of our studies, it became clear that such an effort has a much richer and more diverse physics program. Indeed, in the scenario we have studied in detail (BNL-Homestake), two measurements, ν_μ disappearance oscillations detected via muon events and $\nu_\mu \rightarrow \nu_e$ appearance oscillations via electron events together provide a wealth of information.

During the initial research program, a run of 5×10^7 sec (probably distributed over 5 years), the ν_μ disappearance study will resolve several oscillation maxima and minima (thus firmly establishing oscillations) and measure Δm^2_{32} to 1% or better and $\sin^2 2\theta_{23}$ to 1% or better, significant improvements over existing or planned measurements. In the $\nu_\mu \rightarrow \nu_e$ appearance mode, the $\nu_e + n \rightarrow e^- + p$ quasi-elastic events over the 0.5 GeV range will allow the following investigations to be completed:

1. Search for and measurement of $\sin^2 \theta_{13}$ to below 0.005 via matter enhanced oscillations.
2. Determine the sign of Δm^2_{31}, i.e. whether m_3 is the largest or smallest of the 3 neutrino masses, also via matter enhancement or suppression effects in the 3-7 GeV region.
3. Measure $\sin\delta$ (and $\cos\delta$) to about $\pm 25\%$ thus determining J_{cp} and the δ quadrant.
4. Measure Δm^2_{21} and θ_{12} from the $\nu_\mu \rightarrow \nu_e$ oscillations of low energy $0.5 - 1.0$ GeV neutrinos with about the same sensitivity as Kamland, but in an appearance rather than disappearance mode.

The above program is extremely rich, covering essentially all the parameters of 3 generation neutrino mixing as currently envisioned. It is also robust, offering important measurements even if some parameters whose values we have assumed in our calculations change

significantly. Together with the search for proton decay and study of cosmic neutrinos, our accelerator based long baseline neutrino oscillation program represents a major step forward in the advancement of science. Beyond the first research period, one could envision further accelerator and beam upgrades, antineutrino runs, or additional beams from other accelerator facilities. Indeed, the large detector that forms the centerpiece of this effort should be expected to function for half a century or more expanding our knowledge of all the above noted research areas.

This report will show that the bold program envisioned above is technically feasible and economically attractive. We show that the existence of the AGS machine at BNL with its straightforward and economical upgrade to the needed 1 MW power level, taken together with the needed very long baseline available for at least two appropriate detector sites, makes this approach to a practical facility the best one for the next-generation U.S. neutrino physics program. The identified physics goals are compelling and not covered by less ambitious alternatives. Nevertheless, its realization will require strong commitment and vision. The high payoff is worth the effort.

2 Introduction

Brookhaven National Laboratory and collaborators started a neutrino working group to identify new opportunities in the field of neutrino oscillations and explore how our laboratory facilities can be used to explore this field of research. The memo to the working group and the charge are included in Appendix I.

This report is the result of the deliberations of the working group. Previously, we wrote a letter of intent to build a new high intensity neutrino beam at BNL [1]. A new intense proton beam will be used to produce a conventional horn focussed neutrino beam directed at a detector located in either the Homestake mine in Lead, South Dakota at 2540 km or the Waste Isolation Pilot Plant (WIPP) in Carlsbad, NM at 2880 km [2, 3]. As a continuation of the study that produced the letter of intent, this report examines several items in more detail. We mainly concentrate on the use of water Cherenkov detectors because of their size, resolution, and background rejection capability, and cost. We examine the prospects of building such a detector in the Homestake mine.

The accelerator upgrade will be carried out in phases. We expect the first phase to yield a 0.4 MW proton beam and the second phase to result in a 1.0 MW beam. The details of this upgrade will be reported in a companion report. In this report we assume accelerator intensity of 1 MW for calculating event rates and spectra. We also assume a total experimental duration of 5 years with running time of 10^7 seconds per year.

We examine the target station and the horn produced neutrino beam with focus on two topics: target and horn design for a 1 MW beam and the broad band spectrum of neutrinos from a 28 GeV proton beam.

3 Neutrino Oscillations

The strongest evidence for neutrino oscillations comes from astrophysical observations of atmospheric neutrinos with $\Delta m^2_{32} = (1.6 - 4.0) \times 10^{-3}\ e\mathrm{V}^2$ and maximal mixing [4], and from solar neutrinos with $\Delta m^2_{21} = (3 - 10) \times 10^{-5}\ e\mathrm{V}^2$ assuming the LMA solution [5]. The observation by the LSND experiment [6] will soon be re-tested at Fermilab by the mini-Boone [7] experiment. Therefore we will not discuss it further in this document. There are several accelerator based experiments (K2K, MINOS, and CNGS) [8, 9, 10, 11, 12] currently in the construction phase or taking data to confirm the atmospheric neutrino signatures for

oscillations. There is now a consensus that there are four main goals in the field of neutrino oscillations that should be addressed soon with accelerator neutrino beams:

1. Precise determination of Δm^2_{32} and $\sin^2 2\theta_{23}$ and definitive observation of oscillatory behavior.

2. Detection of $\nu_\mu \rightarrow \nu_e$ in the appearance mode. If the measured Δm^2 for this measurement is near Δm^2_{32} then this appearance signal will show that $|U_{e3}|^2 (= \sin^2 \theta_{13})$ from the neutrino mixing matrix in the standard parameterization is non-zero.

3. Detection of the matter enhancement effect in $\nu_\mu \rightarrow \nu_e$ in the appearance mode. This effect will also allow us to measure the sign of Δm^2_{32}, i.e. which neutrino is heavier.

4. Detection of CP violation in neutrino physics. The neutrino CP-violation in Standard Model neutrino physics comes from the phase multiplying $\sin \theta_{13}$ in the mixing matrix. This phase causes an asymmetry in the oscillation rates $\nu_\mu \rightarrow \nu_e$ versus $\bar{\nu}_\mu \rightarrow \bar{\nu}_e$.

In this report we describe how all of these goals can be achieved under reasonable assumptions for the various parameters using the new intense AGS based beam and the very long baseline of BNL to Homestake laboratory of 2540 km.

In Section 3 we estimate the event rates, backgrounds and oscillation signals. This section highlights the physics measurements achievable with the detector being proposed, focusing on its sensitivity to various oscillation parameters.

In Section 4 of this report we briefly describe the accelerator upgrade path to achieve a proton source with intensity greater than 1 MW.

In Section 5 we examine the conventional neutrino beam spectrum and the target-horn station.

In Sections 6 we summarize the report and give a breakdown of the expected costs.

4 Very Long Baseline Experiment

We calculate the event rate without oscillations assuming a 1.0 MW proton beam power with 28 GeV protons (1.1×10^{14} protons per pulse), a 0.5 MT fiducial mass water Cherenkov detector and 5 years of running. Because BNL's Alternating Gradient Synchrotron (AGS)

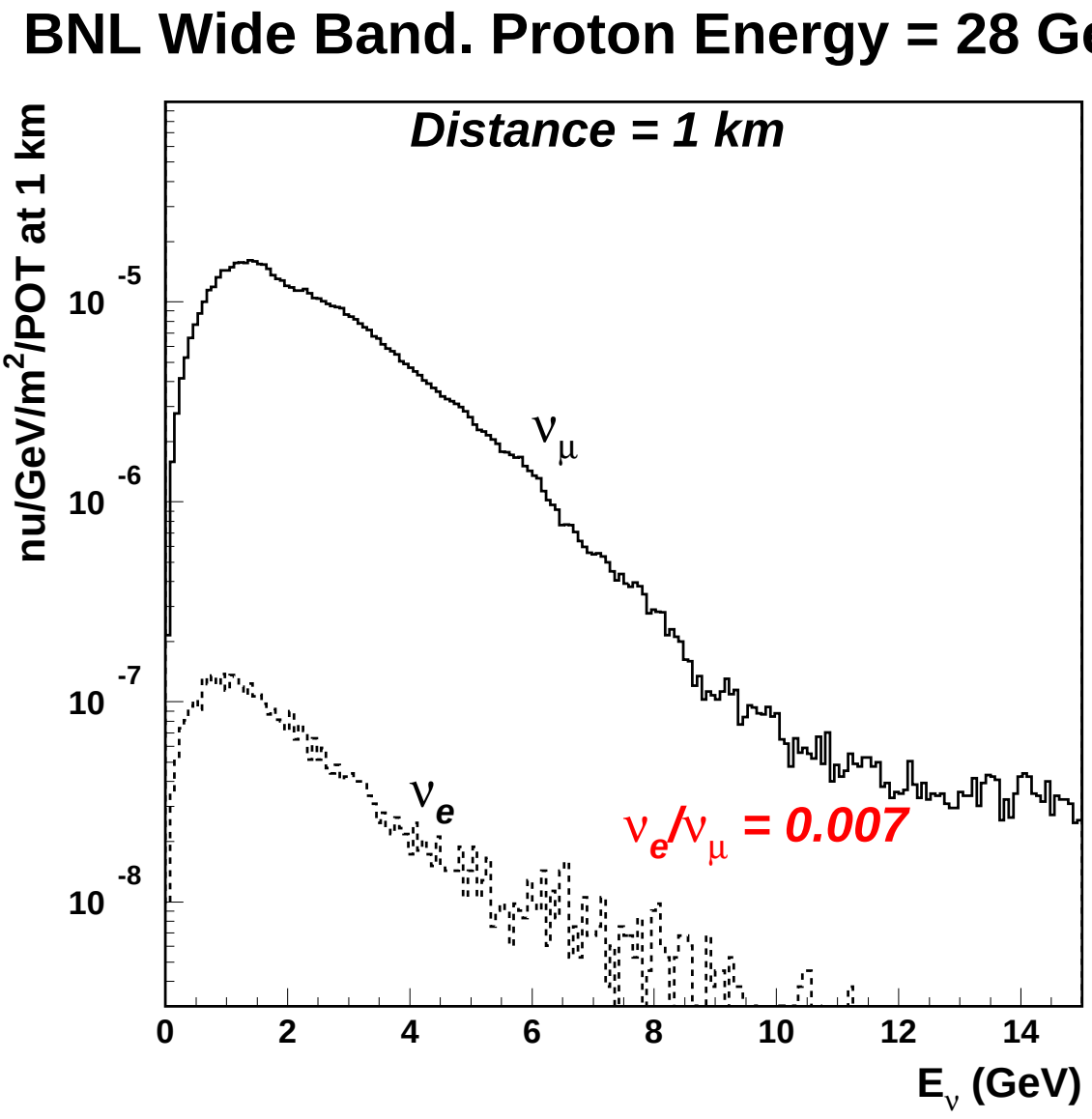

Figure 1: BNL wide band spectrum with the new graphite target and horn design. This spectrum is at 0 degrees with respect to the proton beam on target and the normalization is at 1 km from the target.

Table 1: Number of events of different types for the very long baseline experiment. The parameters are 1 MW of beam, 0.5 MT of fiducial mass, and 5 years of running with 10^7 seconds of live time each year. CC, NC, QE, stands for charged current, neutral current, and quasielastic, respectively. The ν_e interaction rate is from the electron neutrino contamination in the beam.

Reaction	Number
CC $\nu_\mu + N \to \mu^- + X$	51800
NC $\nu_\mu + N \to \nu_\mu + X$	16908
CC $\nu_e + N \to e^- + X$	380
QE $\nu_\mu + n \to \mu^- + p$	11767
QE $\nu_e + n \to e^- + p$	84
CC $\nu_\mu + N \to \mu^- + \pi^+ + N$	14574
NC $\nu_\mu + N \to \nu_\mu + N + \pi^0$	3178
NC $\nu_\mu + O^{16} \to \nu_\mu + O^{16} + \pi^0$	574
CC $\nu_\tau + N \to \tau^- + X$ (if all $\nu_\mu \to \nu_\tau$)	319

can run in a parasitic mode to the Relativistic Heavy Ion Collider (RHIC), we expect to get beam for as much as 1.8×10^7 sec per year. However, we conservatively assume only 1.0×10^7 sec of AGS running per year here. Using these parameters, the 0° flux from Figure 1 and the relevant cross sections, we calculate that the number of quasi-elastic charged current muon neutrino events in a detector located at 2540 km will be $\sim$ 12000 in five years running. Table 1 shows the number of different kinds of events we expect in the absence of oscillations. The large statistics combined with the long baseline make many of the following important measurements possible.

4.1 ν_μ disappearance

The angular distribution of the muons from the quasi-elastic process $\nu_\mu + n \rightarrow \mu^- + p$ produced by the 0^o beam in Figure 42 was measured in experiment E734 (1986) at BNL. It is shown again in Figure 2 along with the principal background, $\nu_\mu + N \rightarrow \mu^- + N + \pi$ [13]. A variety of strategies is possible to reduce this background further in a water Cherenkov detector. Knowing the direction of an incident ν_μ accurately and measuring the angle and energy of the observed muon allows the energy of the ν_μ to be calculated, up to Fermi momentum effects. This method is used by the currently running K2K experiment [8]. The known capability of large water Cherenkov detectors indicates that at energies lower than 1 GeV the ν_μ energy resolution will be dominated by Fermi motion and nuclear effects[14]. The contribution to the resolution from water Cherenkov track reconstruction depends on the photo-multiplier tube coverage. With coverage greater than $\sim$ 10%, we expect that the reconstruction resolution should be more than adequate for our purposes [21]. In the following discussion we assume a 10% resolution on the ν_μ energy. This is consistent with the resolution projected for 10% coverage from the K2K experience [15].

The range of $\Delta m^2_{32} \sim 1.24 \frac{E_\nu[\mathrm{G}e\mathrm{V}]}{L[\mathrm{km}]}$ covered by the proposed experiment using the beam in Figure 1 extends to the low value of about 5×10^{-4} $e\mathrm{V}^2$. The lower end of this extensive range of values is considerably below the corresponding values for other long baseline terrestrial experiments [11, 12]. If the value of Δm^2_{32} turns out to be towards the lower end ($\sim 10^{-3}$) of its current range, or if the value of Δm^2_{21} turns out to be towards its high end ($\sim 10^{-4}$ $e\mathrm{V}^2$), then large and very interesting interference effects in the very long baseline experiment will be possible.

Extra-long neutrino flight paths open the possibility of observing multiple nodes (minimum intensity points) of the neutrino oscillation probability in the disappearance experiment. Observation of one such pattern will for the first time directly demonstrate the oscillatory nature of the flavor changing phenomenon. The nodes occur at distances $L_n = 1.24(2n-1)E_\nu/\Delta m^2_{32}$, $n = 1, 2, 3, \ldots$. In Figure 3, as an example, we show the flight path L versus E_ν relationship of the nodes for $\Delta m^2 = 0.003$ eV^2, a value close to the value measured in atmospheric neutrino experiments [4]. An advantage of having a very long baseline is that the multiple node pattern is detectable over a broad range of Δm^2. For Δm^2_{32} as small as 0.001 $e\mathrm{V}^2$, the oscillation effects will be very large.

The two single charged pion reactions $\nu_\mu + p \rightarrow \mu^- + p + \pi^+$ and $\nu_\mu + n \rightarrow \mu^- + n + \pi^+$ produce a signal which is somewhat larger than the quasi-elastic total in Table 1. For these

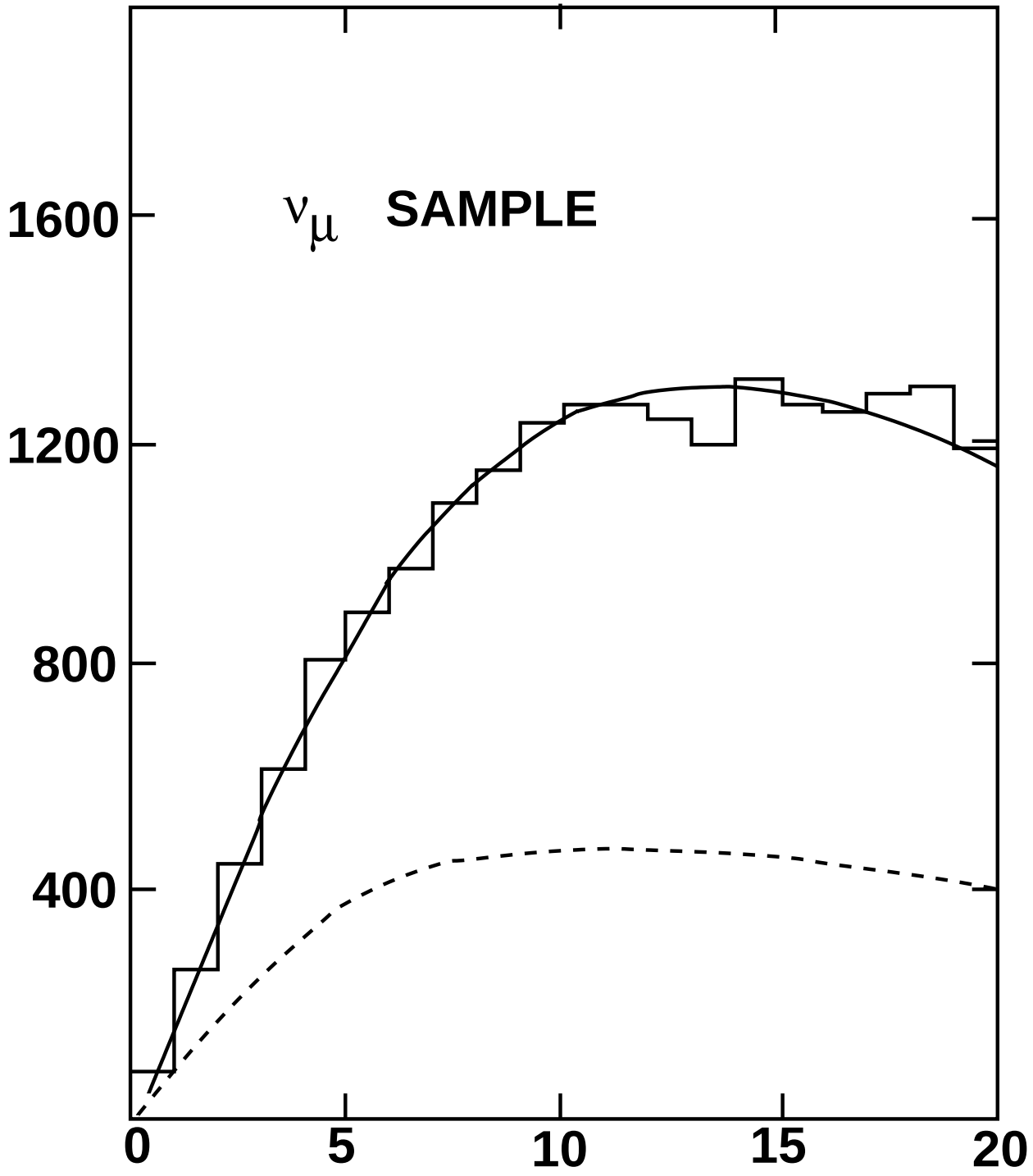

Figure 2: Angular distribution of muons from the process $\nu_\mu n \to \mu^- p$ (top curve) and background from $\nu_\mu N \to \mu^- N' \pi$ (bottom curve). The histogram is data from AGS experiment E734 (year 1986) and the lines are Monte Carlo.

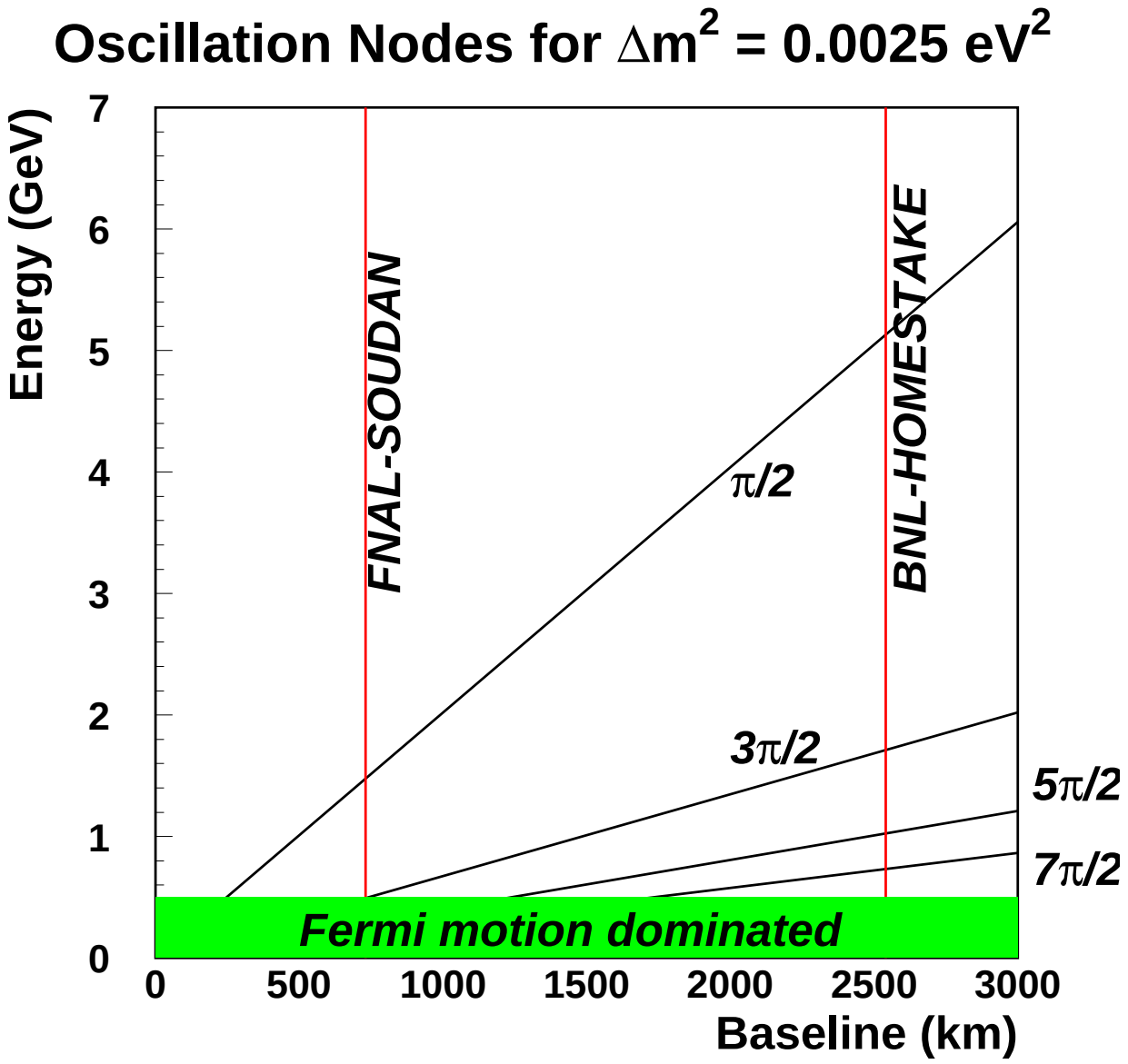

Figure 3: Nodes of neutrino oscillations for disappearance (Not affected by matter effects) as a function of oscillation length and energy for $\Delta m^2_{32} = 0.0025\ e\mathrm{V}^2$. The distances from FNAL to Soudan (the distance from BNL to Morton salt works is approximately the same[36]) and from BNL to Homestake are shown by the vertical lines.

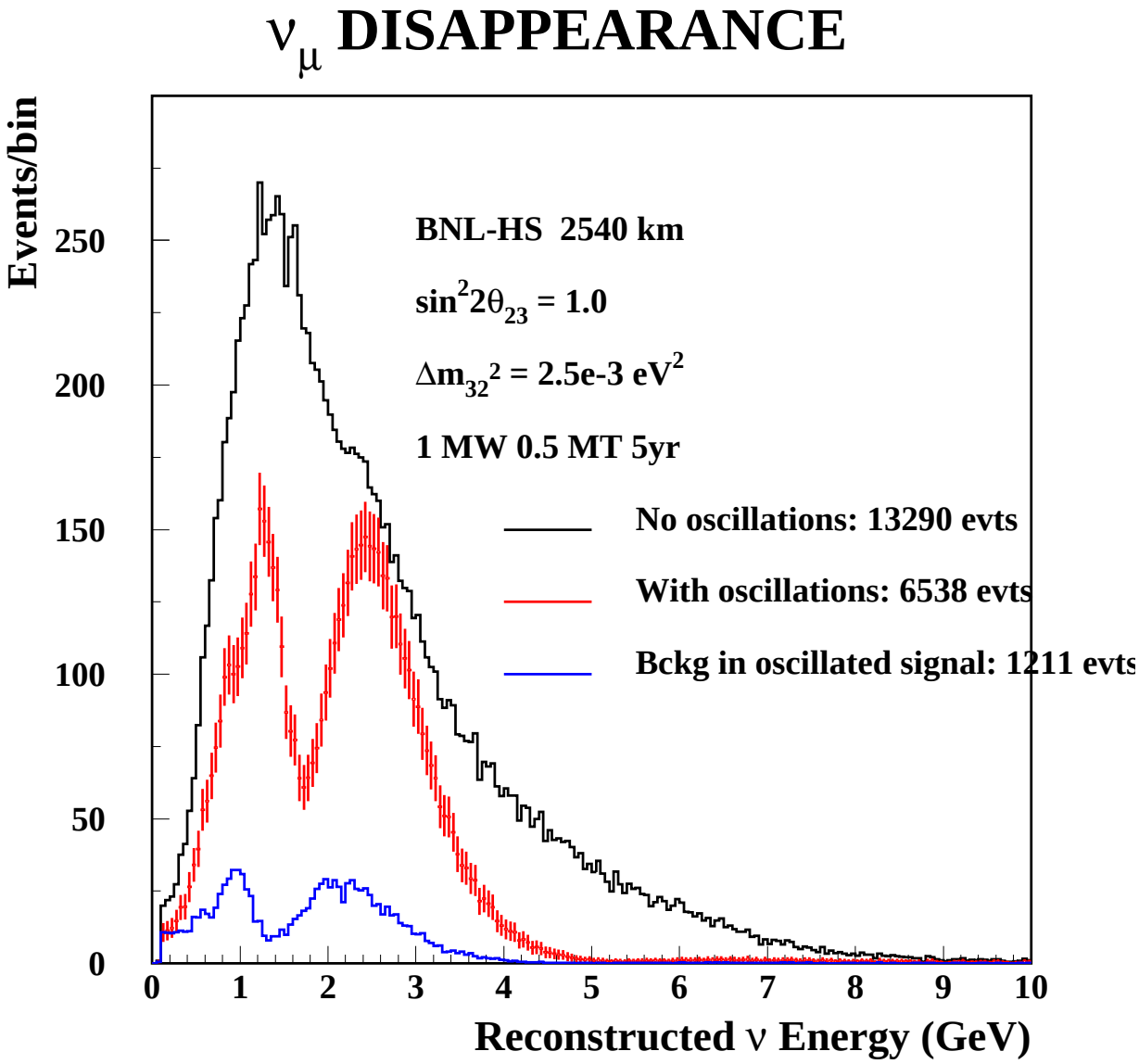

Figure 4: Spectrum of detected events in a 0.5 MT detector at 2540 km from BNL including quasielastic signal and CC-single pion background. We have assumed 1.0 MW of beam power and 5 years of running. The top histogram is without oscillations; the middle error bars are with oscillations and the bottom histogram is the contribution of the background to the oscillated signal only. This plot is for $\Delta m^2_{32} = 0.0025\ eV^2$. The error bars correspond to the statistical error expected in the bin. A 10 % detector energy resolution is assumed. At low energies the Fermi movement, which is included in simulation, will dominate the resolution.

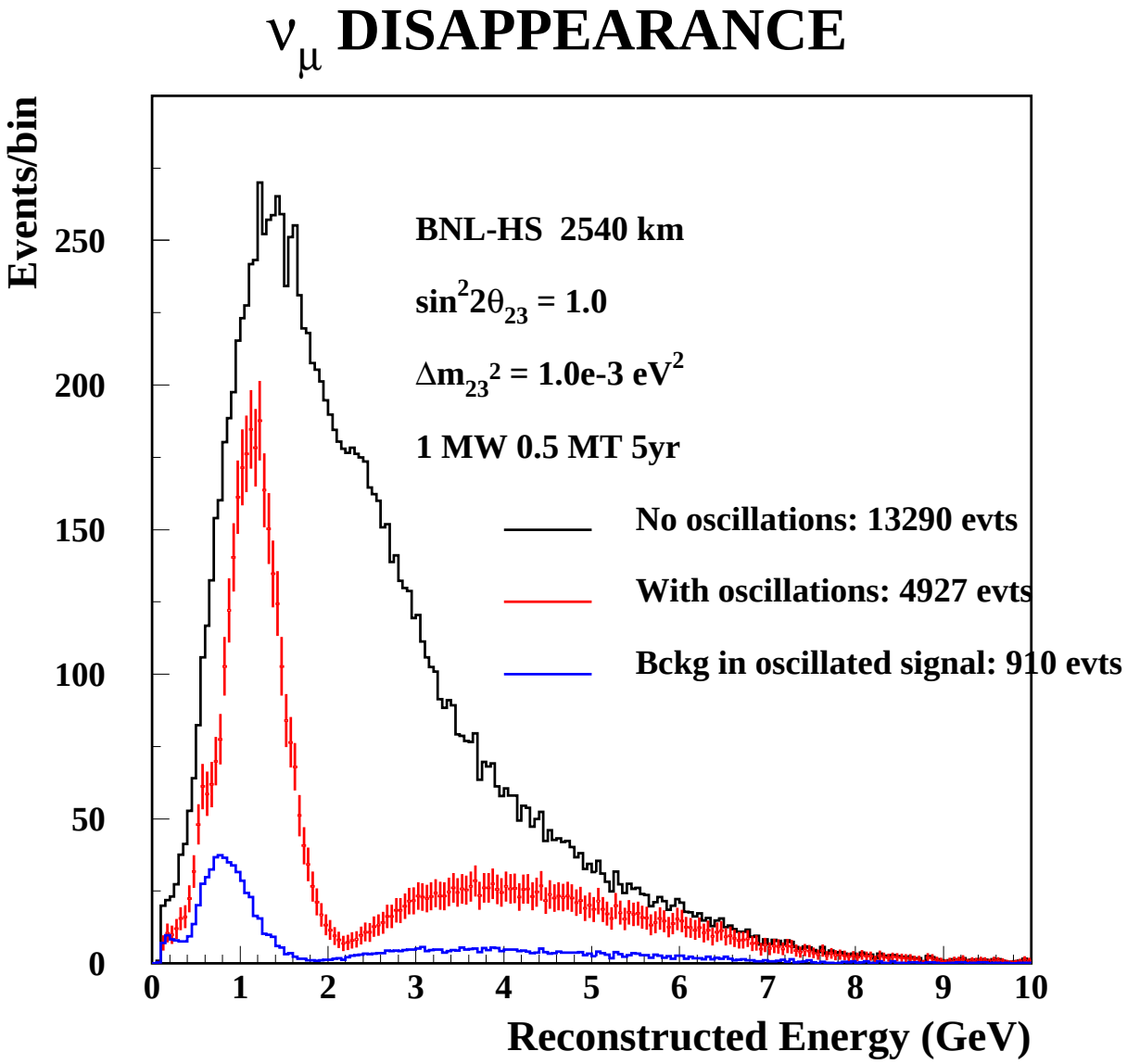

Figure 5: Spectrum of detected events in a 0.5 MT detector at 2540 km from BNL including quasielastic signal and CC-single pion background. We have assumed 1.0 MW of beam power and 5 years of running. The top histogram is without oscillations; the middle error bars are with oscillations and the bottom histogram is the contribution of the background to the oscillated signal only. This plot is for $\Delta m^2_{32} = 0.001$ eV^2. The error bars correspond to the statistical error expected in the bin. A 10 % detector energy resolution is assumed. At low energies the Fermi movement, which is included in simulation, will dominate the resolution.

events, if both the muon and the pion produce more than 50 photoelectrons each, the event can be easily identified as a two ring event in a water Cherenkov detector and rejected. 50 photoelectrons corresponds to about 170 MeV/c (250 MeV/c) for muons (pions) for a detector with 10% photo-multiplier coverage. An additional cut to require the muon to be within 60^o of the neutrino direction reduces the background further. With such a cut, we find that 18% of the events will show one ring (principally the μ^-). The detection of two muon decays, one from the μ^- the other from the decay chain $\pi \rightarrow \mu \rightarrow e$, could be used to further suppress this background by approximately a factor of 2. More importantly, background events can be tagged by the two muon decays to determine the shape of the background from the data itself. This will greatly increase the confidence in the systematic error due to this background. The reaction $\nu_\mu + n \rightarrow \mu^- + p + \pi^0$ (the only allowed CC-π^0 reaction) is $\sim$15% of the total quasi-elastic rate. The momentum distribution of μ^- and π^0 are essentially the same as those for CC-charged pion production. Only 0.5% of the CC-π^0 events will look like quasi-elastic muon events because at least one of the gamma rays from the π^0 decay is usually visible. Thus this background is negligible in the quasi-elastic sample.

The expected plot of signal and background is shown in Figures 4 and 5. They show the disappearance of muon type neutrinos as a function of neutrino energy measured in quasi-elastic events. The background, which will be mainly charged current, will also oscillate, but the reconstructed neutrino energy will be systematically lower for the background. Nevertheless, the main effect will be to slightly broaden the large dips due to disappearing muon neutrinos.

In Figure 6 we show the statistical precision expected on the measurement of Δm^2_{32} and $\sin^2 2\theta_{23}$ for several different points in the parameter space. It is clear that since the signal and the statistics are large, the systematic error in fitting the spectrum will dominate the final error. We list various effect that must be considered for the measurement with brief comments about each.

- The determination of Δm^2 has a statistical uncertainty of approximately $\pm 0.7\%$ at $\Delta m^2 = 0.0025\ eV^2$ with maximum mixing. It is about $\pm 1.0\%$ when $\sin^2 2\theta_{23} = 0.75$. Clearly, the knowledge of the energy scale will be very important in measuring this number. If the energy scale uncertainty is $\delta E/E$ then the final error will be given by

$$(\frac{\sigma(\Delta m^2)}{\Delta m^2})^2 = (\frac{\sigma_{stat}}{\Delta m^2})^2 + (\frac{\delta E}{E})^2$$

  Therefore, it will be very important to understand the energy calibration of the detector to about 1 % for muon energy of $\sim$ 1 GeV. One solution could be a magnetic

spectrometer to measure the momentum of cosmic ray muons entering the detector. This consideration could affect the depth at which this detector should be mounted. Another option could be a linear accelerator that could provide protons or electrons at a rate of few Hz at ~ 100 MeV.

- Even if the overall energy scale is known well, the energy calibration could vary non-linearly over the entire spectrum. The worst effects of these fluctuations will be where the spectrum has the maximum slope. This effect will cause additional smearing of the spectrum and reduce the resolution on Δm^2. We assume a 5% uncertainty of the energy calibration over the entire range.

  It should be pointed out that the oscillation minima should be at energies that are in precisely known ratios of integers: 3, 5, 3/5, etc. This could be used to determine the relative energy scale precisely. On the other hand these ratios could be important to determine the presence of new physics (non-sinusoidal depletion of muon neutrinos) in the oscillations.

- The model of Fermi motion and reconstruction resolution will affect both the shape of the signal and the background used in the fit. The consequences of this effect are probably the same as the previous one in terms of the resolution of fitted parameters.

  It was pointed out earlier that some of the the CC-π^+ background could be tagged by two muon decays. This sample of events can be used in separate fits to put more constraints on the detector simulations. The large number of charged current events (~ 52000) that are not quasielastic could also be used in the same manner.

- The statistical uncertainty in the determination of $\sin^2 2\theta_{23}$ is ± 0.016 at $\sin^2 2\theta_{23} = 0.75$ and $\Delta m^2_{32} = 0.0025\ eV^2$. This determination is somewhat better at smaller Δm^2. At maximum mixing, Figure 6 shows that we can determine $\sin^2 2\theta_{23} > 0.99$ at 90% confidence level.

  We expect this error to be even smaller if proper background subtraction is performed on the data. Normally the determination of this quantity depends on the systematic error for the normalization of the flux. However, in the case of very long baseline, the largest part of the sensitivity comes from the shape of the spectrum or how deep the valleys are compared to the peaks (see Figure 4). Therefore, this determination is not affected greatly by the systematic error for the overall normalization. This is demonstrated as follows: for $\Delta m^2_{32} = 0.003\ eV^2$, even without background subtraction, the valleys at $\pi/2$ and $3\pi/2$ have only 2% and 30% of the un-oscillated event rate (see

Figure 4). If we assume the flux normalization error to be 5%, which is consistent with what has been achieved by the K2K experiment[15], then the expected error due to flux normalization on $\sin^2 2\theta_{23}$ is $0.02 \times 0.05 = 0.001$.

- We note that within the parameter region of interest there should be very little correlation in the determination of Δm^2_{32} and $\sin^2 2\theta_{32}$.

With the assumption on the systematic errors as above we obtain Figure 7. The systematic errors introduce a small correlation in the Δm^2_{32} vs. $\sin^2 2\theta_{32}$ measurement. The error on the determination of Δm^2_{32} at 0.0025 eV^2 increases to about $\pm 1.2\%$ at maximum mixing, but there is only a small effect on the determination of $\sin^2 2\theta_{23}$. As mentioned before, the energy scale uncertainty must be added in quadrature to the calculated uncertainty on Δm^2_{32}. The precision of this experiment can be compared with the precision expected from MINOS (Figure 7) and the precision obtained so far from the K2K experiment (Figure 8). It is expected that K2K will obtain twice as much data; therefore we could naively estimate that the precision on the parameter determination will improve as $1/\sqrt{2}$.

Finally, we note that the flux normalization is usually obtained by placing a detector close to the neutrino source. For example, both K2K and MINOS have large near detectors to determine the flux. Since absolute flux determination is not very important for parameter determination in our case, we argue that the requirements on a near detector need not be very severe for this measurement. It may not be necessary to build a near detector until sufficient statistics are obtained in the far detector to demand the required systematic error reduction of a near detector.

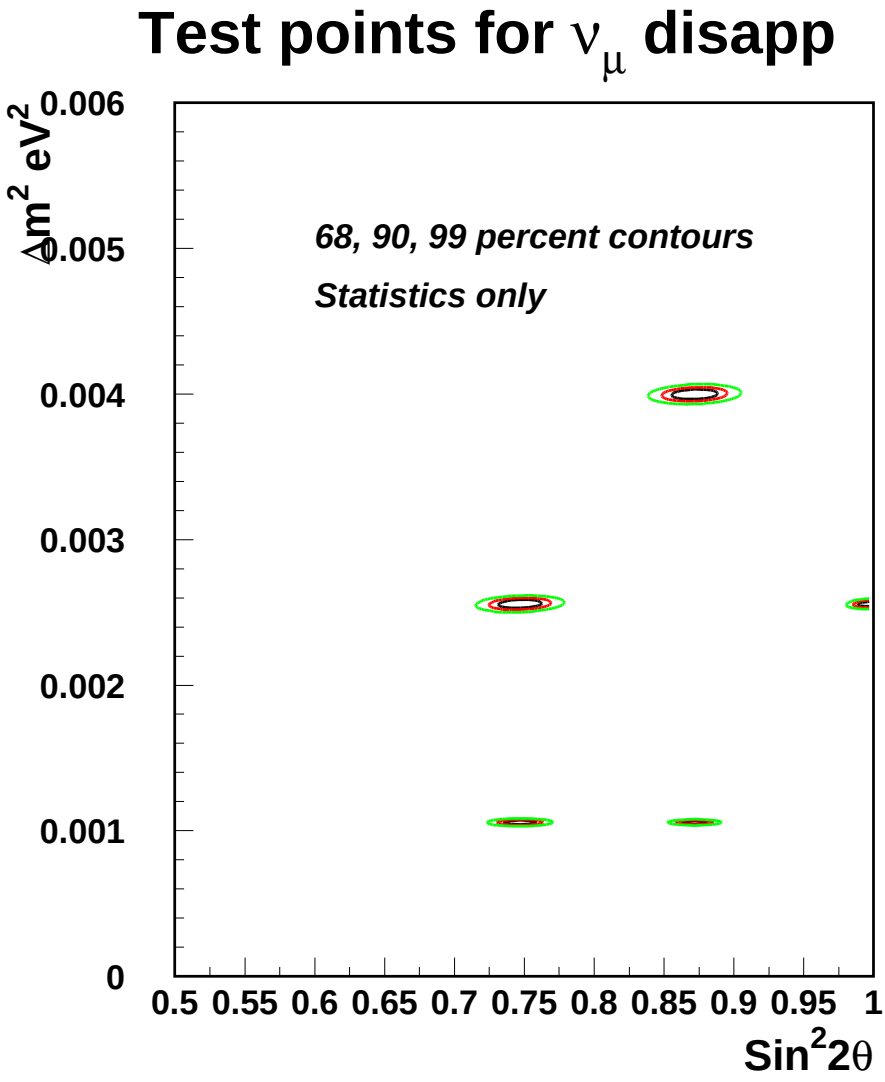

Figure 6: Statistical resolution at 68%, 90% and 99% confidence level on Δm^2_{32} and $\sin^2 2\theta_{23}$ for the 2540 baseline experiment; assuming 1 MW, 0.5 MT, and 5 years of exposure.

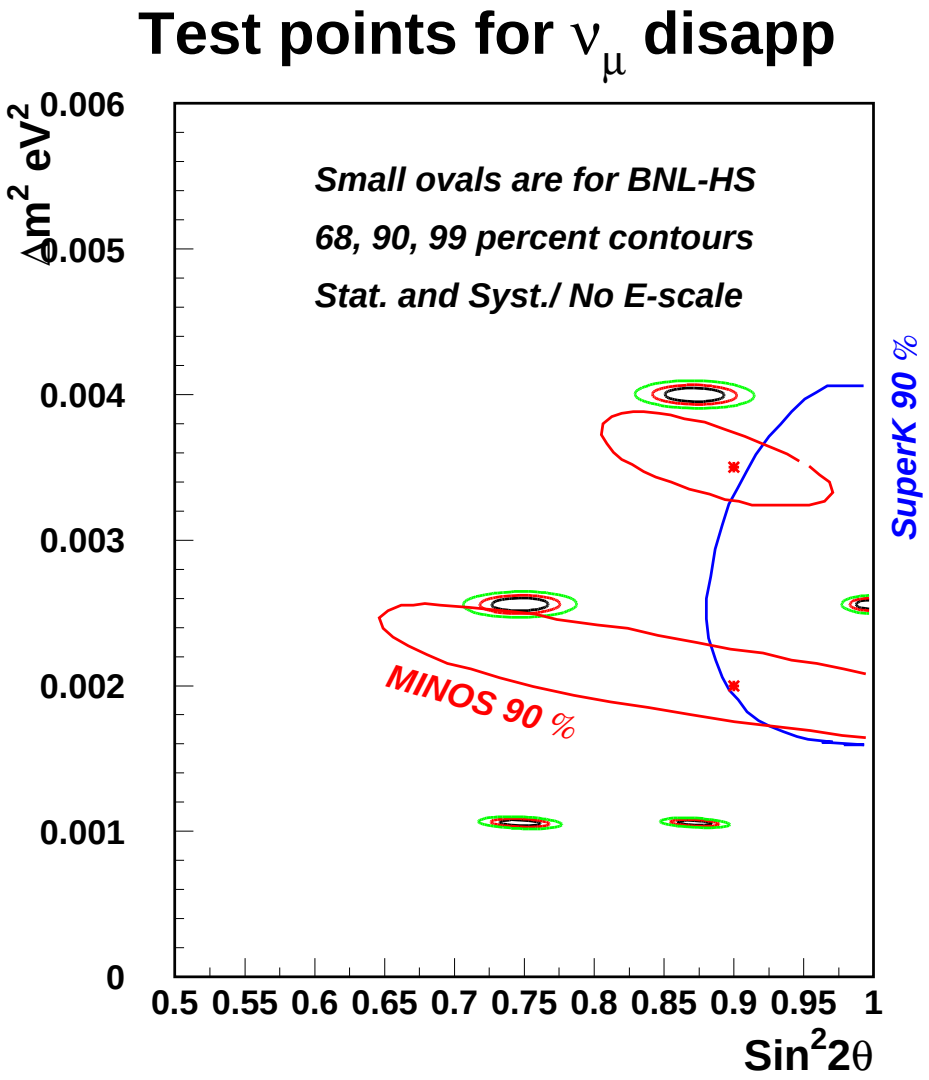

Figure 7: Resolution including statistical and systematic effects at 68%, 90% and 99% confidence level on Δm^2_{32} and $\sin^2 2\theta_{23}$ for the 2540 baseline experiment; assuming 1 MW, 0.5 MT, and 5 years of exposure. We have included a 5% bin-to-bin systematic uncertainty in the energy calibration as well as a 5% systematic uncertainty in the normalization. The expected resolution from the MINOS experiment at Fermilab and the allowed region from SuperK is also indicated.

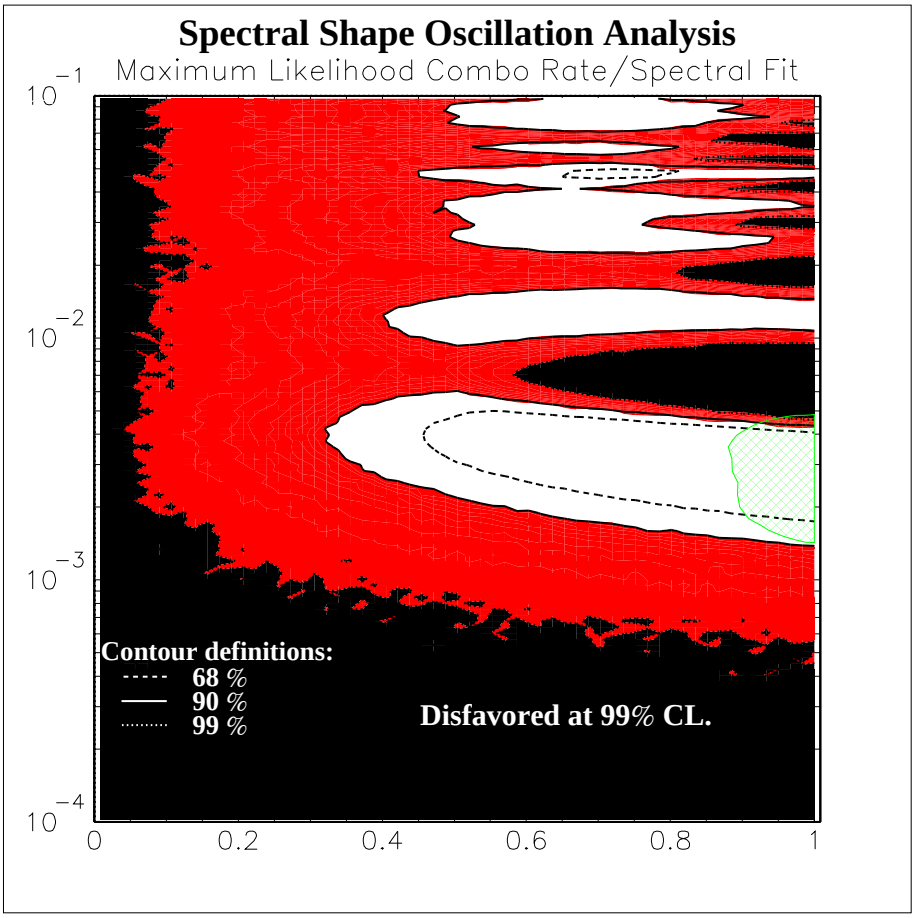

Figure 8: The allowed region for Δm^2_{32} and $\sin^2 2\theta_{23}$ from the K2K experiment. From thesis by Eric Sharkey, SUNY at Stony Brook.

4.2 $\nu_\mu \rightarrow \nu_e$ appearance

The oscillation of $\nu_\mu \rightarrow \nu_e$ is discussed is several recent papers [16, 17, 18, 19]. This oscillation in vacuum is described fully by the following equation:

$$\begin{aligned} P(\nu_\mu \rightarrow \nu_e) &= 4(s_{23}^2 s_{13}^2 c_{13}^2 + J_{CP} \sin\Delta_{21}) \sin^2 \frac{\Delta_{31}}{2} \\ &+2(s_{12}s_{23}s_{13}c_{12}c_{23}c_{13}^2 \cos\delta - s_{12}^2 s_{23}^2 s_{13}^2 c_{13}^2) \sin\Delta_{31} \sin\Delta_{21} \\ &+4(s_{12}^2 c_{12}^2 c_{23}^2 c_{13}^2 + s_{12}^4 s_{23}^2 s_{13}^2 c_{13}^2 - 2s_{12}^3 s_{23}s_{13}c_{12}c_{23}c_{13}^2 \cos\delta - J_{CP}\sin\Delta_{31}) \sin^2 \frac{\Delta_{21}}{2} \\ &+8(s_{12}s_{23}s_{13}c_{12}c_{23}c_{13}^2 \cos\delta - s_{12}^2 s_{23}^2 s_{13}^2 c_{13}^2) \sin^2 \frac{\Delta_{31}}{2} \sin^2 \frac{\Delta_{21}}{2} \end{aligned} \quad (1)$$

where

$$J_{CP} \equiv s_{12}s_{23}s_{13}c_{12}c_{23}c_{13}^2 \sin\delta \quad (2)$$

J_{CP} is an invariant that quantifies CP violation in the neutrino sector. The abbreviations $s_{ij} \equiv \sin\theta_{ij}$, $c_{ij} \equiv \cos\theta_{ij}$, and $\Delta_{ij} \equiv \Delta m_{ij}^2 L/2E_\nu$ are used. The formula for $P(\bar{\nu}_\mu \rightarrow \bar{\nu}_e)$ is the same as above except that the J_{CP} terms have opposite sign. The vacuum oscillations for a baseline of 2540 km are illustrated in Figure 9 as a function of energy for both muon and anti-muon neutrinos. The main feature of the oscillation is due to the term linear in $\sin^2 \frac{\Delta_{31}}{2}$. The oscillation probability rises for lower energies due to the terms linear in $\sin^2 \frac{\Delta_{21}}{2}$. The interference terms involve CP violation and they create an asymmetry between neutrinos and anti-neutrinos. The vacuum oscillation formula (Eq.1) and Figure 9 show that the CP asymmetry also grows as $1/E$ in the 0.5-3.0 GeV region. The parameters listed in the figure are $\sin^2 2\theta_{12} = 0.8$, $\sin^2 2\theta_{23} = 1.0$, and $\sin^2 2\theta_{13} = 0.04$ and $\Delta m_{21}^2 = 5.0 \times 10^{-5}\ eV^2$, $\Delta m_{32}^2 = 0.0026\ eV^2$. Similar notation for parameters will be followed in the rest of the document. Because of this effect it is argued that the figure of merit for measuring CP violation is independent of the baseline. For very long baselines the statistics for a given size detector at a given energy are poorer by one over the square of the distance, but the CP asymmetry grows linearly in distance [17]. The background to the electron neutrino signal comes from contamination in the beam ($\nu_e/\nu_\mu \sim 0.7\%$) and neutral current events. At small distances the systematic error on this background could limit the ability to extract the CP violating effect, but at large distance the background reduces as $1/(distance)^2$ and allows us to greater sensitivity to CP violating effects. We rely on this important observation in the rest of this section.

The vacuum oscillation formulation must be modified to include the effect of matter [18]. The $\nu_\mu \rightarrow \nu_e$ probability in the presence of matter is shown in Figures 10 and 11. When

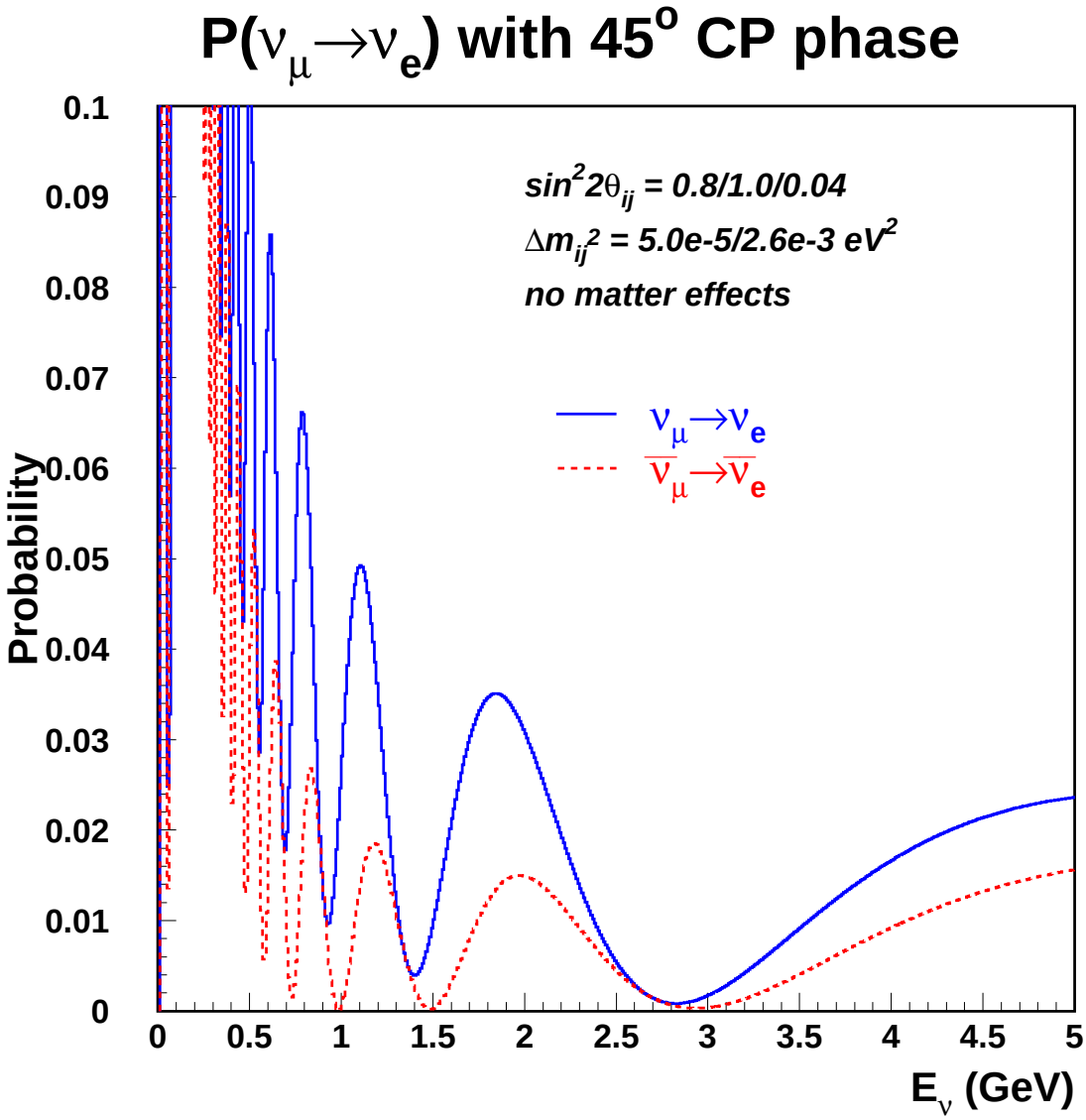

Figure 9: Probability of $\nu_\mu \to \nu_e$ and $\bar{\nu}_\mu \to \bar{\nu}_e$ oscillations at 2540 km in vacuum assuming a $\delta_{CP} = +45^o$ CP violation phase. It can be seen that the CP asymmetry between ν_μ and $\bar{\nu}_\mu$ increases for lower energies because the CP asymmetry is proportional to $\Delta m^2_{21} L/E$ which increases for lower energies. The parameters listed in the figure are $\sin^2 2\theta_{12} = 0.8$, $\sin^2 2\theta_{23} = 1.0$, and $\sin^2 2\theta_{13} = 0.04$ and $\Delta m^2_{21} = 5.0 \times 10^{-5}\ eV^2$, $\Delta m^2_{32} = 0.0026\ eV^2$.

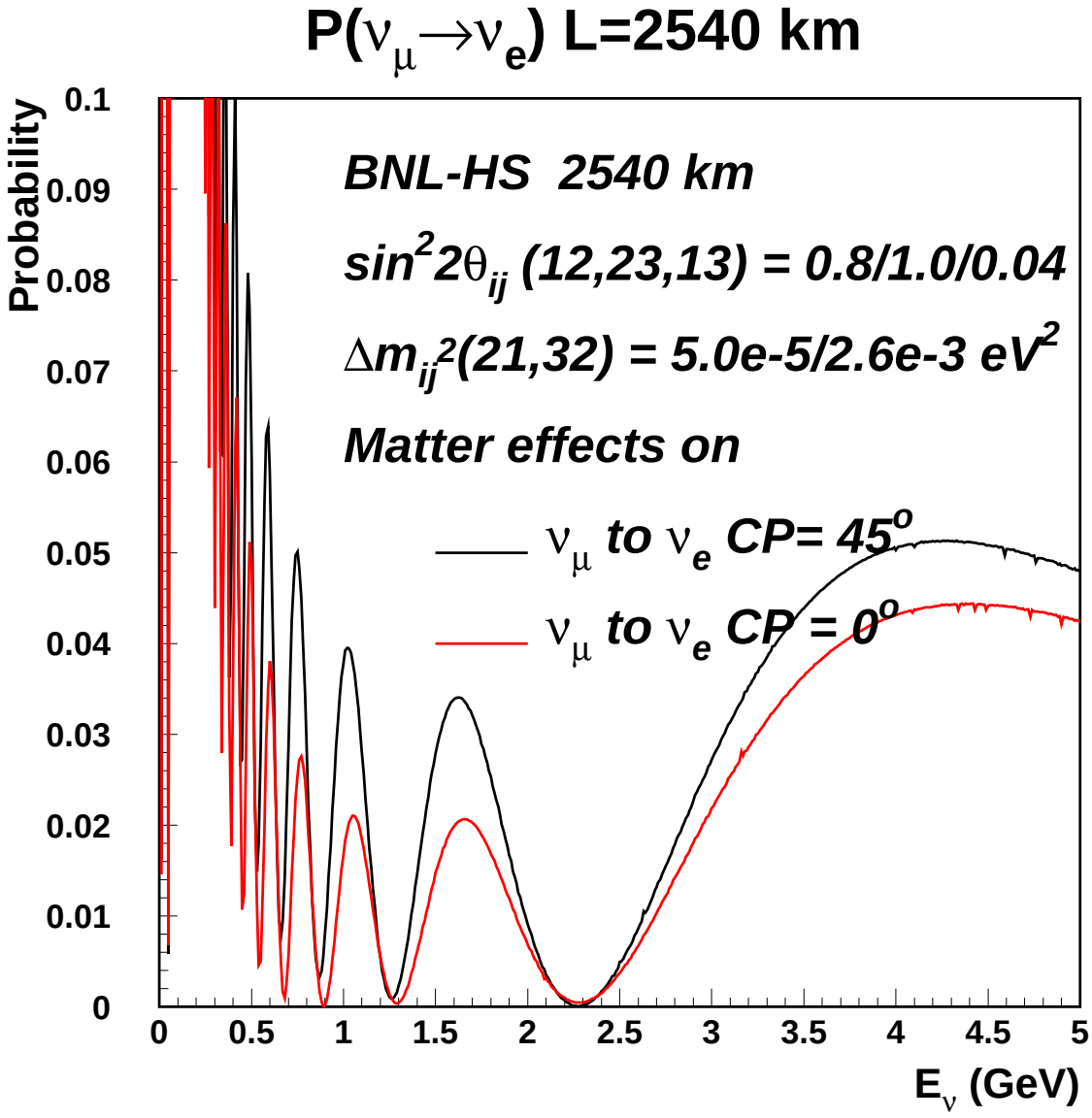

Figure 10: Probability of ν_μ oscillating into ν_e after 2540 km. The parameters assumed are listed in the figures. The upper and lower curves correspond to CP phase angle of $+45^o$ and 0^o respectively. We point out that the effect of CP phase increases for lower energies.

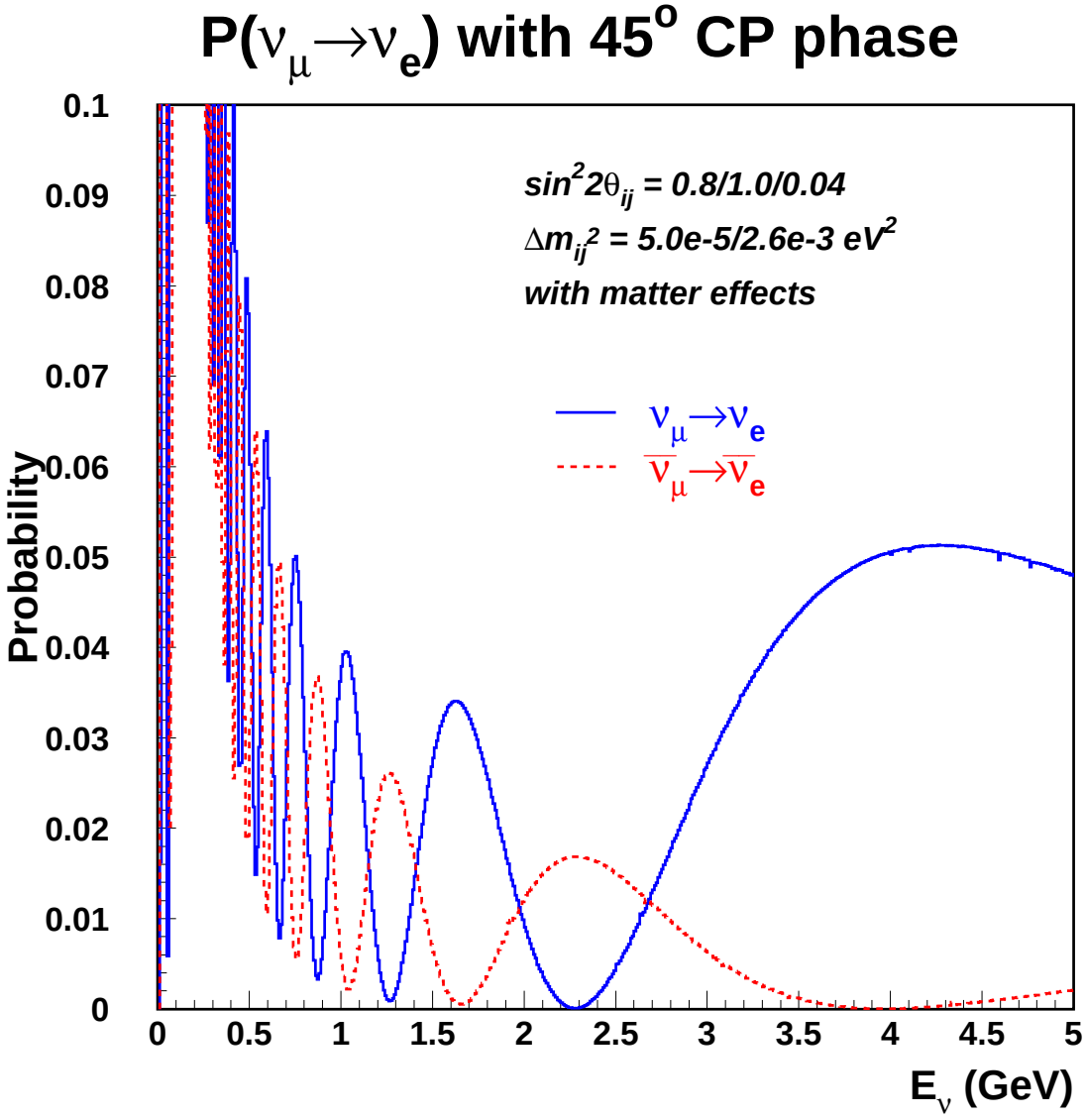

Figure 11: Probability of ν_μ oscillating into ν_e after 2540 km. The parameters assumed are listed in the figures. This plot assumes a CP violation phase of $+45^o$. The upper and lower curves are for neutrinos and anti-neutrinos, respectively. We see that for distance of 2540 the matter effects will be large and will lead to almost complete reversal of nodes and anti-nodes for neutrinos and anti-neutrinos. The probability for neutrinos with $\Delta m^2_{32} < 0$ will be similar to (but not exactly the same as) anti-neutrinos.

compared to Figure 9 we can see that matter will enhance (suppress) neutrino (anti-neutrino) conversion at high energies and will also lower (increase) the energy at which the oscillation maximum occurs. The effect is opposite (enhancement for anti-neutrinos and suppression for neutrinos) if the sign of Δm^2_{32} is negative. The Figures 9 to 11 gives us hints about possible strategies in understanding neutrino oscillation parameters.

In the low energy region from 0 to 1.0 GeV, the probability for $\nu_\mu \rightarrow \nu_e$ is dominated by the effects of Δm^2_{21} if the solution to the solar neutrino deficit is the large mixing angle (LMA) solution. An excess of electron like events in this region would be sensitive to Δm^2_{21} and $\sin^2 2\theta_{12}$.

In the intermediate energy region from 1.0 to 3.0 GeV, we see that the CP violating phase δ_{CP} has a large effect on the oscillation probability and the effects of matter are relatively small. Therefore this energy region could be used to measure the CP violating phase δ_{CP} from the observed spectrum of electron like events.

The higher energy region with energy greater than 3.0 GeV is clearly the region of discovery for $\nu_\mu \rightarrow \nu_e$ oscillations as well as the sign of Δm^2_{32}. In the case of the normal mass hierarchy ($m_3 > m_2 > m_1$) the oscillation signal in the high energy region for neutrinos will be enhanced by more than a factor of 2. Moreover, as we will discuss below, the backgrounds from both neutral currents and intrinsic ν_e will fall in this region. Therefore the appearance signal will have a distinctive shape to distinguish it from the background. In the case of ($m_2 > m_1 > m_3$) the oscillation signal in the high energy region will be almost completely suppressed. However, there will be a peak between 2 and 3 GeV. If $\sin^2 2\theta_{13}$ is sufficiently large, this will be a clear signature for $\Delta m^2_{32} < 0$, a very important result in particle physics.

Finally, matter enhancement of the oscillations has been postulated for a long time without experimental confirmation [20]. Detection of such an effect by measuring a large asymmetry between neutrino and anti-neutrino oscillations or by measuring the spectrum of electron neutrinos is a major goal for neutrino physics. This measurement will also yield the sign of Δm^2_{32}.

4.3 Backgrounds

While the ν_μ disappearance result will be affected by systematic errors, the $\nu_\mu \rightarrow \nu_e$ appearance result will be affected mainly by the backgrounds. The signal we are looking for consists of clean, single ring electron events in the detector. The signal will mainly result from the quasielastic reaction $\nu_e + n \rightarrow e^- + p$. The main backgrounds will be from neutral

current reactions and the intrinsic electron neutrinos in the beam. Most of the $\sim$ 17000 neutral current reactions from Table 1 are either elastic scattering off nucleons or single pion production channels. Of these, the channels that produce single π^0 will be the major source of backgrounds. We estimate that approximately 2800 NC events will have multiple pions in the final state. Half of these will have at least one π^0. We expect that these can be rejected much more effectively than the single π^0 production channels which will have $\sim$ 3700 events (see Table 1). This number includes the coherent production channel of $\nu_\mu + O^{16} \rightarrow \nu_\mu + O^{16} + \pi^0$. The charged current background channel, $\nu_\mu + n \rightarrow \mu^- + p + \pi^0$, in which the muon remains invisible was shown to be small for a similar beam spectrum in the E889 proposal [21].

For a baseline of 2540 km, the matter enhanced oscillation signal will be above 3 GeV. Our strategy for obtaining a unique, clear signal therefore depends on the observation that neutral current background will peak at low energies and fall rapidly as a function of observed energy. This is demonstrated in Figures 12 and 13 for the neutral current single pion production channel. In Figure 12 we see that the q^2 distribution peaks at low values and is nearly independent of the neutrino energy. The neutrino energy only determines the kinematic limit of the q^2 value. This behavior leads most neutral current events to be at low energies.

Figure 13 shows the distribution of total π^0 energy for single pion production events with no detector cuts. We see that the distribution is about 3 orders of magnitude suppressed above 2.5 GeV where we expect the signal from $\nu_\mu \rightarrow \nu_e$ appearance (see Figure 10). Therefore, we propose that even a modest rejection of neutral current background above 2.5 GeV is sufficient to provide us with good sensitivity for $\nu_\mu \rightarrow \nu_e$ appearance.

This modest rejection can be obtained by first cutting all events with visible energy less than 500 MeV. Further rejection is obtained by getting rid of events with two showers each with energy greater than 150 MeV separated by more than 9 degrees in angle and by cutting events with angle between the shower and the neutrino direction of greater than 60 degrees; this was calculated using a fast Monte Carlo with appropriate angle and energy resolution corresponding to a water Cherenkov detector. At high energies, above 3 GeV, a full simulation of a large water Cherenkov detector showed us that it is possible to obtain about a 50% rejection based on the Cherenkov ring characteristics. The overall rate of π^0 misidentification is shown in Figure 14.

It should be noted that the advantage of the very long baseline is in applying a simple cut on the total visible energy to eliminate most of the background. The rate of π^0 misidentification for neutral current events (Figure 13) above 500 MeV is 6%. The efficiency for electrons

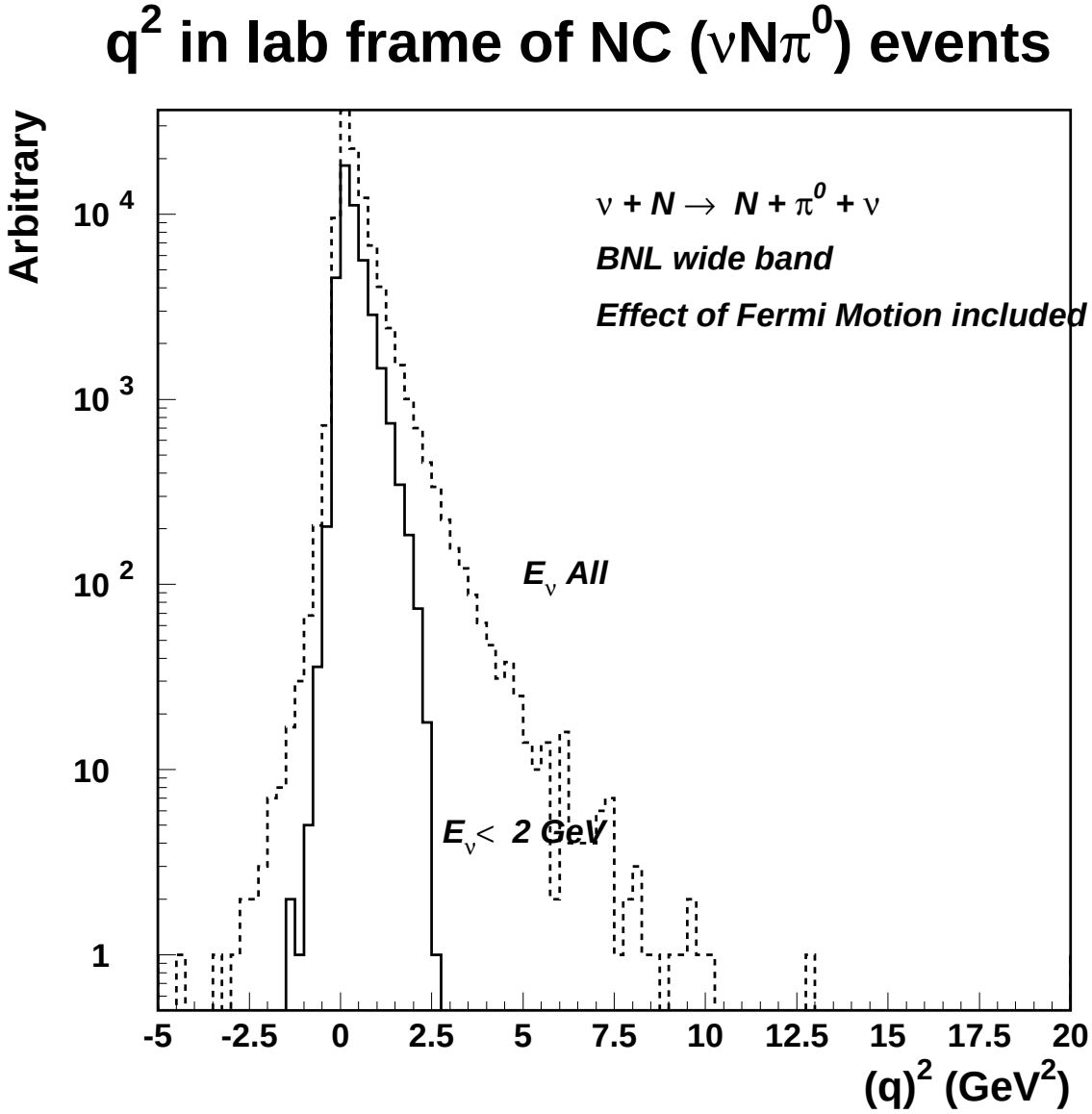

Figure 12: The q^2 distribution of $\nu_\mu + N \to \nu_\mu + N + \pi^0$ channels. Here $q^2 = ((p'_N + p'_\pi) - p_N)^2$. p_N is the initial 4 momentum of the target nucleon (assumed to be at rest in the lab frame). p'_N and p'_π are the 4-momenta of the final state nucleon and pion, respectively. The peak of the distribution is independent of neutrino energy. The neutrino energy only determines the physical cutoff of the q^2 distribution. The slightly negative behavior of the distribution is caused by the Fermi motion of the target nucleus which was assumed to be at rest in the above formula.

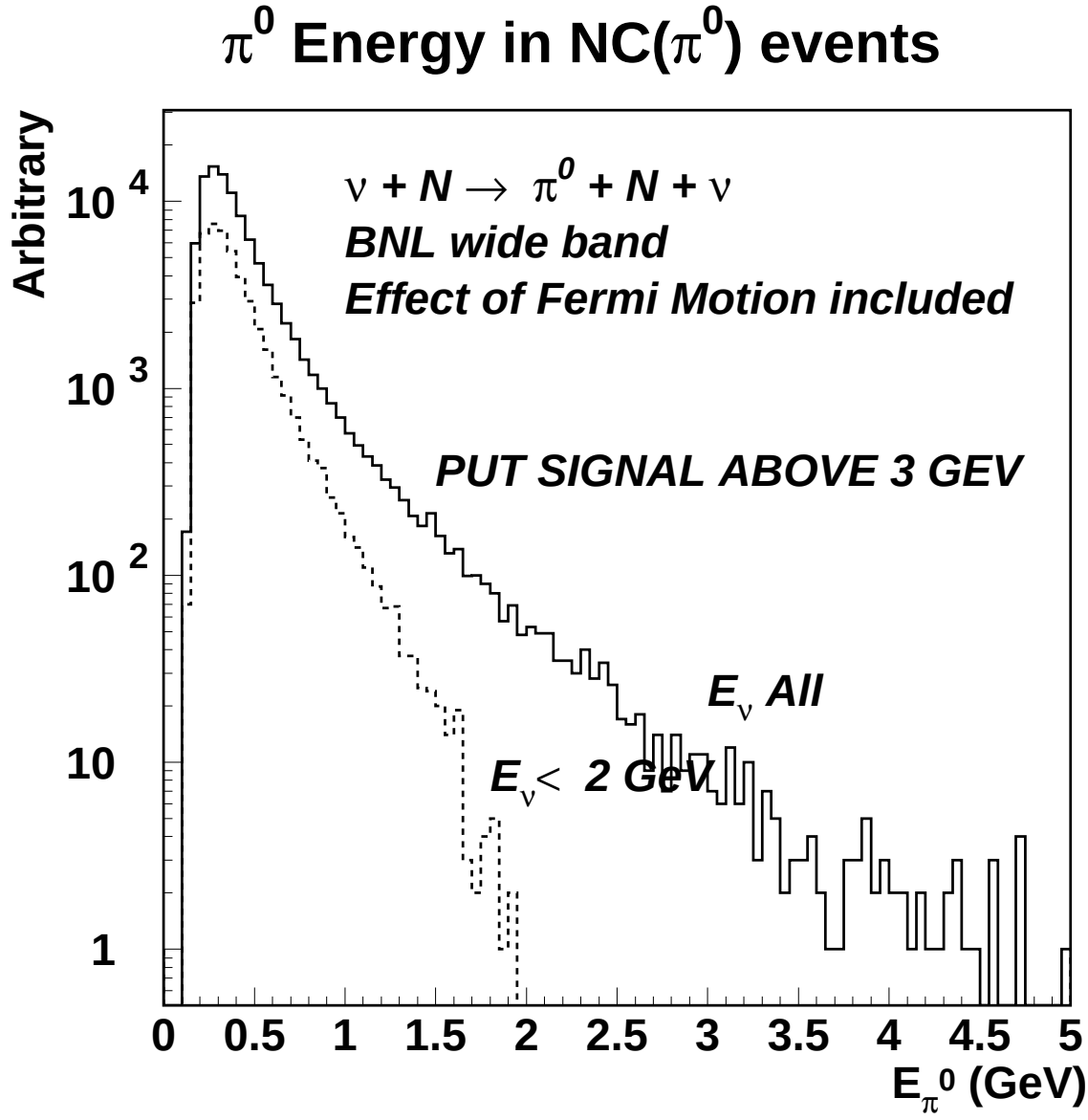

Figure 13: The π^0 energy distribution of $\nu_\mu + N \rightarrow \nu_\mu + N + \pi^0$ channels with no cuts. The peak of the distribution is independent of neutrino energy. The neutrino energy determines the high energy cutoff of the distribution. The distribution is about 3 orders of magnitude suppressed above 2.5 GeV where we expect the signal from $\nu_\mu \rightarrow \nu_e$ appearance.

is shown on the right hand side of Figure 14. The efficiency for quasielastic electron neutrino events is 64% at energy less than 1.5 GeV. Above 1.5 GeV the efficiency is 90%. Using appropriate resolution and efficiency factors we obtain the predicted background spectrum of electron like showering events in Figure 15. The reconstructed electron energy and the angle of the electron with respect to the neutrino direction is used to reconstruct the neutrino energy assuming a quasielastic scattering event. Figure 15 includes backgrounds from the neutral current single π^0 production off nucleon as well as coherent π^0 production off O^{16}, which has a much more energetic spectrum. The spectrum also includes the background from ν_e contamination in the beam.

The predicted number of total background events is 146 with the beam-ν_e contamination accounting for 70 events. It should be remarked that above 2 GeV the background is dominated by the beam-ν_e contamination: there are 35 ν_e events versus 17 π^0 events. This is despite the rather poor rejection of NC(π^0) events at high energies. Below 2 GeV the background will be dominated by the NC(π^0) events: with 35 ν_e events and 59 π^0 events. Therefore any error in the determination of the NC(π^0) background including contamination from other neutral current background channels (which will have similar energy dependence) will not significantly affect the high energy region above 2 GeV where we expect to see a distinct signal for electron neutrino appearance.

4.4 Sensitivity to $\sin^2 2\theta_{13}$

Figures 16 and 17 show the spectrum of electron like events that will be detected at 2540 km. The signal for $\Delta m^2_{32} = 0.0025\ eV^2$ and $\sin^2 2\theta_{13} \sim 0.04$ will be about 200 events. The advantages of the very long baseline are in obtaining a large enhancement at higher energies and creating a nodal pattern in the appearance spectrum. Both of these can be used to further improve the sensitivity of the experiment. It should be noted that the value of Δm^2_{32} will be known very precisely from the disappearance measurement; this value can then be used to precisely predict the shape of the spectrum of electron-like events. Unlike past experiments in which only a simple counting of signal over background was performed, the node pattern in this experiment will be a strong confirmation of $\nu_\mu \rightarrow \nu_e$. The broadband beam also allows for sensitivity over a broad range of Δm^2_{32}. This can be seen in Figure 17.

We calculated the background electron spectrum assuming $\sin^2 2\theta_{13} = 0$; then we varied the parameters, Δm^2_{31} and $\sin^2 2\theta_{13}$, and calculated the χ^2 with respect to the background spectrum. The other parameters in this calculation were set as follows: $\Delta m^2_{21} = 6 \times 10^5\ eV^2$,

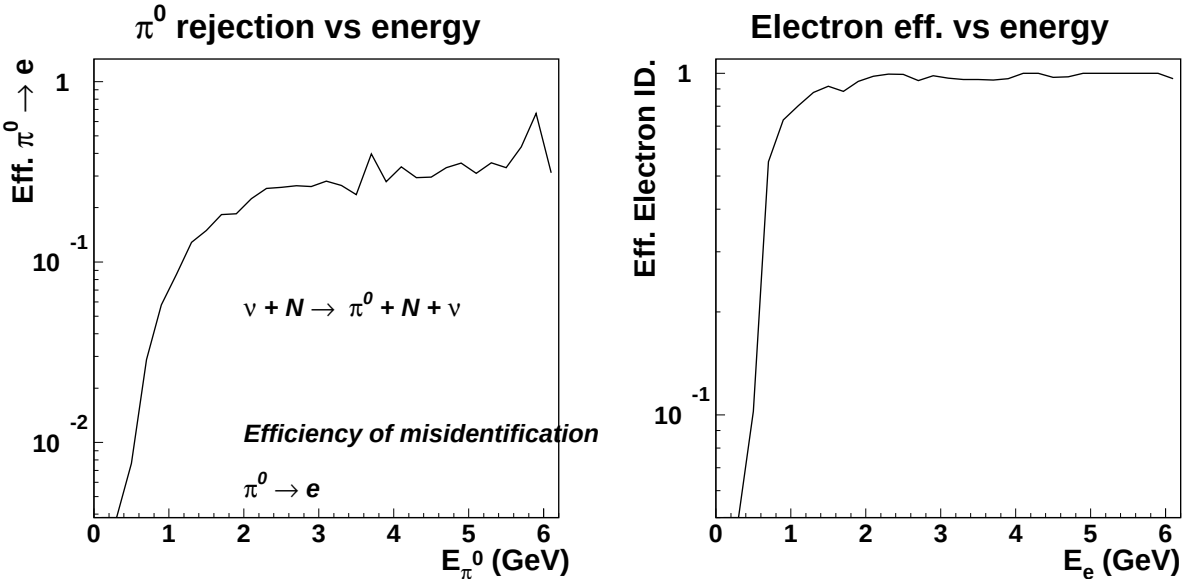

Figure 14: On the left: the rate of misidentification of π^0 events as electrons versus total π^0 energy for the calculations in this paper. On the right: electron efficiency used in this calculation.

$\sin^2 2\theta_{12} = 0.8$, $\sin^2 2\theta_{23} = 1.0$ and $\delta_{CP} = 0$. We assumed that the remaining parameters will be well-known from other experiments. However, the small uncertainty on Δm^2_{21} will cause us to lose sensitivity to $\sin^2 2\theta_{13}$ at values of $\Delta m^2_{32} < 0.001\ eV^2$, outside the region favored by SuperK. For the calculation we assume a 10% systematic error (in addition to the statistical error) on the background spectrum of events. This level of systematic uncertainty is attainable with a modest sized near detector and it compares well with proposals for other such experiments. The 90% confidence level upper limit obtained from this calculation is shown in Figure 18. The same figure also shows the sensitivities of several other proposed experiments as well as the current best limit from the CHOOZ reactor experiment. The current upper limit at $\Delta m^2_{31} = 0.0025\ eV^2$ is $\sin^2 2\theta_{13} = 0.12$. It should be noted that if Δm^2_{32} is lower the current limit becomes much poorer. (We will use the values $\sin^2 2\theta_{13} = 0.04$ and $\sin^2 2\theta_{13} = 0.06$, which are a factor 1/3 and 1/2 below the current limit as benchmark points for some of the plots.)

The sensitivity shown in Figure 18 can be divided in two regions: above $\Delta m^2_{32} = 0.0015\ eV^2$ (in the parameter region preferred by the SuperK data) the electron spectrum shape will be very distinct and show at least two clear nodes; below $\Delta m^2_{32} = 0.0015\ eV^2$

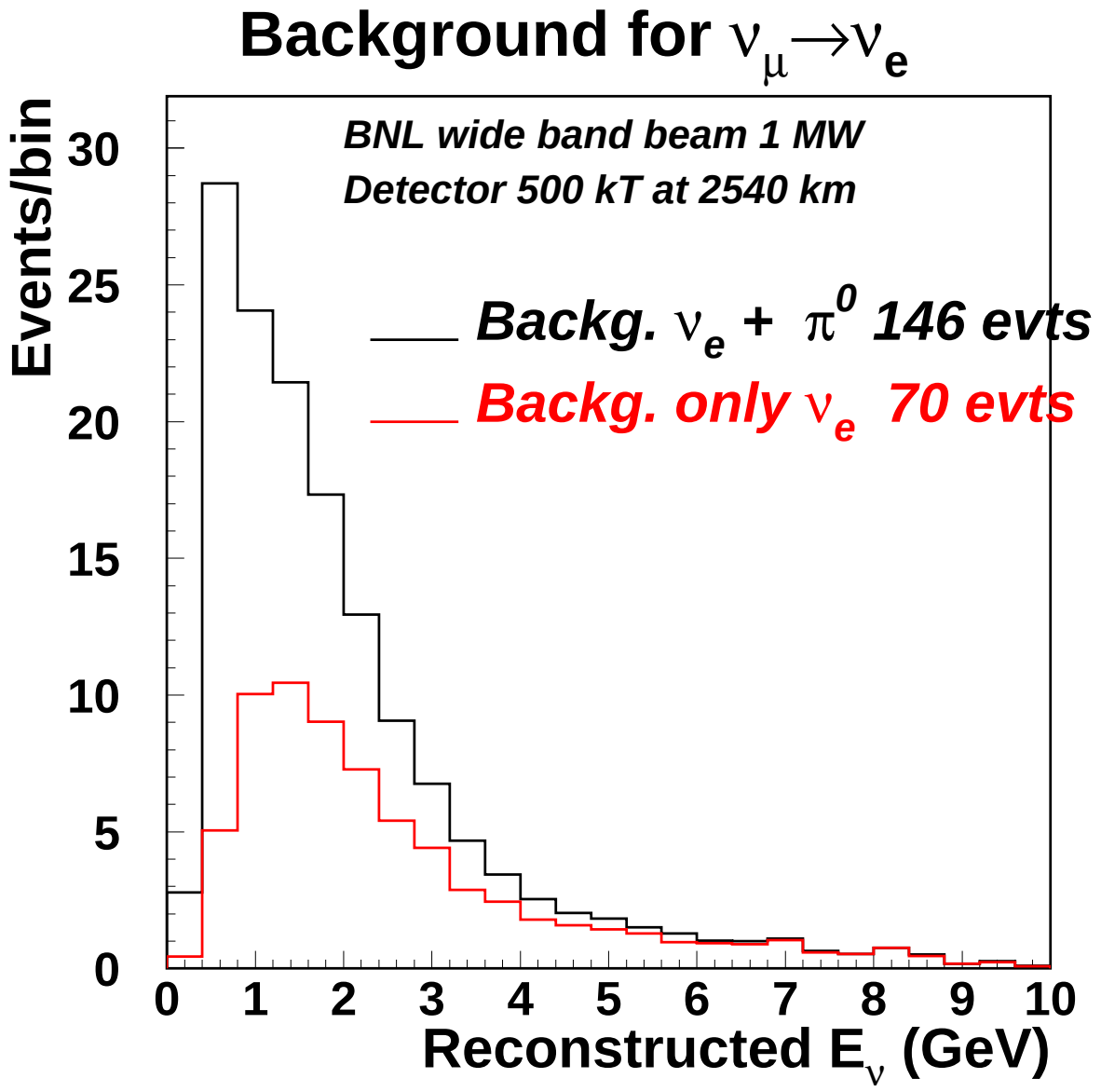

Figure 15: Spectrum of reconstructed electron neutrino energy (assuming quasielastic events) of the background for $\nu_\mu \rightarrow \nu_e$ search. This is for 1 MW beam power, 0.5 MT detectors mass and 5×10^7 sec of running. The top histogram includes both the NC(π^0) and electron contamination backgrounds. The electron neutrino contamination is also shown separately.

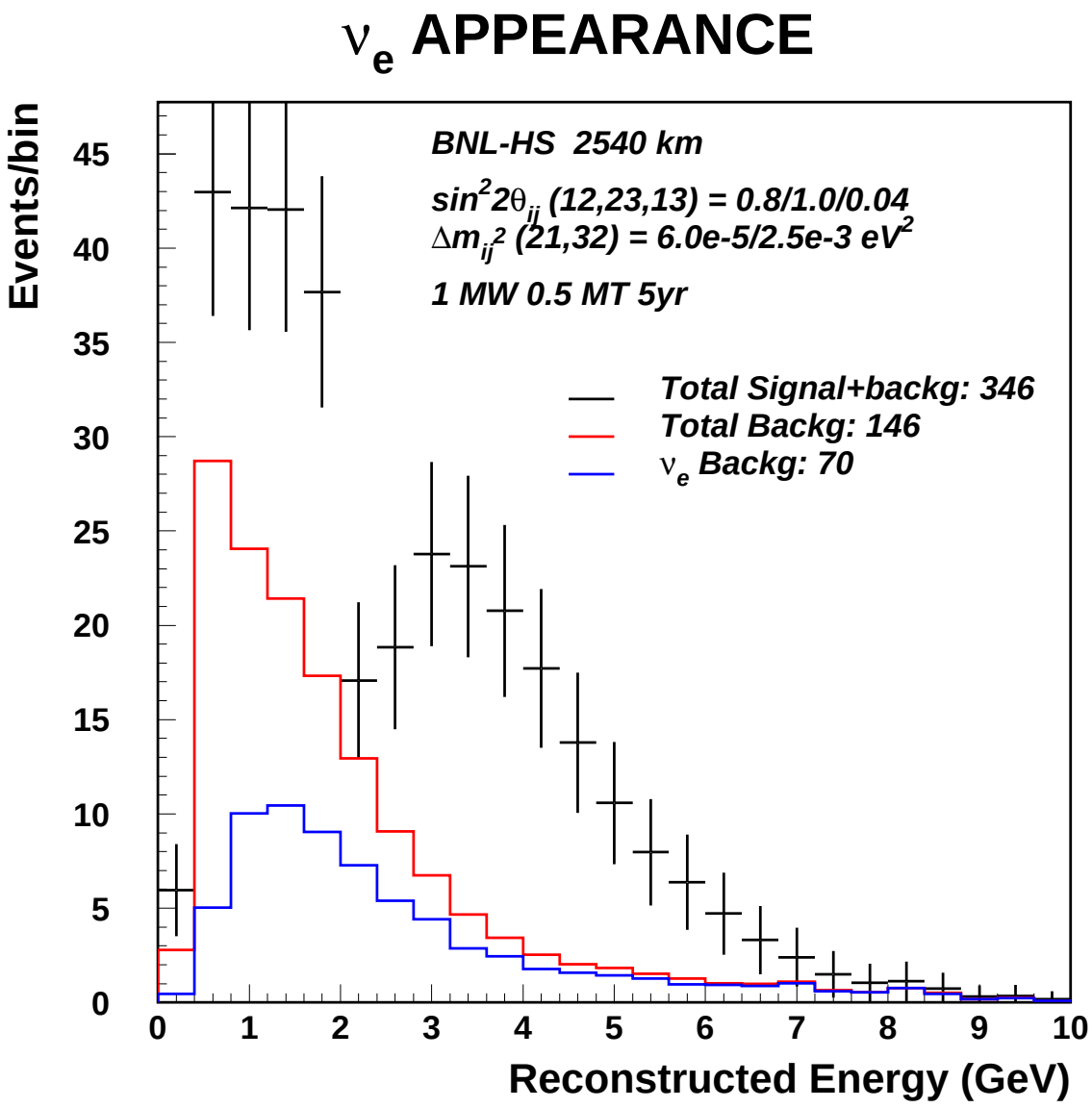

Figure 16: Spectrum of detected quasi-elastic electron neutrino charged current events in a 0.5 MT detector at 2540 km from BNL. We have assumed 1 MW of beam power and 5 nominal years of running. This plot is for $\Delta m^2_{32} = 0.0025\ eV^2$. We have assumed $\sin^2 2\theta_{13} = 0.04$ and $\Delta m^2_{21} = 6 \times 10^{-5}\ eV^2$. The error bars correspond to the statistical error expected in the bin. The spectrum includes effects of Fermi motion, energy resolution and efficiency.

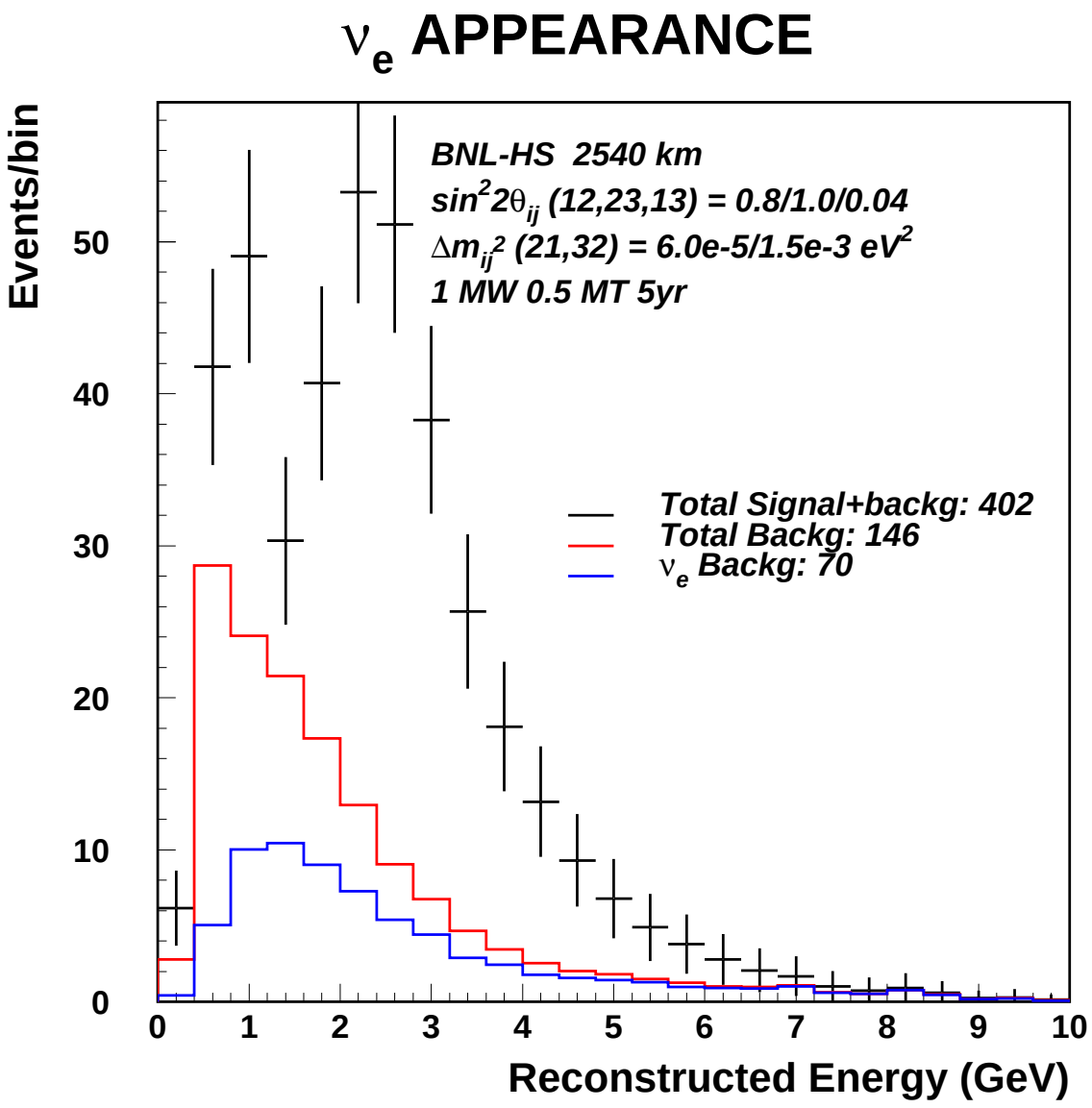

Figure 17: Spectrum of detected quasielastic electron neutrino charged current events in a 0.5 MT detector at 2540 km from BNL. We have assumed 1 MW of beam power and 5 nominal years of running. This plot is for $\Delta m^2_{32} = 0.0015\ eV^2$. We have assumed $\sin^2 2\theta_{13} = 0.04$ and $\Delta m^2_{21} = 6 \times 10^{-5}\ eV^2$.

the statistics will be larger and we will get a better limit, however the signal will not have the distinct shape that will be a strong confirmation of an oscillation signal. Moreover, the $\sin^2 2\theta_{13}$ measurement in the lower region could be correlated with Δm^2_{21}.

The sensitivity for the BNL-to-Homestake experiment declines as Δm^2_{32} becomes larger and the first oscillation node moves to higher energies where our spectrum has much lower flux. This can be improved by adding more focusing elements to the horn-produced beam to increase the high energy flux; however, this will increase the background for the lower energy events. We are in the process of performing these optimization studies to determine the best spectrum shape for this experiment. Lastly, we note that the sensitivity does not depend strongly on the amount of neutral current background. This is shown in Figure 19 where we have calculated the 90% confidence level upper limit assuming that the the neutral current background is twice as high as in Figure 15. This is because the spectrum is already dominated by the intrinsic ν_e background in the higher energy region above 2 GeV. Therefore any additional NC background makes little difference to the statistical sensitivity. Much higher NC background will affect the spectrum below 2 GeV and this could lower the sensitivity to CP parameters as well as Δm^2_{21}.

4.5 Sensitivity to the CP violation parameter

As shown in Figure 9, the effect of CP violation grows linearly as energy is decreased (or the baseline increased). For a very long baseline experiment, it is possible to compare the signal strength in the $\pi/2$ node versus the $3\pi/2$ or higher nodes. Such a comparison will yield a measurement of the CP violation parameter δ_{CP}. Such a measurement can be done with only neutrino beam running over most of the parameter region (anti-neutrino running not necessary). Any such measurement of CP should eventually be augmented by data using a muon anti-neutrino beam in the same experiment. Nevertheless, we have calculated the sensitivity to CP parameter δ_{CP} with only neutrino running. In Figure 20 we plot the reconstructed neutrino spectrum for electron-like events including background for 3 different values of δ_{CP}. The effect of δ_{CP} is clearly large for the lower energy signal region as pointed out earlier. In Figure 21 we further examine the effect of CP on the electron spectrum. This plot shows that both the size of the modulation and the phase shifts as we examine different energy bins. The phase shift is due to the presence of terms involving both $\sin\delta$ and $\cos\delta$ in the $\nu_\mu \rightarrow \nu_e$ probability over the entire spectrum. The broadband beam, therefore, allows us to fit the entire spectrum and gives us good sensitivity to δ_{CP} with much reduced correlation with $\sin^2 2\theta_{13}$.

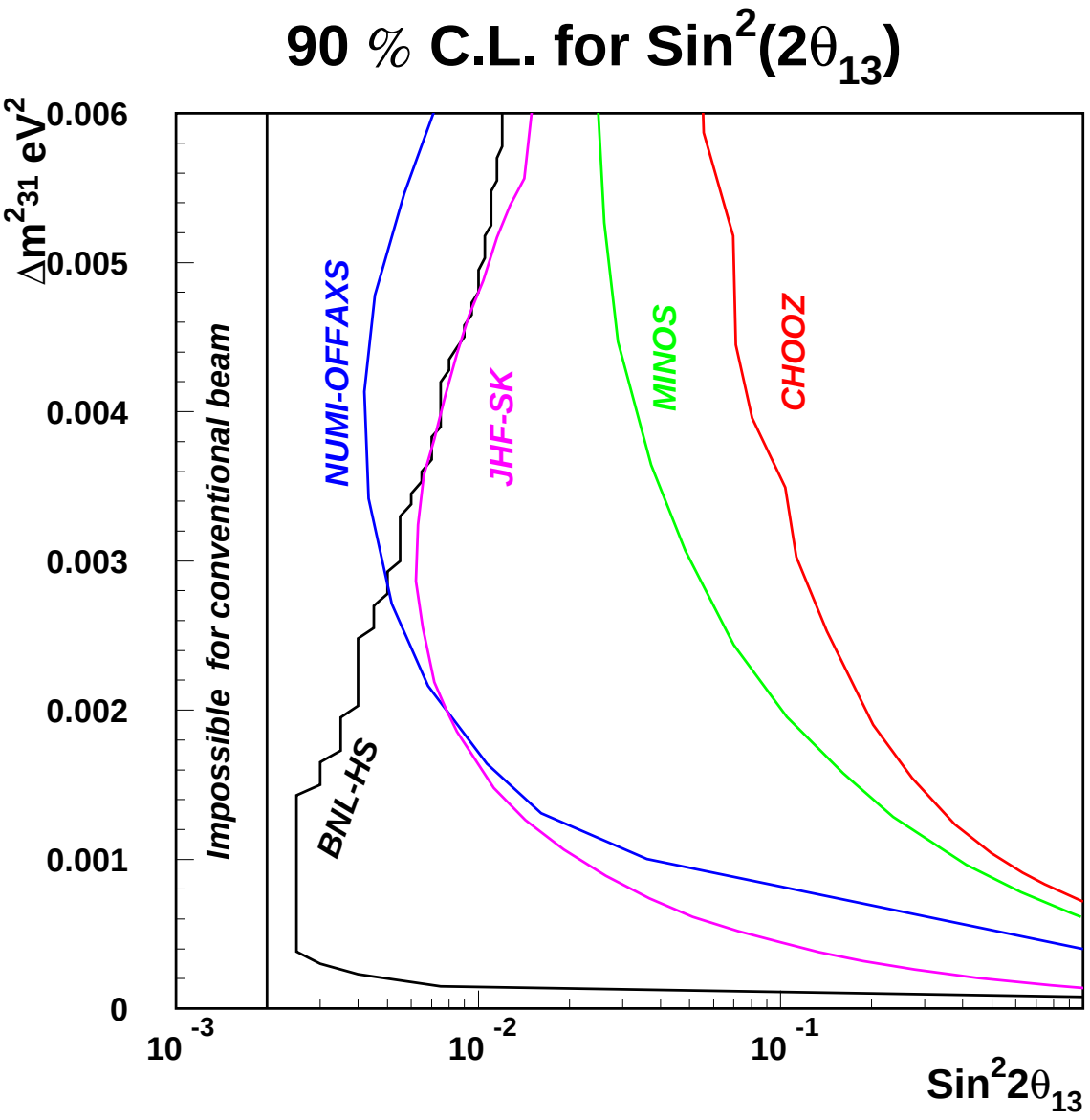

Figure 18: Expected 90% confidence level upper limit on $\sin^2 2\theta_{13}$ versus Δm^2_{31} for the BNL-to-Homestake experiment compared to other proposed experiments. The current limit from the CHOOZ reactor experiment is also shown on the same plot.

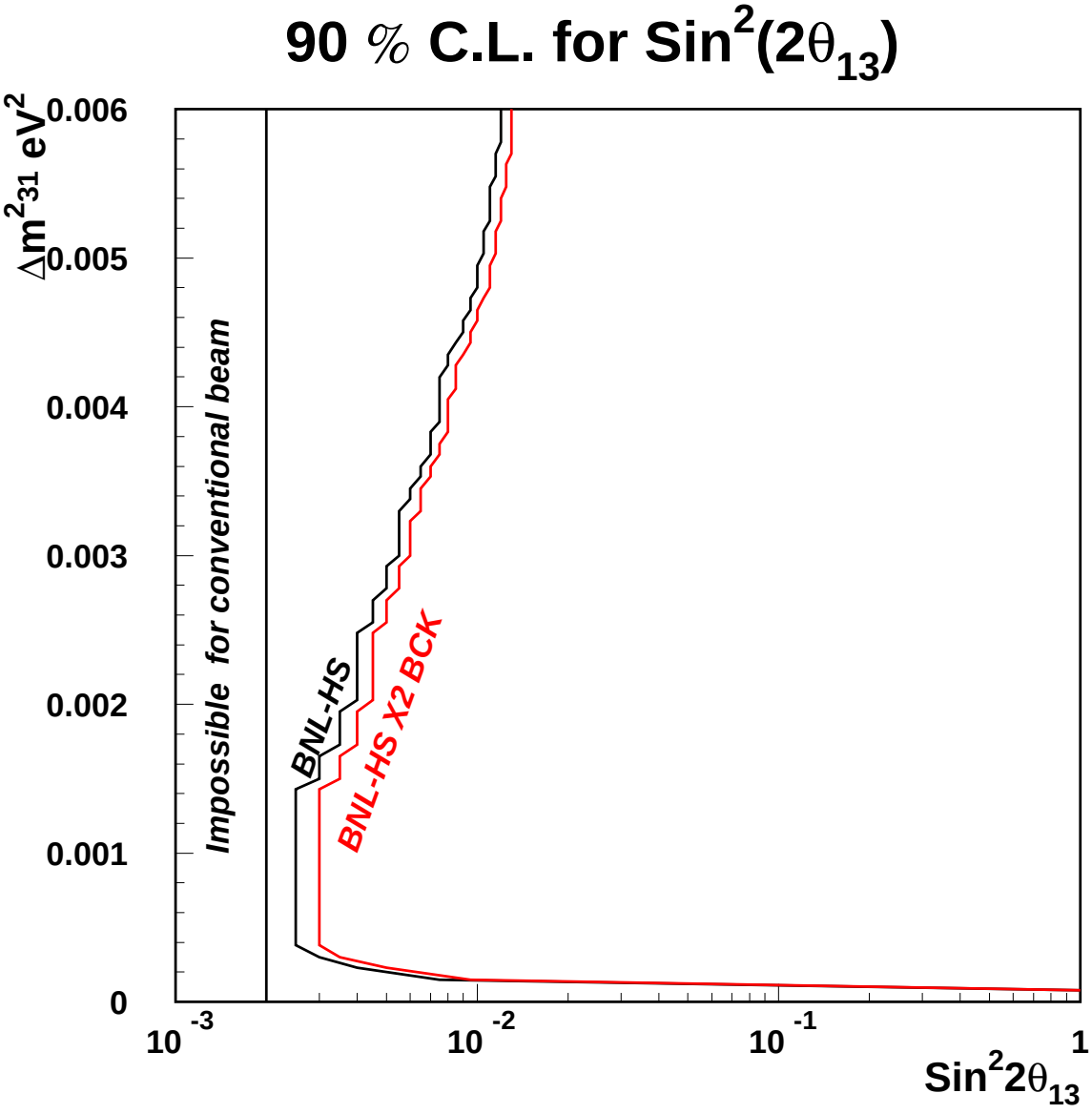

Figure 19: Expected 90% confidence level upper limit on $\sin^2 2\theta_{13}$ versus Δm^2_{31} for the BNL-to-Homestake experiment. The two curves are with the background as predicted in Fig. 15 (the left hand curve) and assuming the neutral current background to be a factor of two larger (the curve to the right).

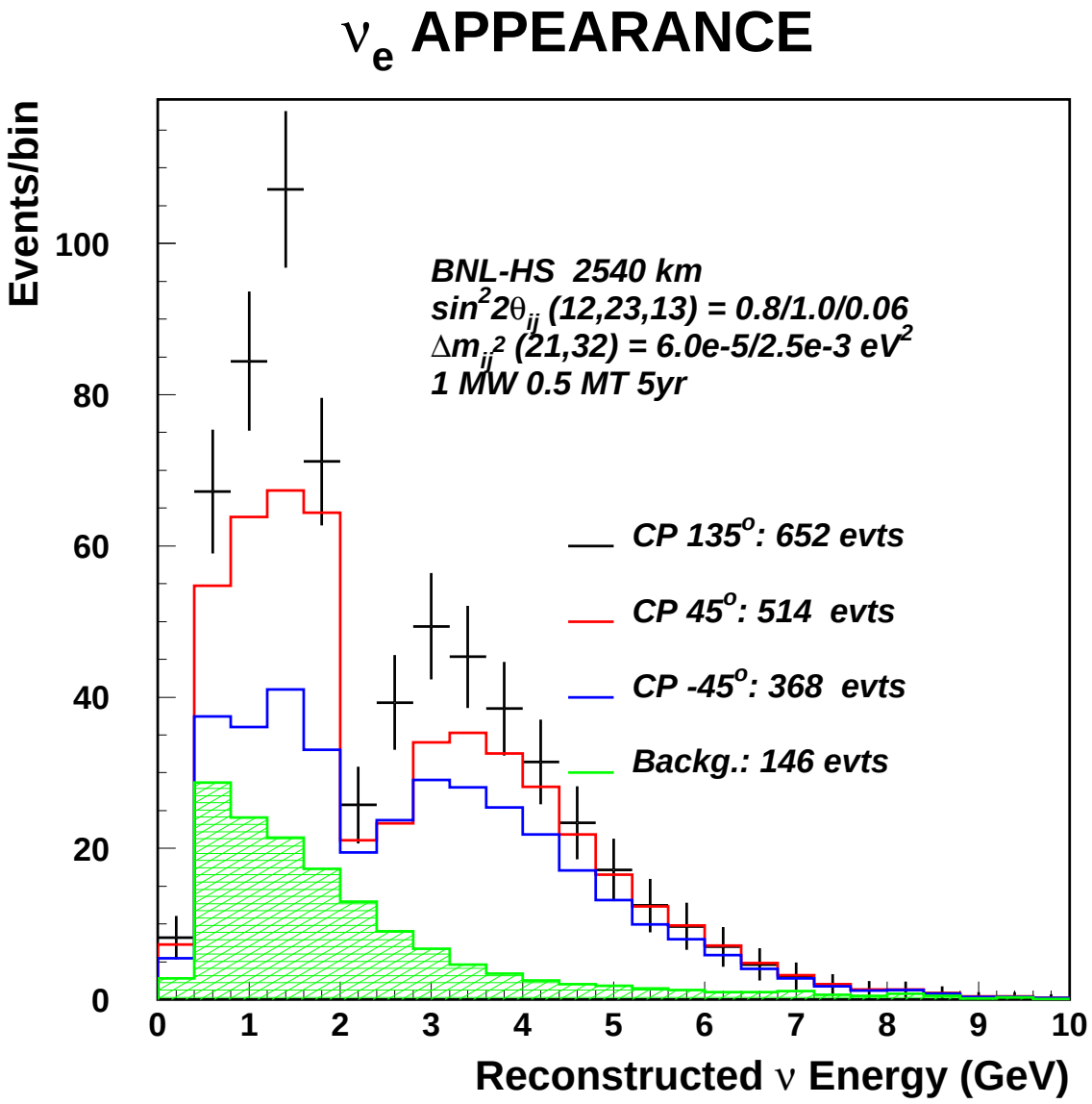

Figure 20: The observed electron neutrino spectrum including background contamination for 3 different values of the CP parameter δ_{CP}. The error bars are for $\delta_{CP} = 135^o$; the errors bars indicate the statistical error on eah bin. The red histogram below the error bars is for $\delta_{CP} = 45^o$, and the blue histogram is for $\delta_{CP} = -45^o$. The green hatched histogram shows just the background (Figure 15). This plot is for $\Delta m^2_{32} = 0.0025$ eV^2. We have assumed $\sin^2 2\theta_{13} = 0.06$ and $\Delta m^2_{21} = 6 \times 10^{-5}$ eV^2. The values of $\sin^2 2\theta_{12}$ and $\sin^2 2\theta_{23}$ are set to 0.8, 1.0, respectively.

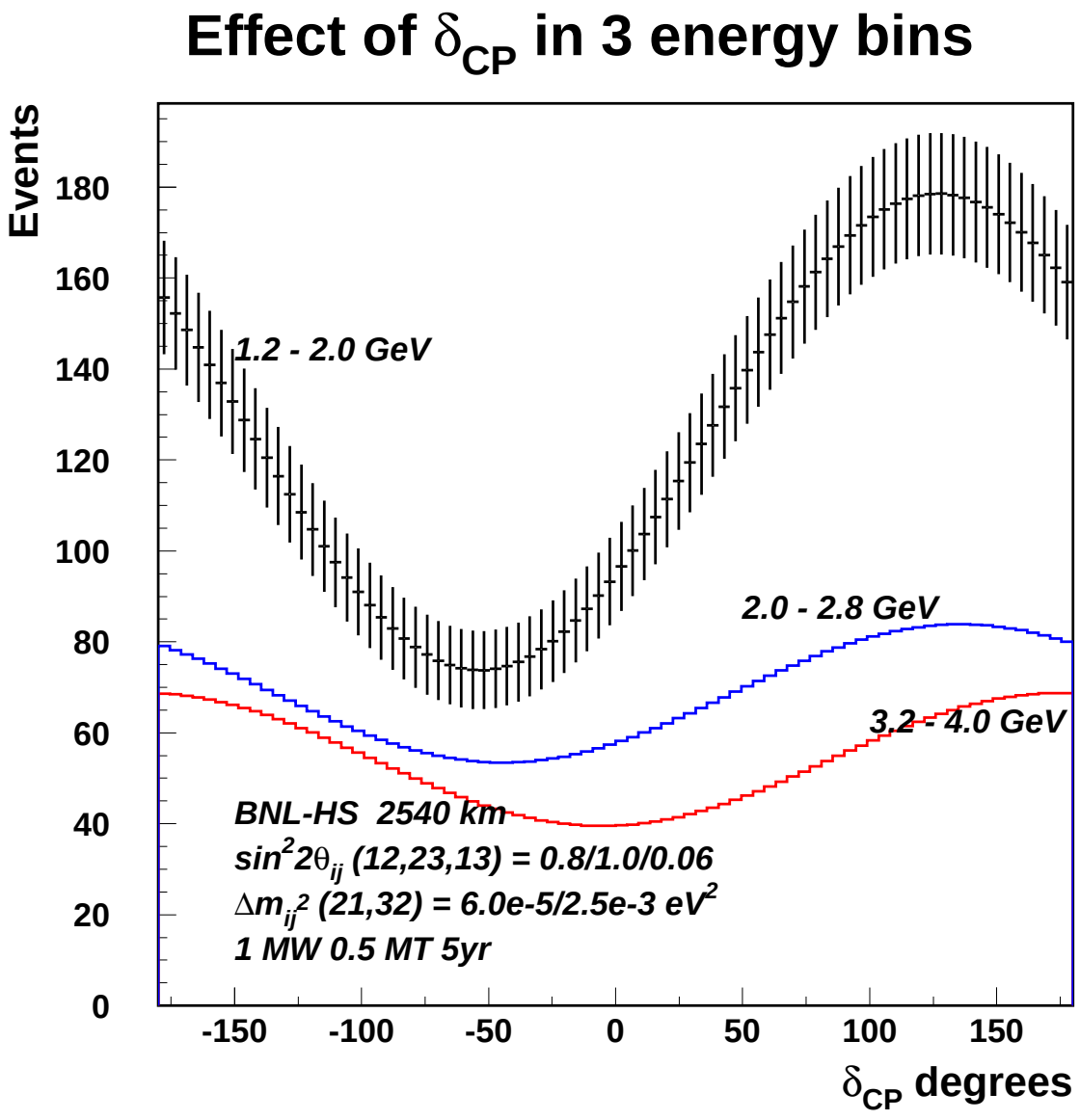

Figure 21: The event rate in 3 energy bins from Fig. 20 as a function of δ_{CP}. This plot also includes the background in each of the 3 energy bins. This plot shows that both the phase and the size of the modulation changes as we examine different energy bins. Thus a fit to the entire spectrum should give us good sensitivity to δ_{CP}.

It is clear from Figure 20 that sensitivity to $\nu_\mu \rightarrow \nu_e$ depends on both $\sin^2 2\theta_{13}$ and δ_{CP}. Therefore, we have calculated the 90% confidence level upper limit on $\sin^2 2\theta_{13}$ as a function of δ_{CP} with all other parameters fixed in Figure 22. The region on the right hand side of the curves in Figure 22 can be excluded if no excess of electrons is found as expected for the parameters shown in the figure.

If $\sin^2 2\theta_{13}$ is reasonably large then a good measurement of δ_{CP} is possible from the neutrino data alone. 68% and 90% confidence level error contours are shown in Figure 23 with statistical errors only for $\delta_{CP} = 45^o$ and $\sin^2 2\theta_{13} = 0.06$ (the other parameters are listed in the figure caption). Systematic errors on the background will mainly affect the low energy (0.5 to 2 GeV) region, which has large sensitivity to the CP parameter. We have calculated the error contours assuming 10% systematic uncertainty on the background in Figure 24. We believe that with the use of a near detector as well as clearly tagged background events we can achieve 10% determination of the expected background. Figures 25 and 26 show the expected error contours at $\sin^2 2\theta_{13} = 0.04, \delta_{CP} = 135^o$ and $\sin^2 2\theta_{13} = 0.06, \delta_{CP} = -90^o$, respectively. Two important observations considering these results are: if we perform the measurement without using a wide band beam in a narrow region of L/E the result will have a severe correlation between $\sin^2 2\theta_{13}$ and δ_{CP}; this correlation is broken by the use of a wide band beam. Secondly, the expected error on δ_{CP} is $\pm 20^o$ over a wide range of $\sin^2 2\theta_{13}$; it can be improved considerably with modest amount of anti-neutrino data running. We will examine the consequences of the anti-neutrino running in an update to this paper.

For the result in this section on the CP measurement we have assumed that the values of Δm^2_{21} and $\sin^2 2\theta_{12}$ will be well known. The measurement of δ_{CP} is, of course, correlated to these quantities. On the other hand, we could fit the observed electron distribution for the quantity $J_{CP} \times \Delta m^2_{21}$ to simply detect the presence of CP-violating terms in the spectrum without attempting to measure δ_{CP}. We will examine these and other subtleties in the next update to this paper.

4.6 Sensitivity to mass hierarchy

There are three possible neutrino mass hierarchies possible with the existing data on atmospheric and solar neutrinos. For most of this paper we have assumed the normal mass hierarchy (NH): $m_3 > m_2 > m_1$. The reversed mass hierarchy (RH), $m_1 > m_2 > m_3$, will be ruled out if the preferred Solar-LMA solution is confirmed in the near future. The LMA solution depends on $m_2 > m_1$ through the MSW mechanism. The third possibility,

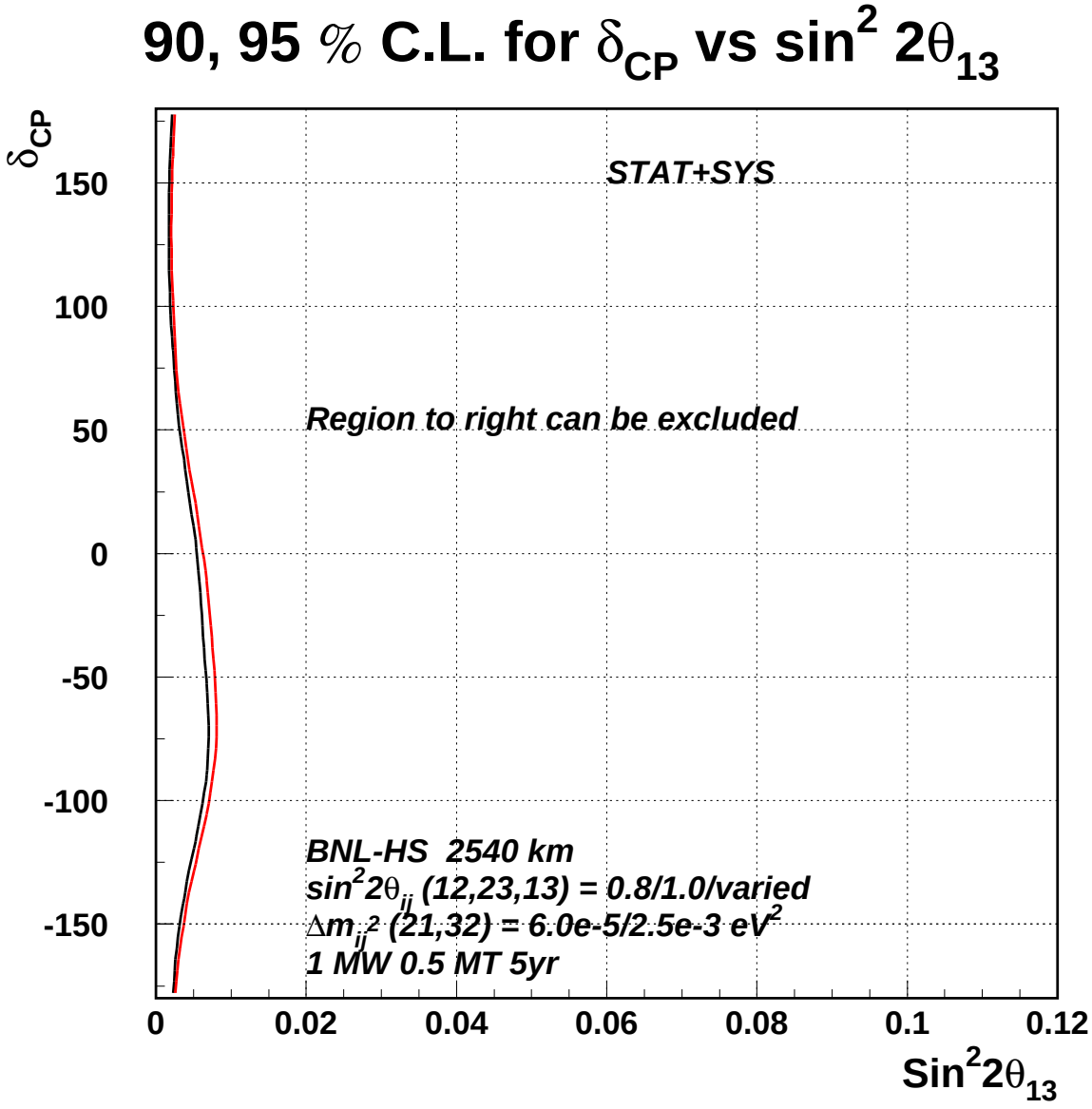

Figure 22: 90% and 95% confidence level upper limit in $\sin^2 2\theta_{13}$ as a function of δ_{CP} if no excess of electron is found as expected for $\Delta m^2_{32} = 0.0025\ e\mathrm{V}^2$, and $\Delta m^2_{21} = 6 \times 10^{-5}\ e\mathrm{V}^2$. The values of $\sin^2 2\theta_{12}$ and $\sin^2 2\theta_{23}$ are set to 0.8, 1.0, respectively.

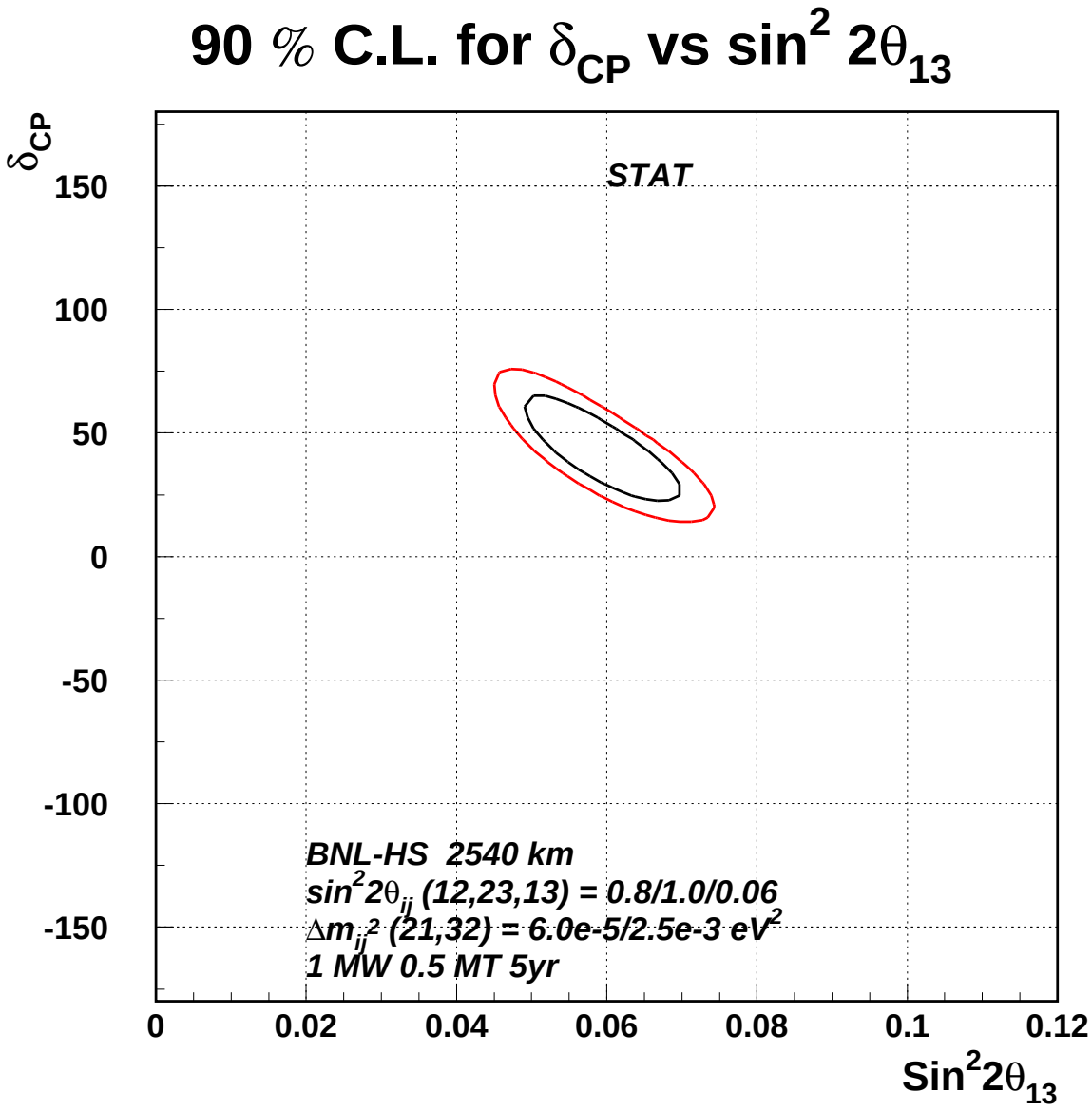

Figure 23: 68% and 90% confidence level error contours in $\sin^2 2\theta_{13}$ versus δ_{CP} for statistical errors only. The test point used here is $\sin^2 2\theta_{13} = 0.06$ and $\delta_{CP} = 45^o$. $\Delta m^2_{32} = 0.0025$ eV^2, and $\Delta m^2_{21} = 6 \times 10^{-5}$ eV^2. The values of $\sin^2 2\theta_{12}$ and $\sin^2 2\theta_{23}$ are set to 0.8, 1.0, respectively.

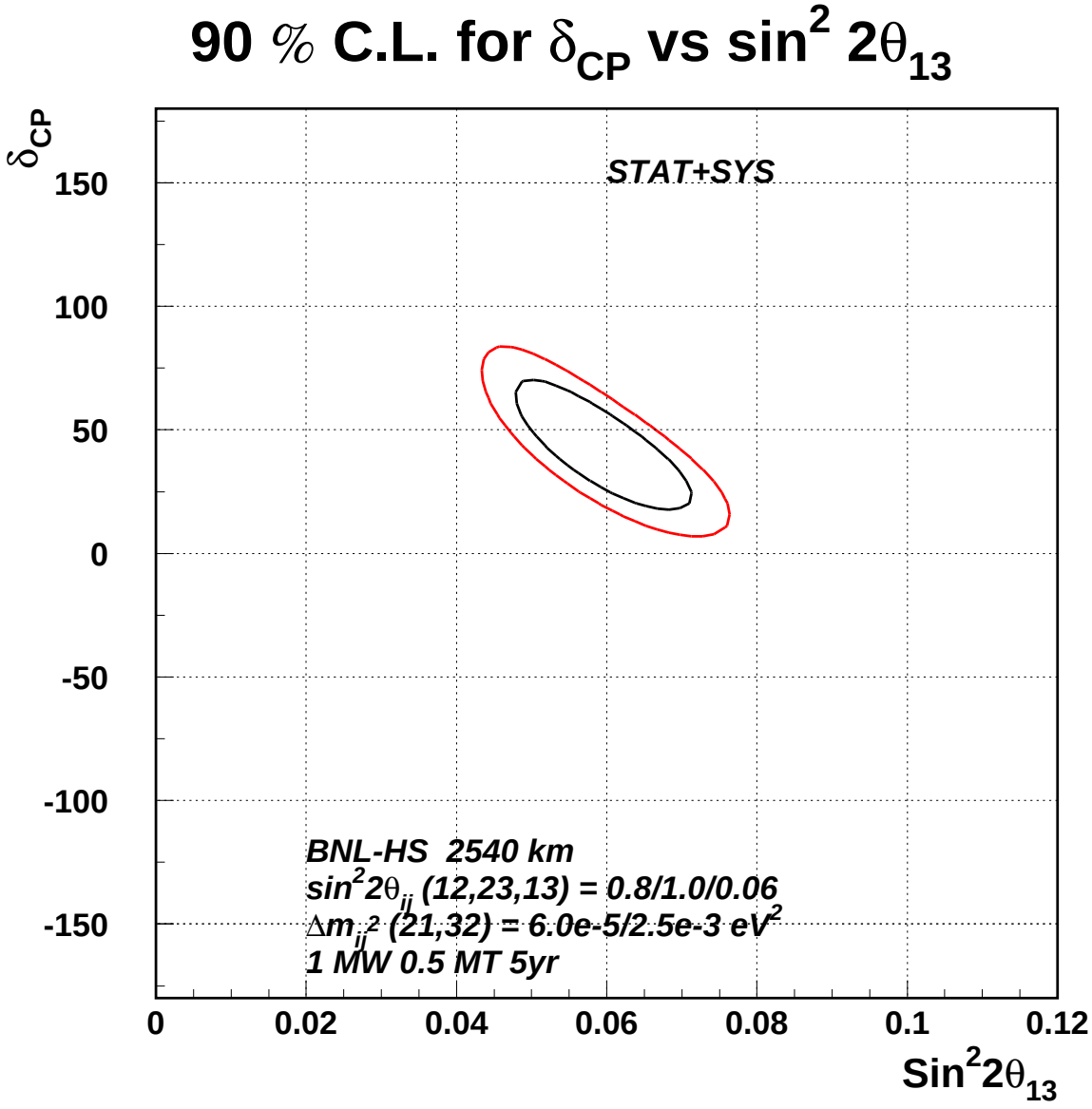

Figure 24: 68% and 90% confidence level error contours in $\sin^2 2\theta_{13}$ versus δ_{CP} for statistical and systematic errors. The test point used here is $\sin^2 2\theta_{13} = 0.06$ and $\delta_{CP} = 45^o$. $\Delta m^2_{32} = 0.0025\ e\mathrm{V}^2$, and $\Delta m^2_{21} = 6 \times 10^{-5}\ e\mathrm{V}^2$. The values of $\sin^2 2\theta_{12}$ and $\sin^2 2\theta_{23}$ are set to 0.8, 1.0, respectively.

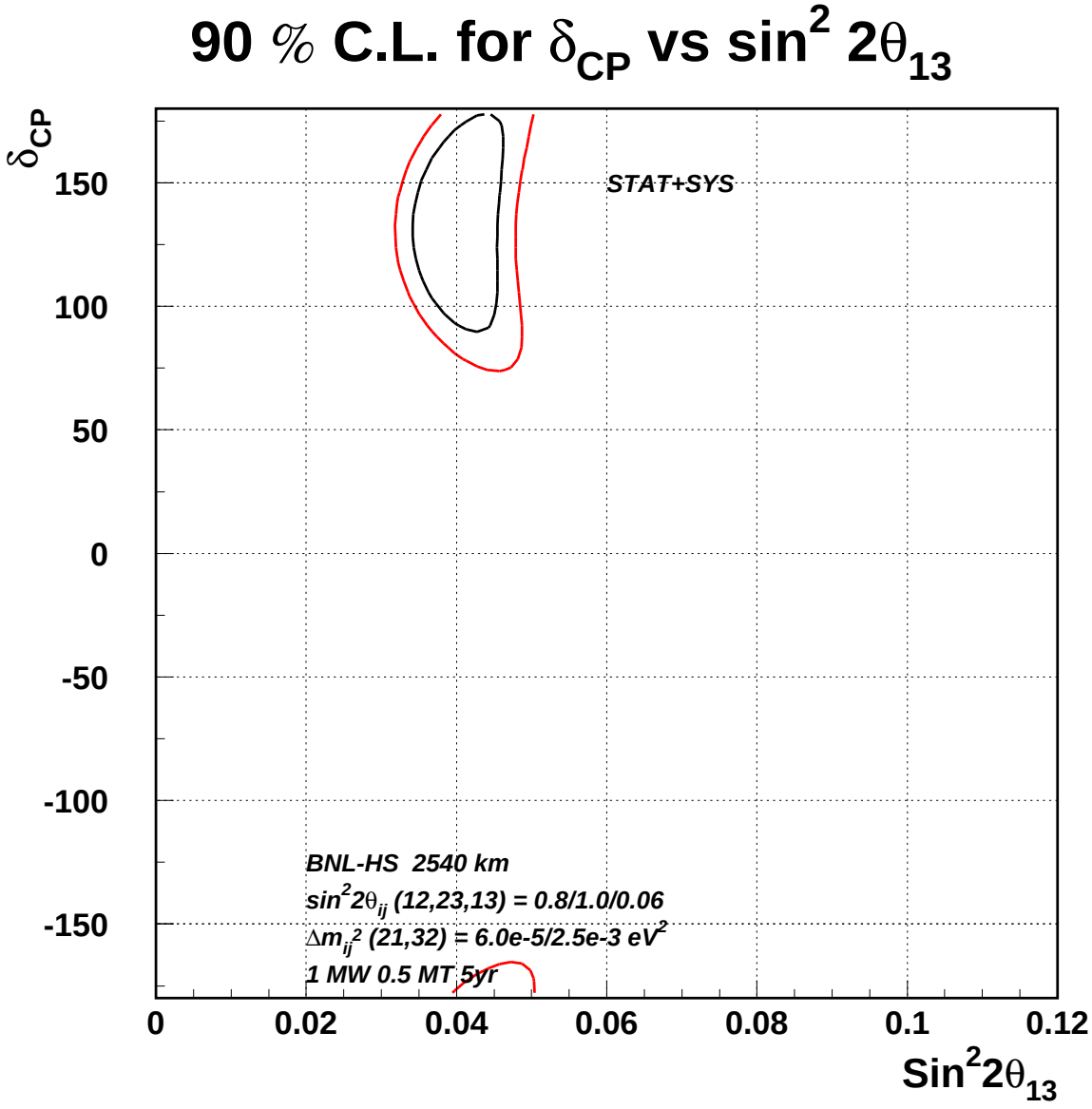

Figure 25: 68% and 90% confidence level error contours in $\sin^2 2\theta_{13}$ versus δ_{CP} for statistical and systematic errors. The test point used here is $\sin^2 2\theta_{13} = 0.04$ and $\delta_{CP} = 135^o$. $\Delta m^2_{32} = 0.0025$ $e\mathrm{V}^2$, and $\Delta m^2_{21} = 6 \times 10^{-5}$ $e\mathrm{V}^2$. The values of $\sin^2 2\theta_{12}$ and $\sin^2 2\theta_{23}$ are set to 0.8, 1.0, respectively.

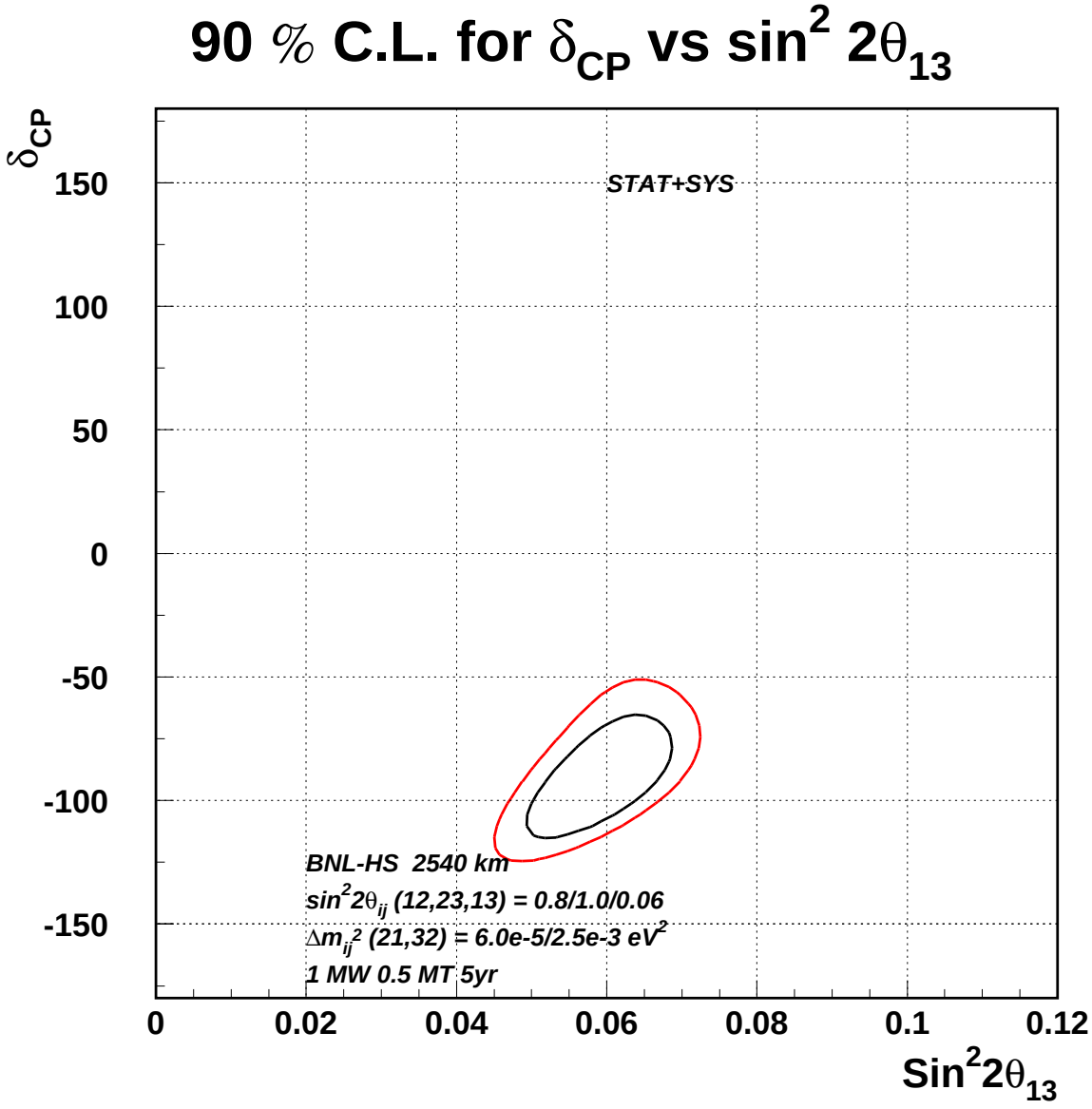

Figure 26: 68% and 90% confidence level error contours in $\sin^2 2\theta_{13}$ versus δ_{CP} for statistical and systematic errors. The test point used here is $\sin^2 2\theta_{13} = 0.06$ and $\delta_{CP} = -90^o$. $\Delta m^2_{32} = 0.0025\ e\mathrm{V}^2$, and $\Delta m^2_{21} = 6 \times 10^{-5}\ e\mathrm{V}^2$. The values of $\sin^2 2\theta_{12}$ and $\sin^2 2\theta_{23}$ are set to 0.8, 1.0, respectively.

$m_2 > m_1 > m_3$, called the unnatural hierarchy (UH), will result in a very different appearance spectrum in the case of the BNL to Homestake experiment. This is illustrated in Figure 27; the UH possibility causes a suppression $\nu_\mu \rightarrow \nu_e$ oscillation in the high energy region. However, the second oscillation maximum is still present and it is quite sensitive to the CP phase. In the case of UH, therefore, we will still obtain reasonable sensitivity to $\sin^2 2\theta_{13}$ with neutrino running, but it will depend strongly on δ_{CP} as shown in Figure 28.

For a large region of parameter space, the UH and NH possibilities can be separated with good significance using the spectrum obtained from the neutrino running only. Nevertheless, anti-neutrino running may be essential if $\sin^2 2\theta_{13}$ is small. The probability of $\bar{\nu}_\mu \rightarrow \bar{\nu}_e$ for the UH case in the of anti-neutrinos is shown in Figure 29. In the UH case the oscillation probability is enhanced in the high energy (> 3 GeV) region. This could be detected easily by changing the polarity of the horn focussed beam to make an anti-neutrino beam.

For this report we have concentrated on first running the beam with the neutrino polarity. In an updated to this report we will examine the event rates, and sensitivities for anti-neutrino running. Nevertheless, we can make a few remarks based on experience from [13]. The horn focussed anti-neutrino flux will be about 80% of the neutrino flux. However, the event rate from anti-neutrino will be suppressed because of the lower cross section. The event rate will also have about 10% contamination from neutrinos. An important feature, however, for the very long baseline experiment can be seen in Figure 30, which shows the cross section for quasielastic events for neutrinos and anti-neutrinos. In the interesting energy region about 3 GeV where we expect the matter enhanced signal for anti-neutrino running, the quasielastic cross section for anti-neutrino running is about 70% of the neutrino cross section. This implies that the sensitivity to $\sin^2 2\theta_{13}$ in the UH case using anti-neutrinos could be quite good with similar amount of running as in the neutrino case for NH.

4.7 Sensitivity to Δm^2_{21}

The distance of 2540 km is sufficient to obtain an appreciable signal for $\nu_\mu \rightarrow \nu_e$ because of the dominant mixing due to Δm^2_{21} and $\sin^2 2\theta_{12}$ if the LMA (Large Mixing Angle) solution holds for the solar neutrino anomaly. This is shown in Figures 31 and 32. The parameters for the best fit point in the LMA solution contour were used for Figure 31. An excess of 62 events is expected in the lower part of the energy spectrum. If the true value of Δm^2_{21} is at the upper end of the LMA solution ($12.0 \times 10^{-5}\ eV^2$) then a rather large excess of 230 events is expected. This signal can result in a reasonably good measurement of Δm^2_{21};

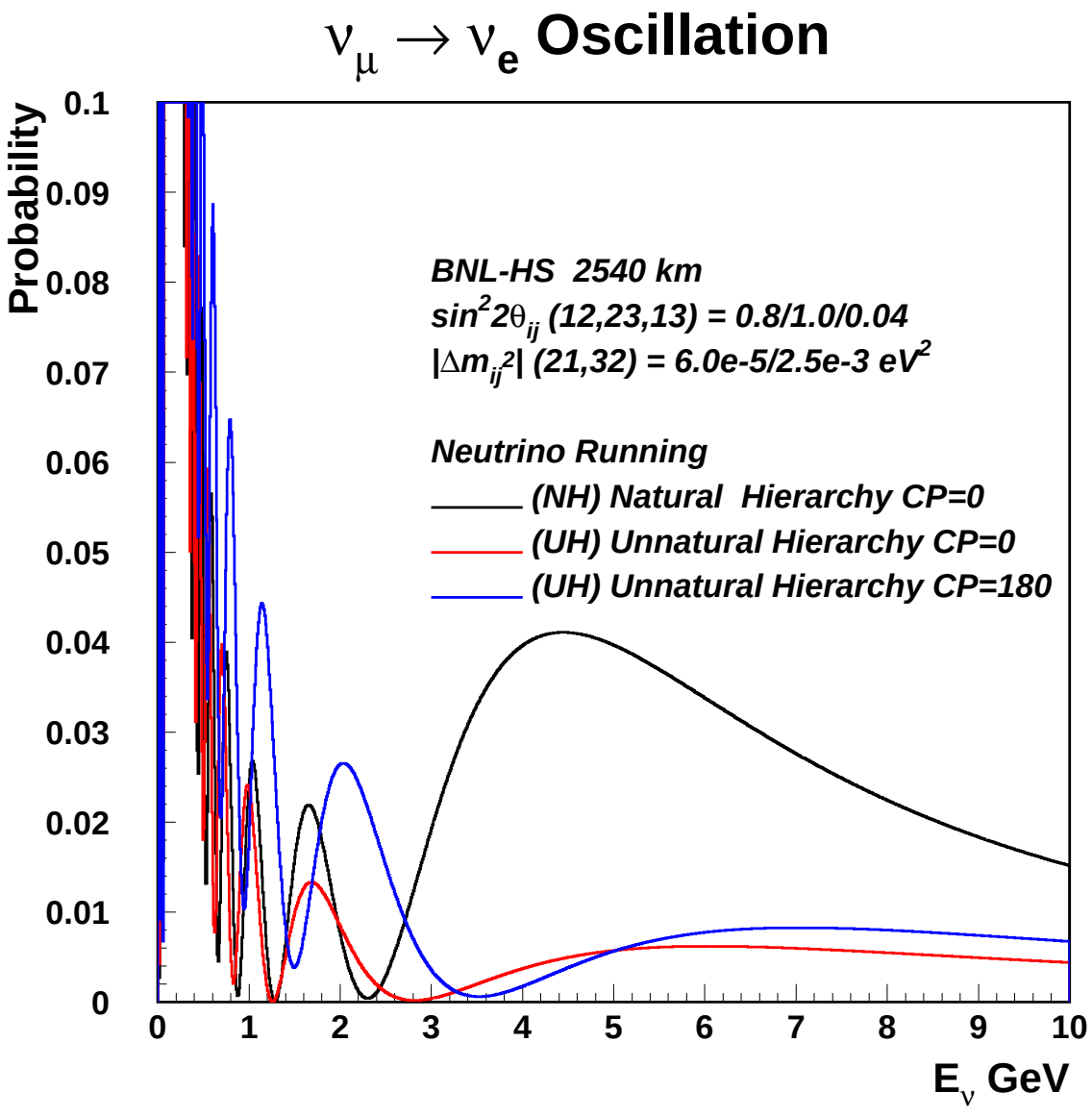

Figure 27: Probability for $\nu_\mu \rightarrow \nu_e$ oscillations as a function of neutrino energy for a baseline of 2540 km. The three curves correspond to regular mass hierarchy (RH) with $\delta_{CP} = 0^o$ (black), irrational mass hierarchy (IRH) with $\delta_{CP} = 0^o$ (red), and irrational mass hierarchy (IRH) with $\delta_{CP} = 180^o$ (blue). The other parameters are indicated in the figure.

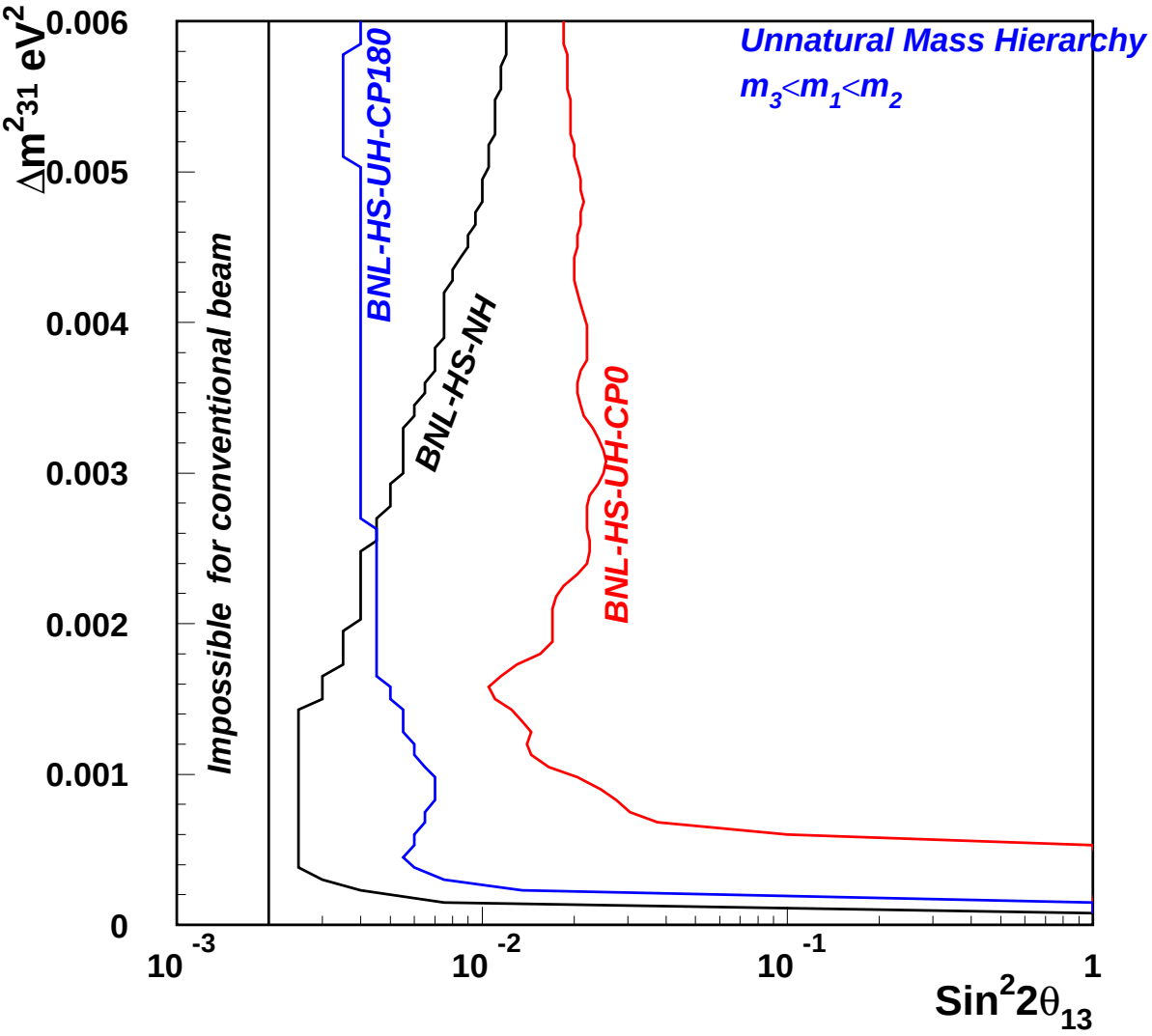

Figure 28: Expected 90% confidence level upper limit on $\sin^2 2\theta_{13}$ versus Δm^2_{31} for the BNL-to-Homestake experiment for the UH hypothesis for running with neutrinos for 5 years. We have used $\delta_{CP} = 0^o$ and $\delta_{CP} = 180^o$ for the two curves labeled BNL-HS-UH-CP0 and BNL-HS-UH-CP180, respectively. The limit that can be obtained for the NH possibility with $\delta_{CP} = 0^o$ is also shown labeled BNL-HS-NH.

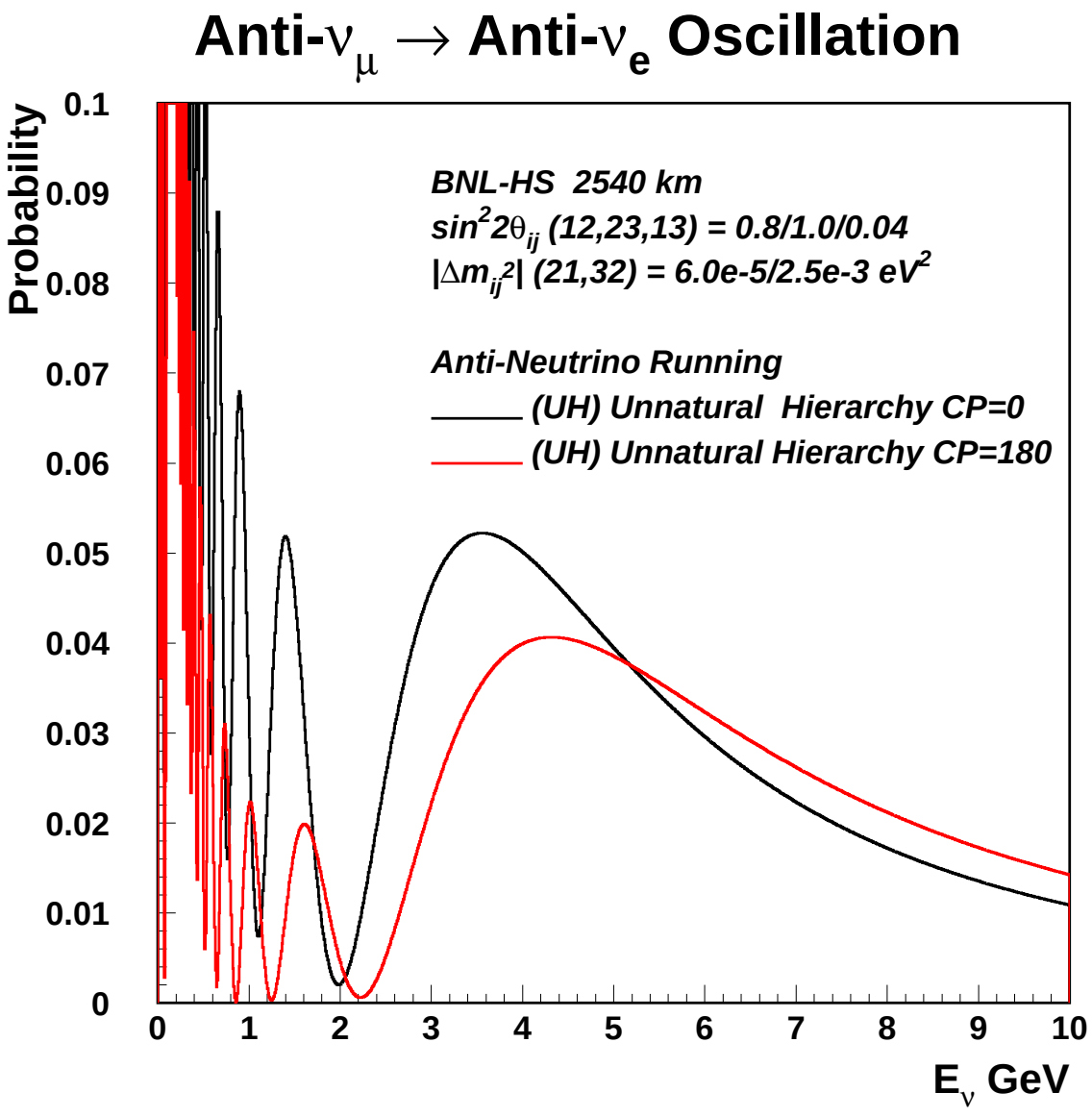

Figure 29: Probability for $\bar{\nu}_\mu \rightarrow \bar{\nu}_e$ oscillations as a function of anti-neutrino energy for a baseline of 2540 km. The two curves correspond to unnatural mass hierarchy (UH) with $\delta_{CP} = 0^o$ (black), and unnatural mass hierarchy (UH) with $\delta_{CP} = 180^o$ (red). The other parameters are indicated in the figure.

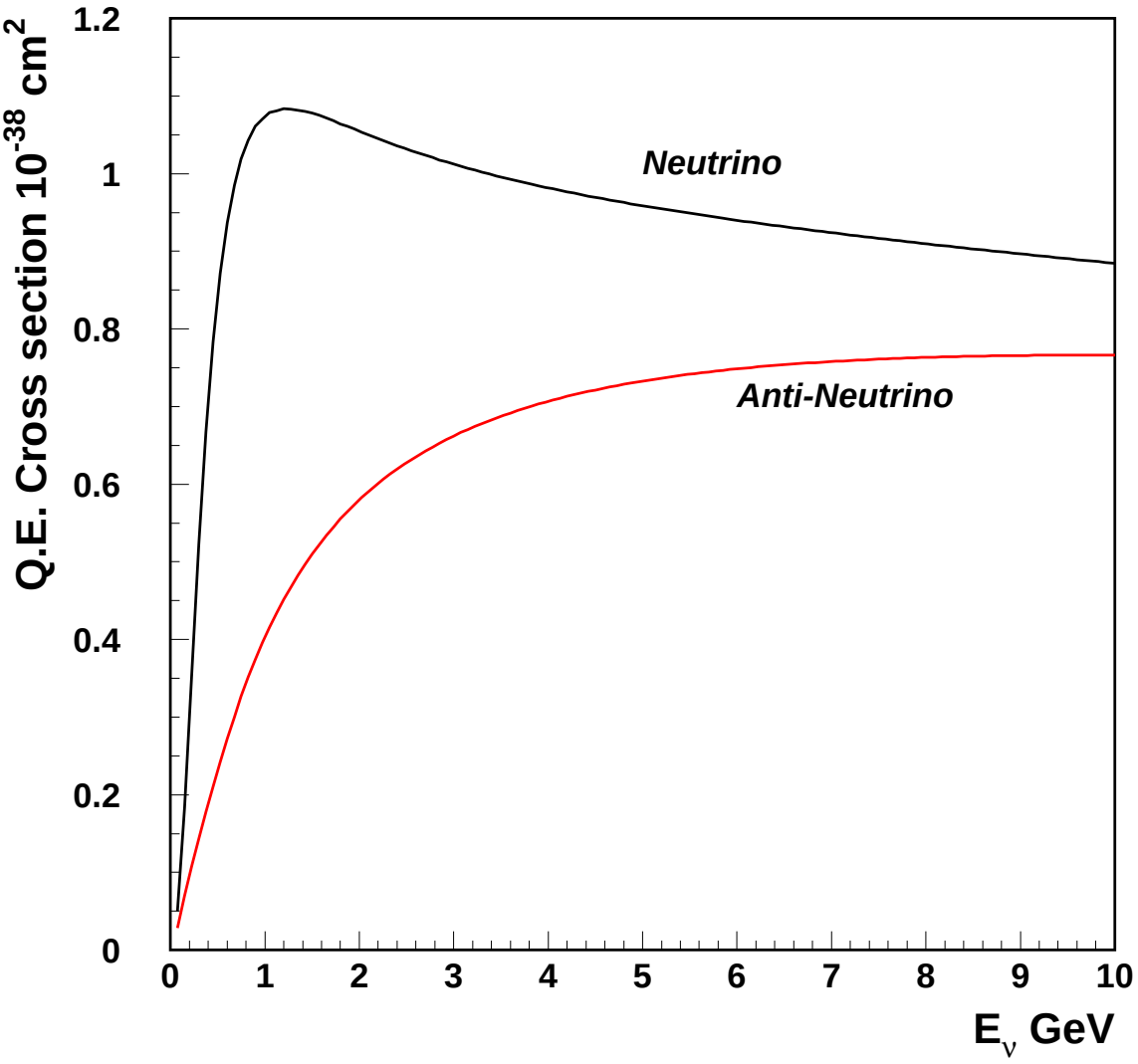

Figure 30: Cross section for quasielastic events. $\nu_e + n \rightarrow e^- + p$ for neutrinos and $\bar{\nu}_e + p \rightarrow e^+ + n$ for anti-neutrinos.

at the LMA best fit point the expected accuracy is ±20%. The confidence level contours are shown in Figure 33 where the LMA allowed contour is approximated as a rectangle. Statistical and 10% systematic error on the background are included in this determination. The accelerator experiment by itself will yield a result with a correlation between Δm^2_{21} and $\sin^2 2\theta_{12}$; therefore another experiment must provide a measurement of $\sin^2 2\theta_{12}$ to give the best result on Δm^2_{21}.

If there is no excess of electron-like events in the spectrum such as Figure 31 then an upper limit can be obtained on the parameters Δm^2_{21} versus $\sin^2 2\theta_{12}$. Such a 90% confidence level limit is shown in Figure 34. This limit was obtained using statistical errors and a 10% systematic error on the background. This experiment can cover most of the LMA solution; if the background can be measured better or suppressed further then all of the LMA region could be covered.

Such a measurement of the parameters governing the solar neutrino anomaly in the ν_e appearance mode is qualitatively very different from measurements in the SNO experiment or long baseline reactor experiments such as KAMLAND [22] and confirms the neutrino oscillation picture in a useful new mode.

4.8 The Experimental Strategy and Program

For most of this document we have shown the possible results of running with a neutrino beam for a total of about 5 years of practical operation. The actual running conditions will, of course, depend on the physics results that will be produced as the experiment progresses. The great advantage of this proposed program is that it is so rich in its physics reach that important new physics results will come forth after every year of running. These results, in turn, will determine the character of running for the next period.

For example, after only about 2 years of running we will have a very accurate determination of Δm^2_{32} and $\sin^2 2\theta_{23}$. At this stage, if we see a substantial peak in the electron spectrum at the expected energy, we will have strong evidence for the natural mass hierarchy (NH) and then continue running with neutrinos to detect the presence of CP violating terms. But if we see no electron signal, we would then switch to antineutrino running. Since at higher energies (> 3 GeV), the antineutrino quasielastic cross section is 70% of the neutrino quasielastic cross section, it will not take a very large amount of antineutrino running to see a peak in the positron spectrum at the expected energy if $\sin^2 2\theta_{13}$ is > 0.01 with the unnatural mass hierarchy. Determination of the mass hierarchy is by itself a major goal of

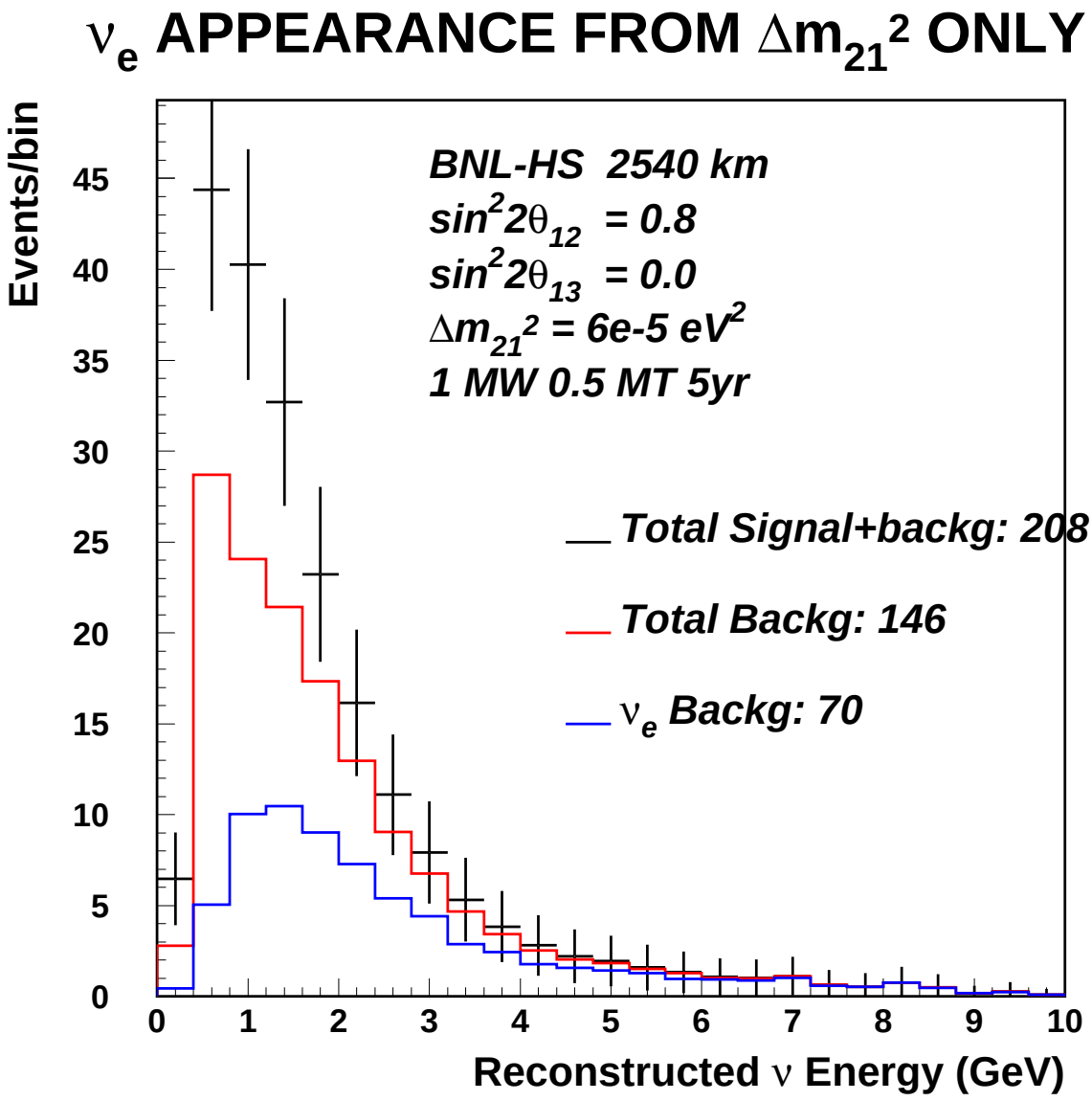

Figure 31: Spectrum of electron-like events for $\sin^2 2\theta_{13} = 0$. The other important parameters are $\Delta m^2_{21} = 6 \times 10^{-5}\ eV^2$ and $\sin^2 2\theta_{12} = 0.8$.

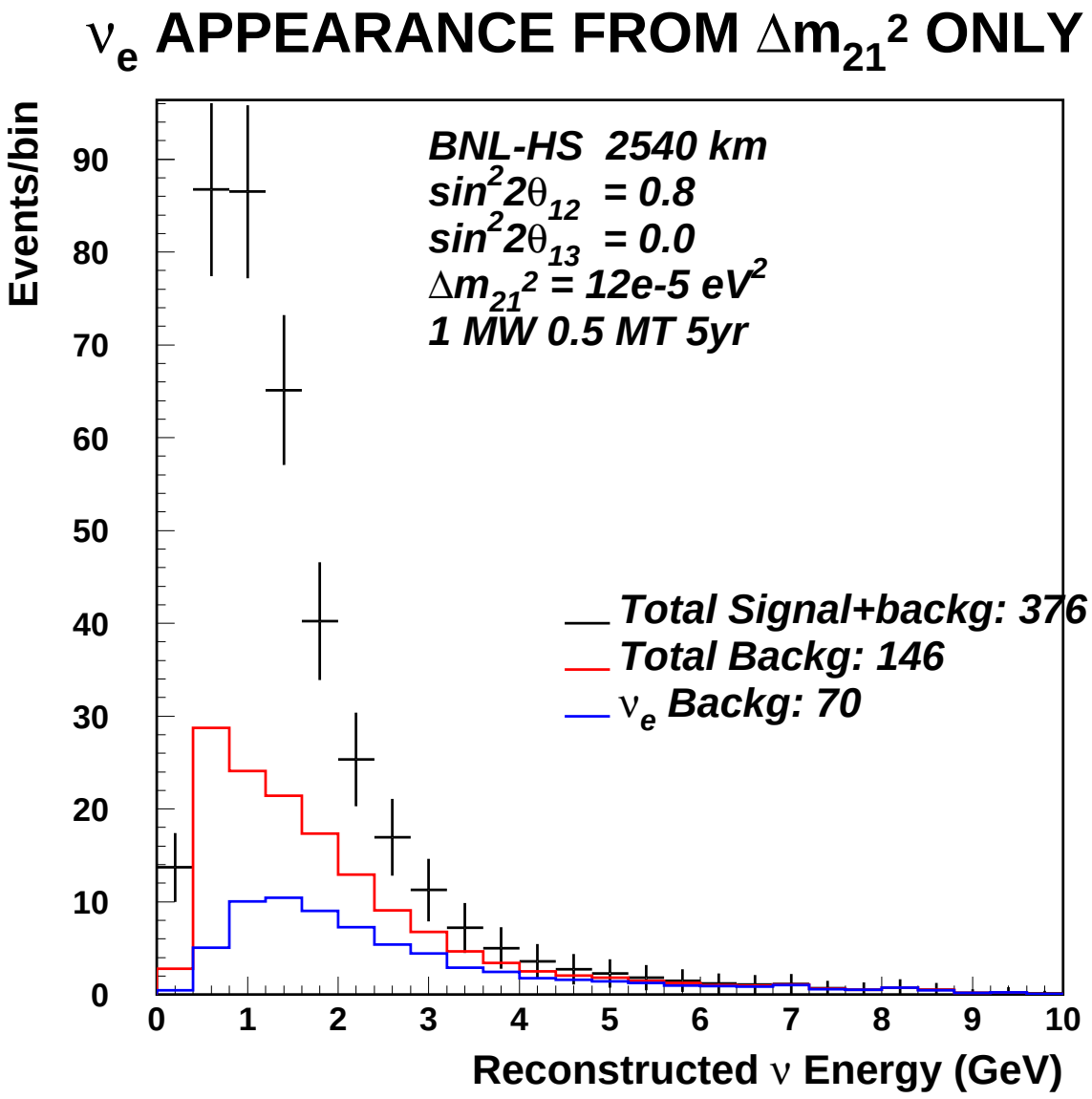

Figure 32: Spectrum of electron-like events for $\sin^2 2\theta_{13} = 0$. The other important parameters are $\Delta m^2_{21} = 6 \times 10^{-5}\ eV^2$ and $\sin^2 2\theta_{12} = 0.8$.

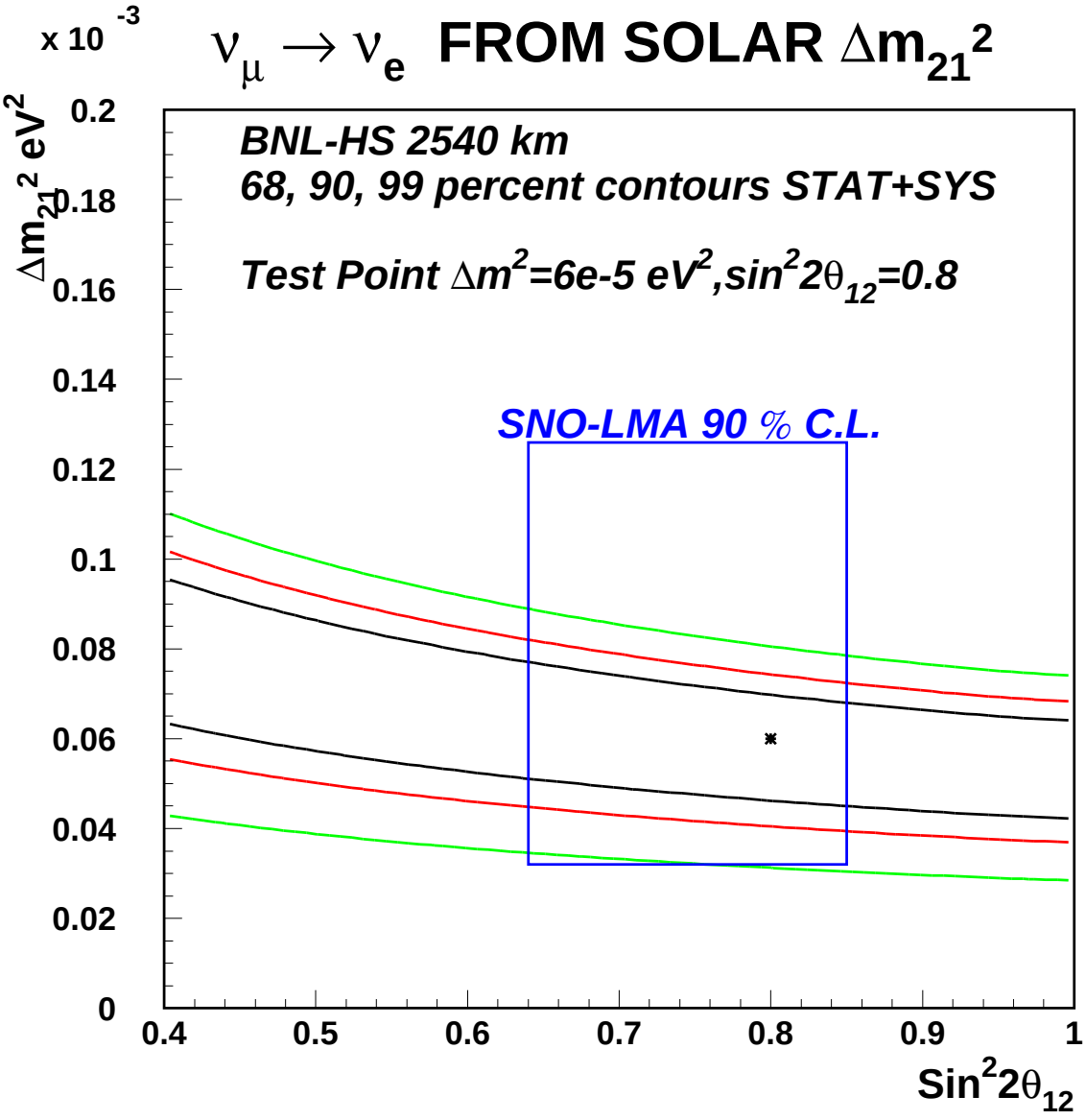

Figure 33: 68, 90, and 99 percent confidence level contours for a measurement at the LMA best fit point. Both statistical and systematic errors are included. We assume a 10% systematic error on the background.

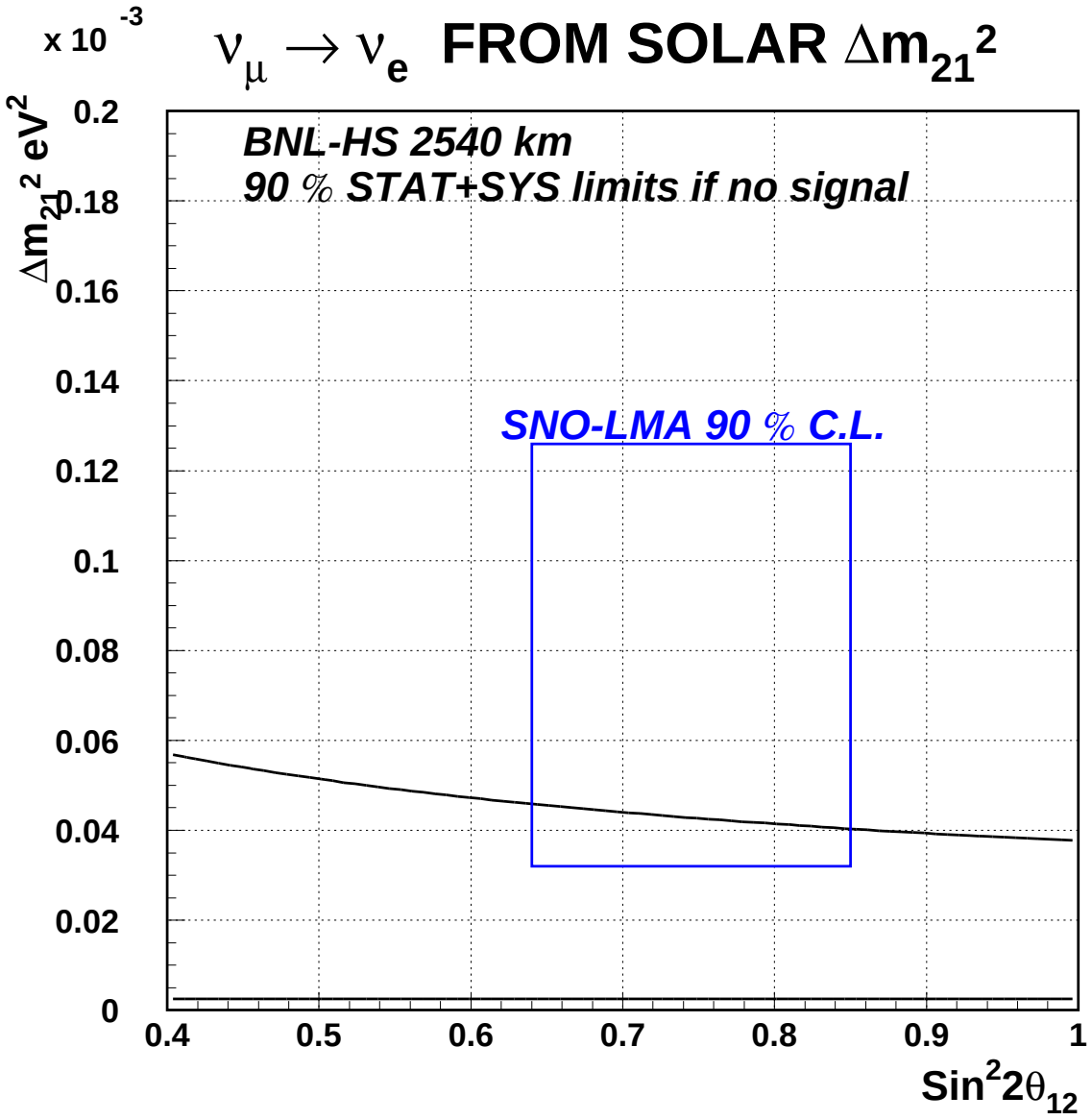

Figure 34: Expected 90% confidence level limit on Δm^2_{21} versus $\sin^2 2\theta_{12}$ if there is no excess of electron-like events. Both statistical and systematic errors are included.

this experimental program.

If the value of $\sin^2 2\theta_{13}$ is too small, one will still complete the experimental program to determine Δm^2_{21} in the appearance mode, a qualitatively different mode from the SNO or the KAMLAND experiments, and a confirmation of the oscillation picture we now have.

It should also be pointed out that although the absolute determination of Δm^2_{32} may be limited by systematic errors on the energy scale, this systematic error is eliminated when we compare the values of Δm^2_{32} obtained from neutrino versus anti-neutrino running. Such a comparison will yield a truly unique test of CPT conservation and more new physics.

Other unexpected results cannot be ruled out because of the spectacular physics reach of such an experiment. These results will influence the running conditions as well as future accelerator, beam, and detector upgrade paths.

We also emphasis that this all-inclusive neutrino oscillations program can be completed in a single facility. Other proposed methods that feature a sequential experiments approach will take much longer to perform and will ultimately cost more. This is an important strategic point for the US particle physics program.

4.9 Detectors for the very long baseline experiment

The conversion of Homestake Gold Mine in Lead, South Dakota, into the National Underground Science and Engineering Laboratory (NUSEL), tentatively to take place in the next few years, will provide a unique opportunity for a program of very-long baseline neutrino oscillation experiments. As explained above, these experiments are possible only due to the length of the baseline, 2540 km, from the Brookhaven National Laboratory (BNL) to Lead. It is proposed that the NUSEL facility will accommodate either an array of detectors or a single monolithic one both with total masses approaching 1 Megaton. Most of these will be water Cherenkov detectors that can observe neutrino interactions in the desired energy range with sufficient energy and time resolution [23]. Details of underground construction of these detectors is provided in Appendix II.

An alternative to Homestake also exists at the Waste Isolation Pilot Plant (WIPP) located in an ancient salt bed at a depth of ~ 700 meters near Carlsbad, New Mexico. One advantage of the WIPP site is that it is owned by the DOE and now has a program of underground science. We note that the recent Neutrino Factory Study [24] at BNL identified the WIPP site as one possible location for a far detector, and the current BNL neutrino beam could use the same concept. The distance from BNL to WIPP is about 2880 km. The cosmic ray

background will be higher at WIPP because the facility is not as deep as Homestake, which has levels as deep as ~ 2500 meters. The increased background, although undesirable, is not an insurmountable problem. However, the mechanical design of a large cavity in a salt bed has to be very different because of the slow movement of salt that causes a cavity to slowly collapse.

The issue of depth is not one that greatly impacts this experiment. A modest overburden is needed so that the detector is not swamped by cosmic ray muon events and thus overwhelmingly dead. Because the beam spill times are well known, simple timing gates suffice to remove virtually all direct cosmic ray backgrounds. This method is successfully used in the K2K experiment. The background from cosmic ray muon spallation events as well as electrons from muon decay are both well below the analysis energy threshold. However, there is a very rich array of physics that a large underground detector can do in the time between beam spills many of which either benefit from or require depths of greater than 3000 meters water equivalent[26]. Figure 35 shows the cosmic ray muon intensity as a function of depth.

In this report we will not address the detailed issues of detector design and cost. A more detailed study of a very large water Cherenkov detector has been done by the UNO collaboration [26]. Figure 36 shows a conceptual design drawing of their detector layout.

Another option for detector technology is a liquid Argon (LAR) time projection chamber. Although a massive LAR detector (500 kT) cannot be ruled out at this stage, a near LAR detector to precisely measure the beam spectrum appears to be a very attractive possibility.

The viability of a large liquid argon detector is presently being demonstrated by the ICARUS collaboration [37] in cosmic-ray tests of a 300-ton module located on the Earth's surface. Currently, a study is in progress to site the LANNDD, 70 KT liquid Argon detector at WIPP [38, 39]. The key issue at this stage is of safety and a proposal to the DOE to study this is in preparation. The LANNDD detector can be used for neutrino physics, as well as the search for proton decay and other astro-particle physics goals. Currently, the ICARUS detector at the Gran Sasso is being constructed with a 3kT detector as a goal. The operation of this detector will provide key information for the eventual construction of LANNDD and for the neutrino physics identified in this paper. A magnetized liquid argon detector would give the maximal discrimination against backgrounds in a neutrino beam, would enhance the ability to perform CP violation experiments, and would permit use of a beam produced by a solenoid focusing scheme [40] that contains both neutrinos and antineutrinos. An R&D experiment is proposed to use a prototype liquid argon detector in a magnetic field to determine the sign of electrons via analysis of their electromagnetic

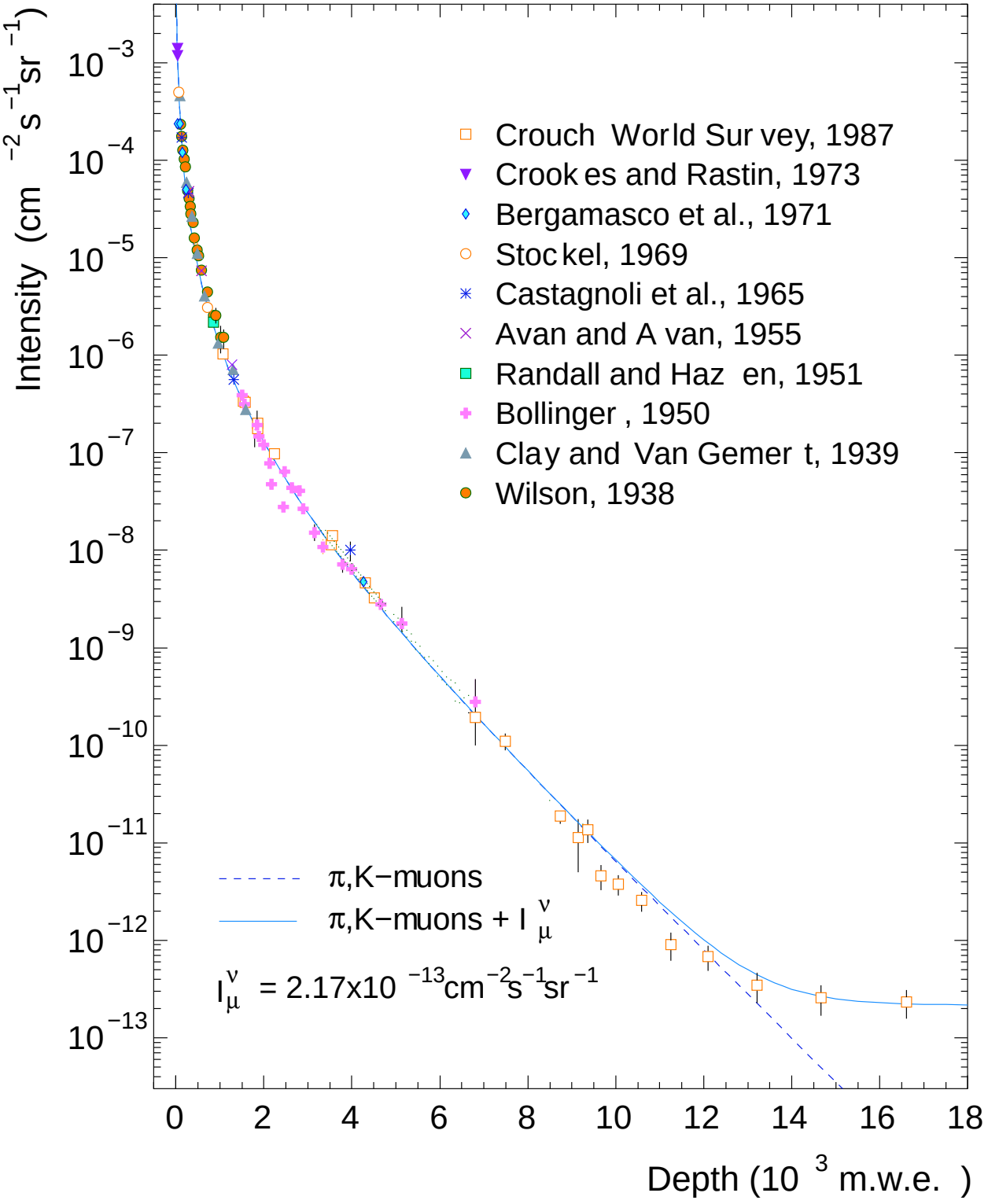

Figure 35: Cosmic ray muon intensity as a function of depth in meters water equivalent (m.w.e) (from ref [25]).

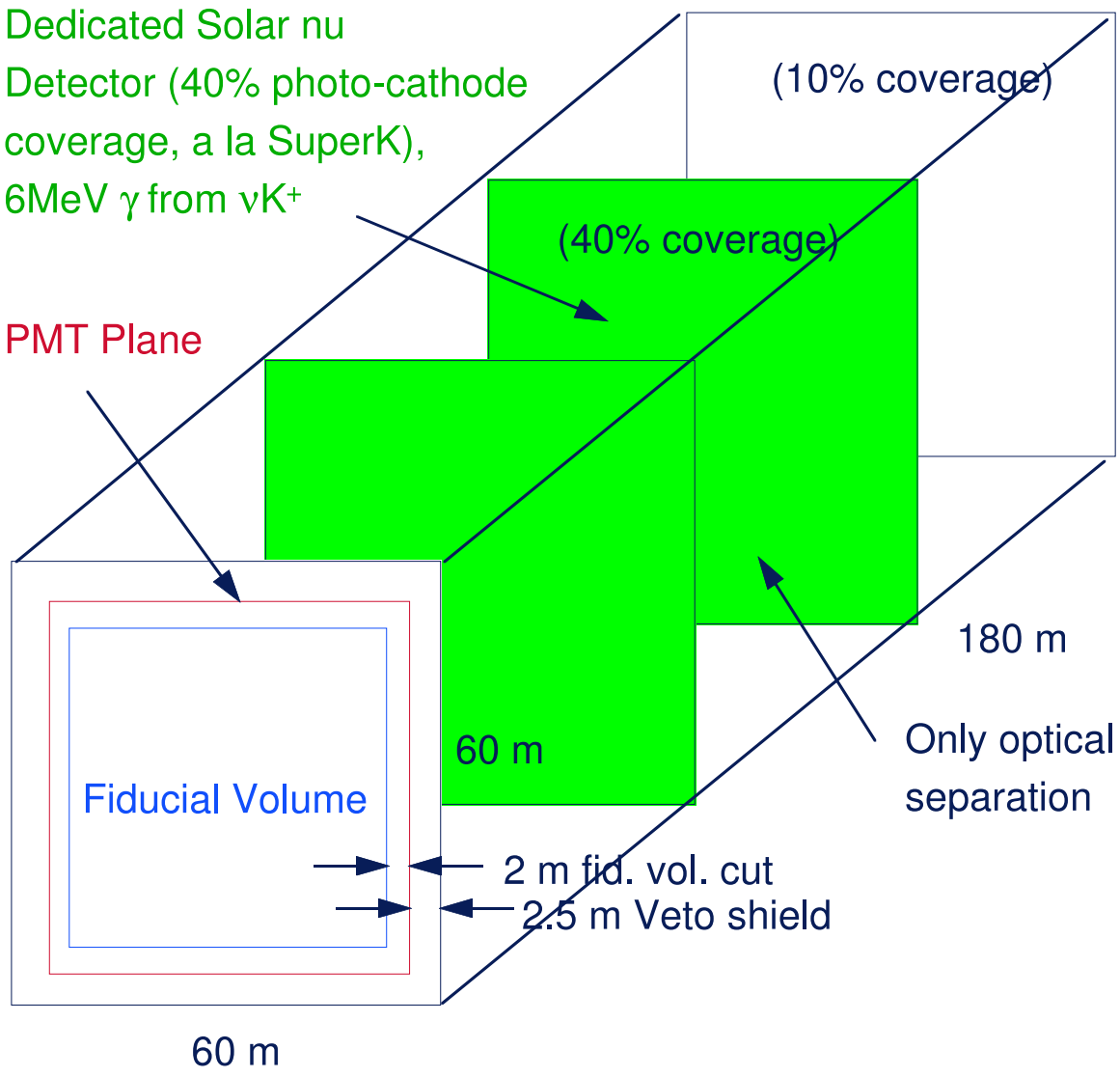

Figure 36: Conceptual design of baseline UNO detector (from ref [26]).

showers up to several GeV [41].

5 AGS Upgrade

The Alternating Gradient Synchrotron (AGS) at BNL is presently the world's highest intensity, multi-GeV proton accelerator and is a natural candidate for the proton driver needed to provide multi-megawatt proton beams (superbeams) for the next generation of neutrino oscillations research program in the U.S. Taking this qualitative fact to the next level, accelerator scientists at BNL have created a credible and effective plan for upgrade of the AGS to the 1 MW proton source needed by the neutrino program advocated in this paper. The increase is a factor of 6 from the present 0.17 MW beam power level. Furthermore, this plan could be time phased to evolve in stages from a 0.4 MW source available in a few years to an ultimate capability of up to 4 MW if such driver power is needed to complete the neutrino research program. At present, we believe a 1 MW source will be adequate for the foreseen program.

Our planned upgrade path would begin with the addition of a 1 GeV superconducting extension to the existing 200 MeV Cu LINAC that currently feeds the Booster ring. The resulting 1.2 GeV hybrid LINAC would bypass the Booster and inject directly into the AGS. The purpose here is to eliminate the need for six complete Booster cycles to fill the AGS and to inject all the needed 1.2 GeV protons in about 0.7 milliseconds. This step increases the average AGS power from 0.17 MW to 0.4 MW, enough to credibly begin the proposed neutrino oscillations program. By next adding new power supplies for the AGS ring, plus added RF power to rapidly accelerate the beam to 28 GeV, the AGS will be operational at the 1 MW power level. Further upgrades could increase the power level to as high as 4 MW if this becomes necessary.

We also note that the technical basis for the proposed upgrade has been documented in a recent study for a muon storage ring, "Feasibility Study-II of a Muon-Based Neutrino Source", June 14, 2001 [24]. Here we present a brief summary of the parameter lists for the required AGS upgrade, along with a summary of the direct costs that were derived in the muon storage ring study. The 1 MW requirements are summarized in Table 2 and a layout of the upgraded AGS is shown in Figure 37.

Table 2: AGS Proton Driver Parameters.

Total beam power	1 MW	Protons per bunch	0.4×10^{13}
Beam energy	28 GeV	Injection turns	230
Average beam current	42 μA	Repetition rate	2.5 Hz
Cycle time	400 ms	Pulse length	0.72 ms
Number of protons per fill	9×10^{13}	Chopping rate	0.75
Number of bunches per fill	24	LINAC average/peak current	20/30 mA

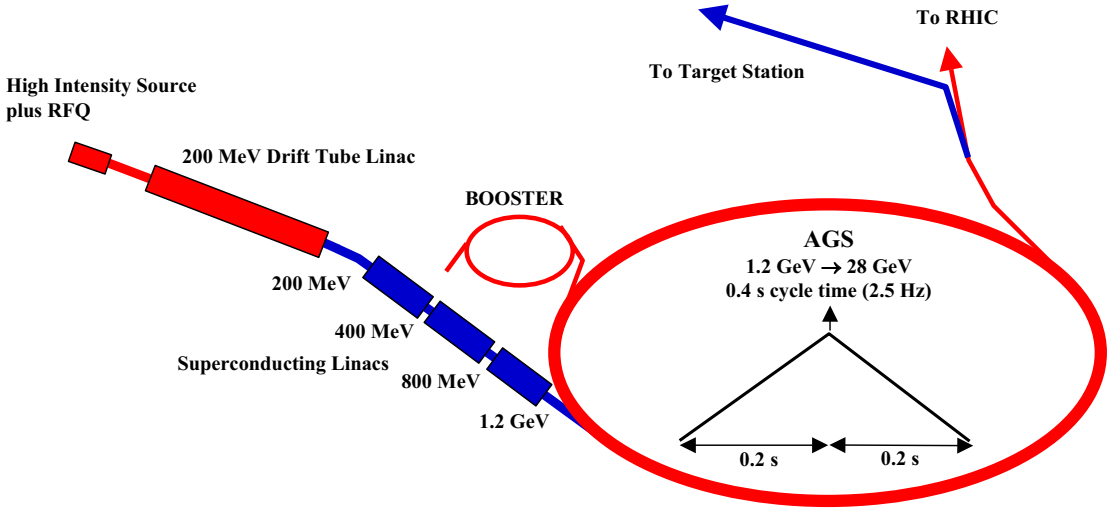

Figure 37: AGS Proton Driver Layout.

5.1 Superconducting LINAC

The superconducting LINAC (SCL) accelerates the proton beam from 200 MeV to 1.2 GeV. The presented configuration follows a similar design described in detail in [27] and [28]. All three LINACs are built up from a sequence of identical periods. The major parameters of the three sections of the SCL are given in Table 3. The low energy section operates at 805 MHz and accelerates proton from 200 to 400 MeV. The following two sections, accelerating to 800 MeV and 1.2 GeV respectively, operate at 1.61 GHz. A higher frequency is desirable for obtaining a larger accelerating gradient with a more compact structure and reduced cost. The SCL will be operated at 2K for the assurance of reaching the desired gradient.

Table 3: General Parameters of the SCL.

LINAC Section	LE	ME	HE
Average Beam Power, kW	7.14	14.0	14.0
Average Beam Current, μA	35.7	35.7	35.7
Initial Kinetic Energy, MeV	200	400	800
Final Kinetic Energy, MeV	400	800	1200
Cell Reference β_0	0.615	0.755	0.887
Frequency, MHz	805	1610	1610
Cells/Cavity	8	8	8
Cavities/Cryo-Module	4	4	4
Cavity Internal Diameter, cm	10	5	5
Total Length, m	37.82	41.40	38.32
Accelerating Gradient, MeV/m	10.8	23.5	23.4
Cavities/Klystron	1	1	1
Norm. rms Emittance, πmm-mrad	2.0	2.0	2.0
Rms Bunch Area, π^oMeV (805 MHz)	0.5	0.5	0.5

5.2 Upgrade to 4 MW

The AGS-based neutrino superbeam can be further upgraded to 4 MW by: 1) increasing the LINAC energy to 1.5 GeV, 2) increasing the AGS intensity to 1.8×10^{14} ppp, and 3) increasing the AGS rep rate to 5.0 Hz. The associated problems in beam dynamics, power supply, RF system, beam losses and radiation protection are under study and appear to be feasible if such a capability is required by the physics experiments.

5.3 Cost of the AGS upgrade

A preliminary cost of upgrading the accelerator complex to 1 MW is shown in Table 4. This upgrade could be done in phases if required by the funding plan. We are still in the process of creating a detailed staging plan.

Table 4: Preliminary direct costs of upgrading the AGS to 1 MW. These costs do not include EDIA, contingency, and overheads.

1.2 GeV Superconducting LINAC	
LE SC LINAC	\$36.1 M
ME SC LINAC	\$25.9 M
HE SC LINAC	\$28.2 M
AGS upgrades	
AGS Power Supply	\$32.0 M
AGS RF upgrade	\$8.6 M
AGS injection channel	\$ 3.7 M
Full turn extraction	\$ 5.5 M
Total	\$140 M

6 Neutrino Beam Design

The geographic location of BNL on one side of the continent allows us to send beams to a variety of distances including very long baselines of 2000 km or more. This is shown in Figure 38. The distances from BNL to Lead, SD (Homestake), and WIPP in NM are 2540 and 2880 km, respectively. The respective dip angles are 11.5, and 13.0 degrees. The difficulty of building the beam and the cost increases with the dip angle but all these angles and distances are feasible.

Our conceptual design for a beam to Homestake is shown in Figures 39 and 40. It can be adapted to any far location in the Western direction. Our design addresses a number of issues. At BNL we are constrained to keep the beam line above the water table which is at a shallow depth ($\sim$ 10 m) on Long Island. Therefore the beam has to be constructed on a hill that is built with the appropriate 11.5 degree slope. Fortunately, it is relatively easy, and inexpensive to build such hills on Long Island because of the flat, sandy geology. It is important to keep the height of the hill low so that the costs are not dominated by its construction. The proton beam must be elevated to a target station on top of the hill. The cost of the hill can be lowered by bending the proton beam upwards as quickly as possible. We have, however, chosen the design and the bend angle used for the RHIC injection lines in our proposal because the RHIC injection lines have well known costs.

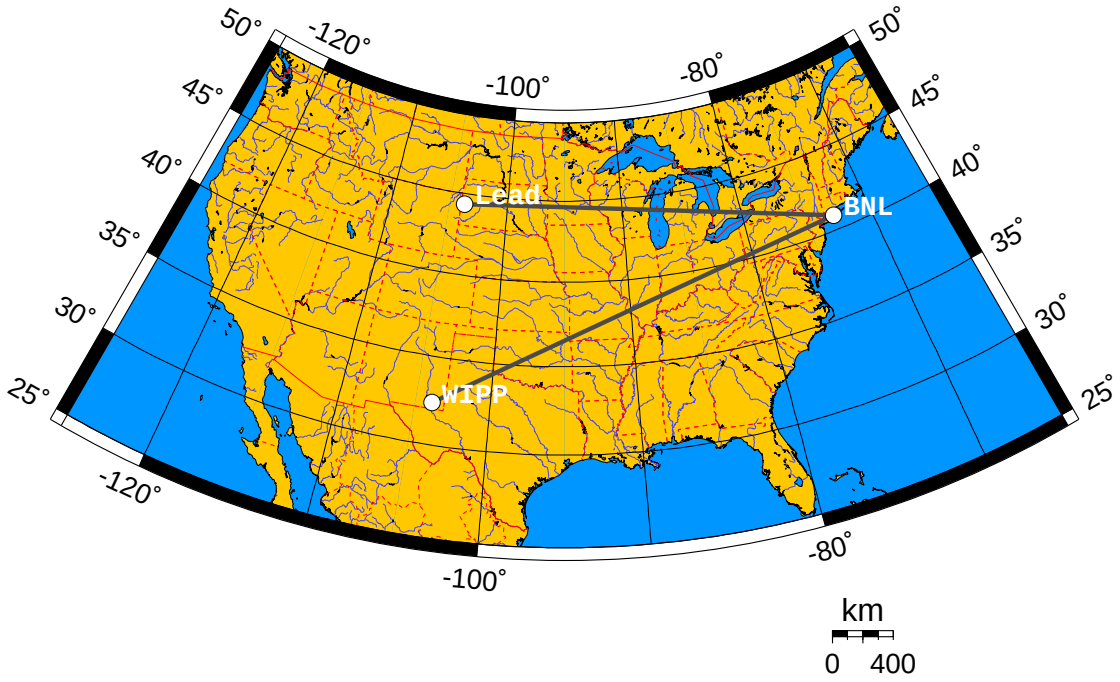

Figure 38: Possibilities for very long baselines from BNL. The distances from BNL to Lead (Homestake), and WIPP are 2540, and 2880 km, respectively.

The proposed fast-extracted proton beam line in the U-line tunnel will be a spur off the line feeding RHIC. It will turn almost due west, a few hundred meters before the horn-target building. In addition to its 90 degree bend, the extracted proton beam will be bent upward through 13.76 degrees and then down by 15 degrees to strike the proton target. The downward 11.30 degree angle of the 200 meter meson decay region will then be aimed at the 4850 feet level of the Homestake laboratory. This will require the construction of a 54 meter hill to support the target-horn building, so as to avoid any penetration of the water table. At its midpoint (about Lake Michigan) the center of the neutrino beam will be roughly 120 km below the Earth's surface.

6.1 Optimization of the wide band spectrum

For this report we have attempted to optimize the beam for the Homestake distance (2540 km). However, our optimization process could be applied to any distance. As already explained, the ideal beam for Homestake will be a broadband beam that covers ∼0.5 GeV to ∼7.0 GeV range. The $\nu_\mu \rightarrow \nu_e$ process through Δm^2_{21} (solar oscillations) will generate

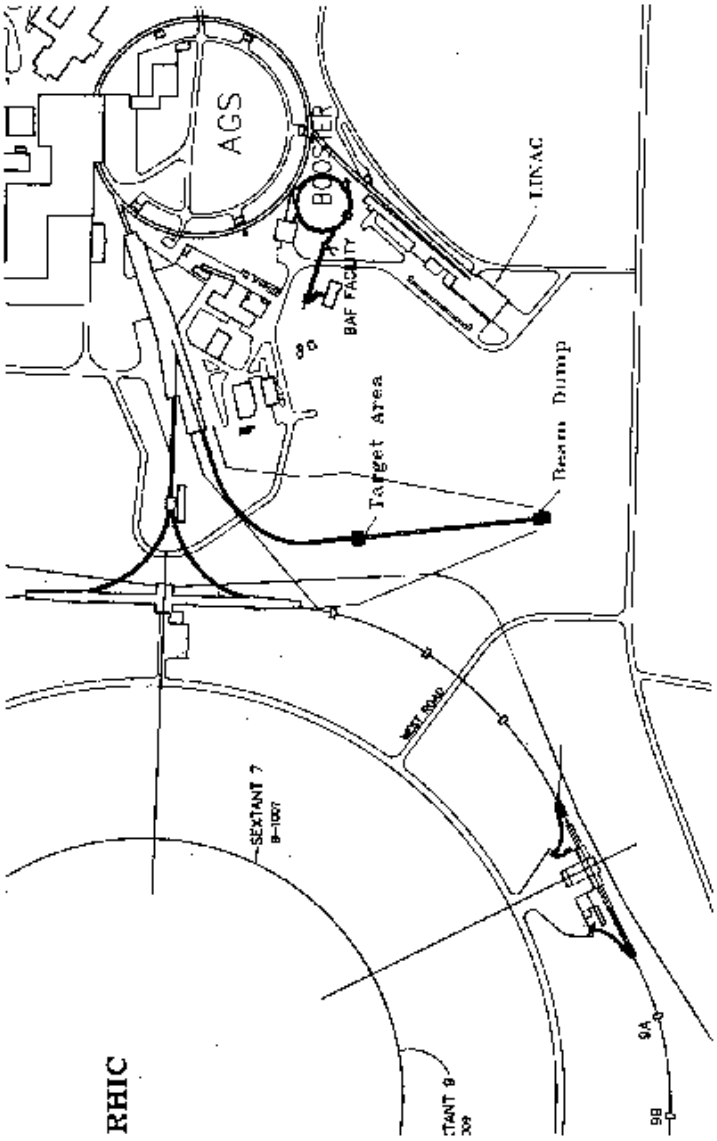

Figure 39: The beam line for sending a neutrino beam to Homestake mine, South Dakota. This same beam line can be adapted for any far location in the Western direction.

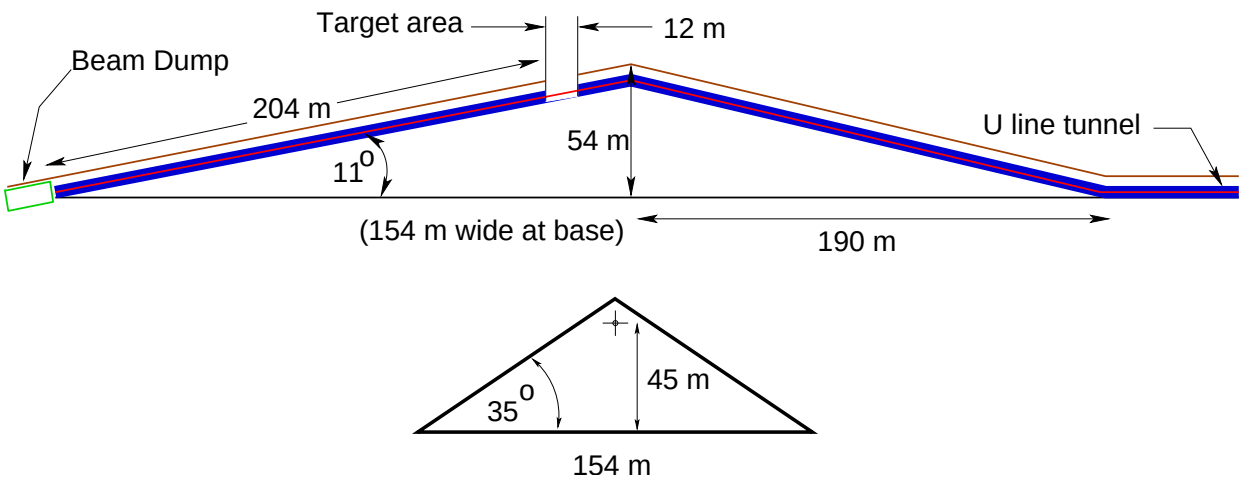

Figure 40: Elevation view of the neutrino beam line to Homestake, South Dakota. For a nearer location a much smaller hill can be constructed. In this beam we assume a decay tunnel length of 200 m. For a shorter tunnel the cost of the hill will reduce as shown in Table 5.

a sizable effects at the lowest energies. The energy range $1-3$ GeV will be important for the detection of CP violation. The energy region $3-5$ GeV contains the first matter enhanced (for neutrinos with regular mass hierarchy) $\nu_\mu \to \nu_e$ oscillation maximum. Recall that the highest energies are important for establishing the existence of $\nu_\mu \to \nu_e$ signature because this region is free from the neutral current π^0 background and should have very good efficiency for the signal. Lastly, the energy region $6-7$ GeV is important for the ν_μ disappearance measurement.

To obtain a broad band neutrino spectrum we have adapted the standard scheme of multiple parabolic horns, each one focuses a different pion momentum region. The difficulty with this approach is that the lowest energy pions we need to capture and focus are approximately 1-2 GeV and come from a long target. Figures 41 and 43 shows the design of the target and horn geometry for a conventional wide band neutrino beam, similar to that used in previous experiments at BNL, such as E734. The E734 design used a water cooled 1.5 interaction length copper target. The calculated energy distributions of a ν_μ beam produced by 28 GeV protons is shown in Figure 42 [21]. The 0° calculation has been shown consistent with neutrino beam data [29]. A copper target will not survive the 1 MW intensity proton beam that we propose. Therefore, both new materials and new focusing geometries must be considered.

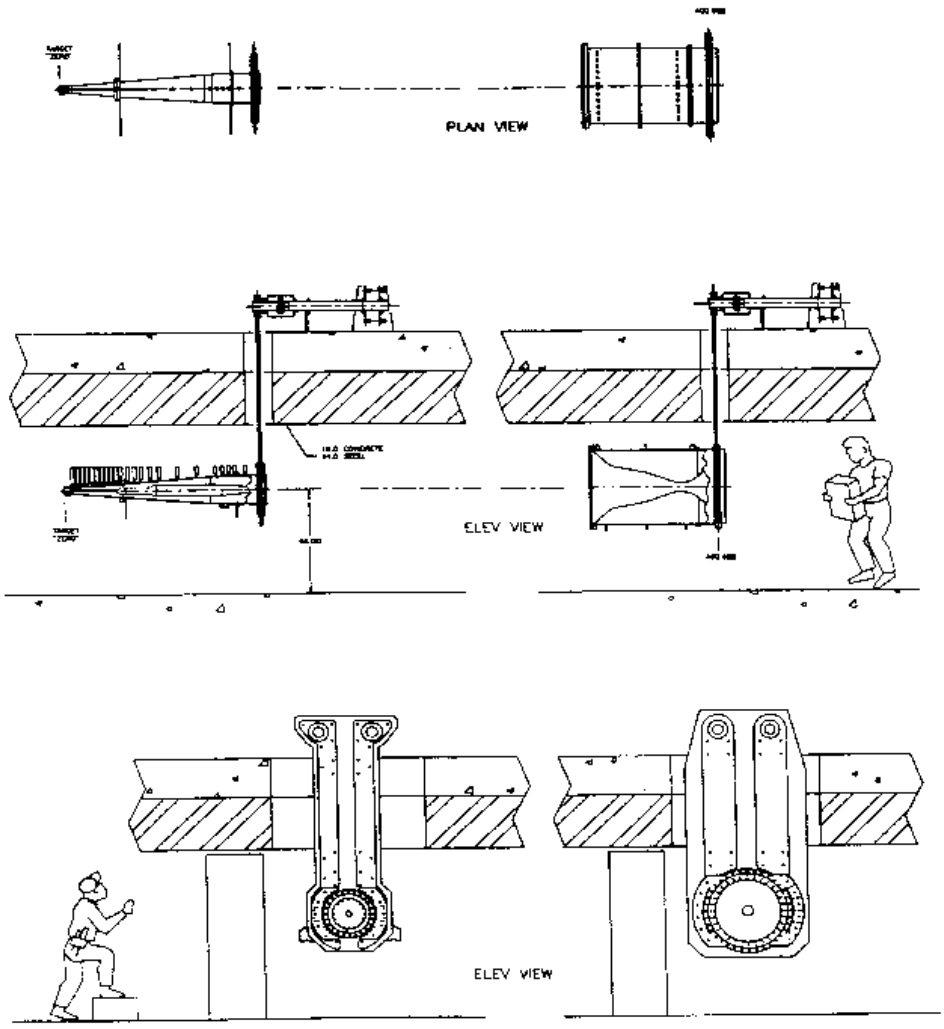

Figure 41: The design of the horn focusing system used for the E734 experiment adapted from the E889 proposal.

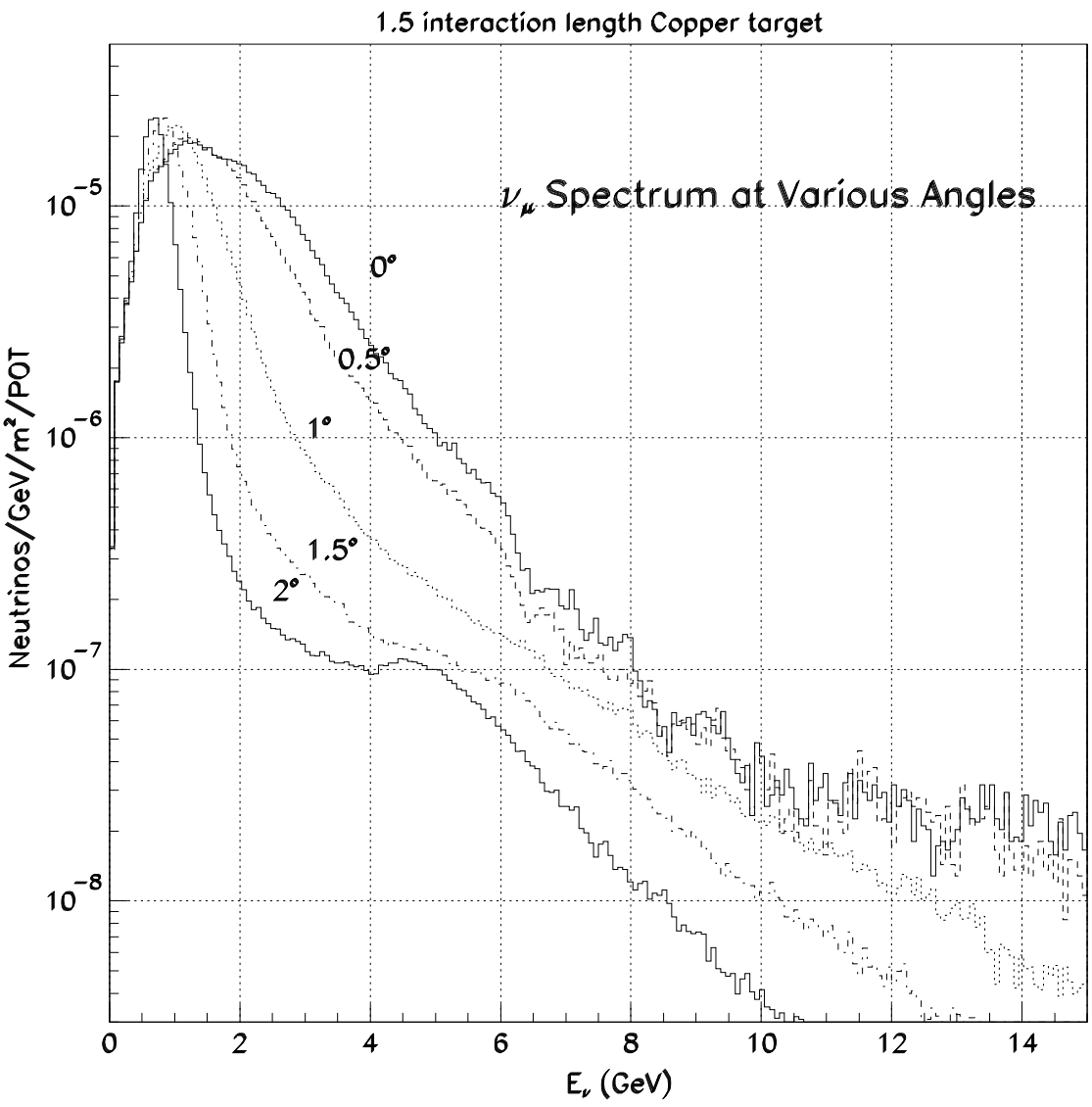

Figure 42: Wide band horn focussed neutrino spectrum for 28 GeV protons on a copper target. The spectrum is approximately the same if Super-Invar is used as target material. Spectra of neutrinos are calculated at various angles with respect to the 200 m decay tunnel axis at the AGS and at a distance of 1 km from the target.

We discuss the target in much more detail in a later section. The two main issues in the target design are the target material and the space available for cooling. If a dense material, such as Super-Invar, is used then the spectrum will be approximately the same as shown in Figure 42. A better approach is to use graphite as the target material and modify the horn geometry to allow for a longer target (Figure 43). The result of these modifications is shown in Figure 44. The electron neutrino contamination is shown on the same scale in Figure 45. We have used a 1.5 interaction length graphite target. As shown in the figures, the flux resulting from a graphite target is considerably higher in the 3.5 to 8 GeV region. There is no significant change in the ratio of electron type neutrinos to muon type neutrinos between a graphite and a copper target. We have used the neutrino flux from Figures 44 and 45 for the calculation of event rates and backgrounds in the rest of this report.

There is a large ($\sim$ 50%) model dependent uncertainty on the neutrino flux at high energies ($>$ 4 GeV). In particular the hadron production model in MARS gives lower flux than in GEANT [30]. This uncertainty will most likely be resolved by new experiments [31, 32] in the near future.

Further work on the optimization of this spectrum for the very long baseline experiment is ongoing. Further optimization focuses on enlarging the horns to accept more lower energy pions so that the flux near 0.5 GeV can be enhanced, using an evacuated or helium filled decay tunnel, and as using the hadron hose [33] to capture more higher energy particles.

6.2 Target Station

To use the 1 MW proton driver proposed for BNL, serious consideration must be given to the target selection. It is desirable to choose a solid target for generating a high intensity neutrino beam. For pion production with high power proton beams, target integrity becomes an important issue. Up to now, the production of secondary particles has been limited to proton beams with average beam power on the order of 100 to 200 kW. We now have to consider a target which can survive a 1 MW (or greater) average proton beam power. For a 28 GeV proton beam, 1 MW beam power implies 2.23×10^{14} proton/sec. For a rep-rate of 2.5 Hz we then must consider nearly 100 TP per spill. A number of options have been considered and investigated both in terms of the material selection as well as the feasibility of target configuration. In evaluating the target choices the following concerns are being addressed:

- Heat removal from the target.

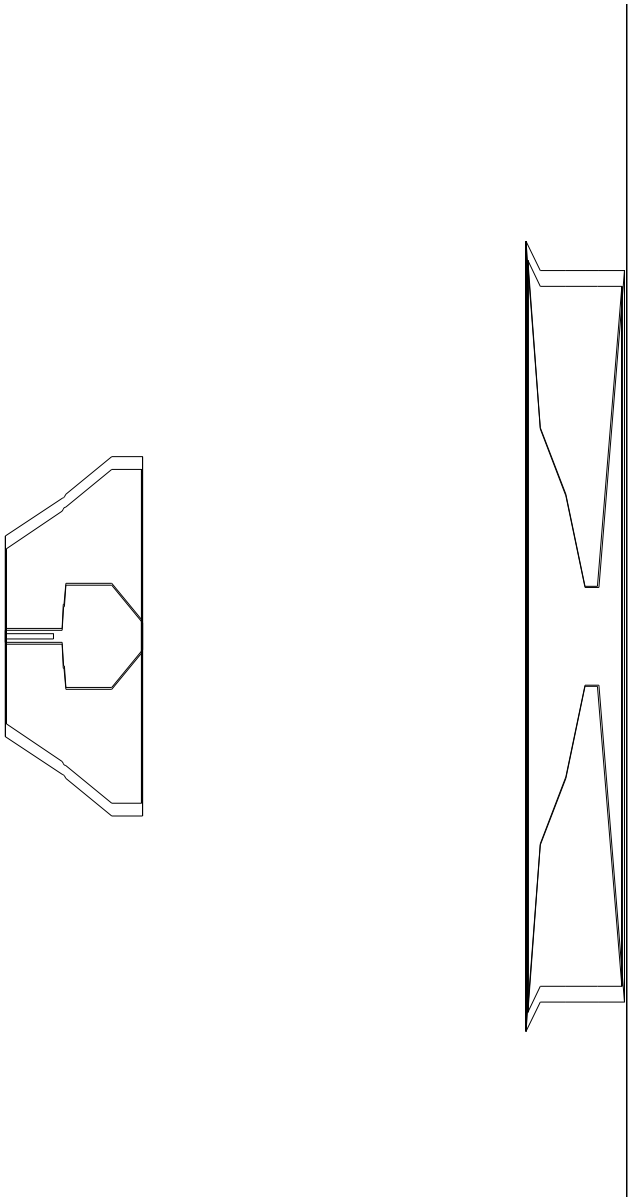

Figure 43: The horn geometry in the GEANT simulation. The vertical and horizontal scales are in the ratio of 1 to 13. The beam is incident from the left.

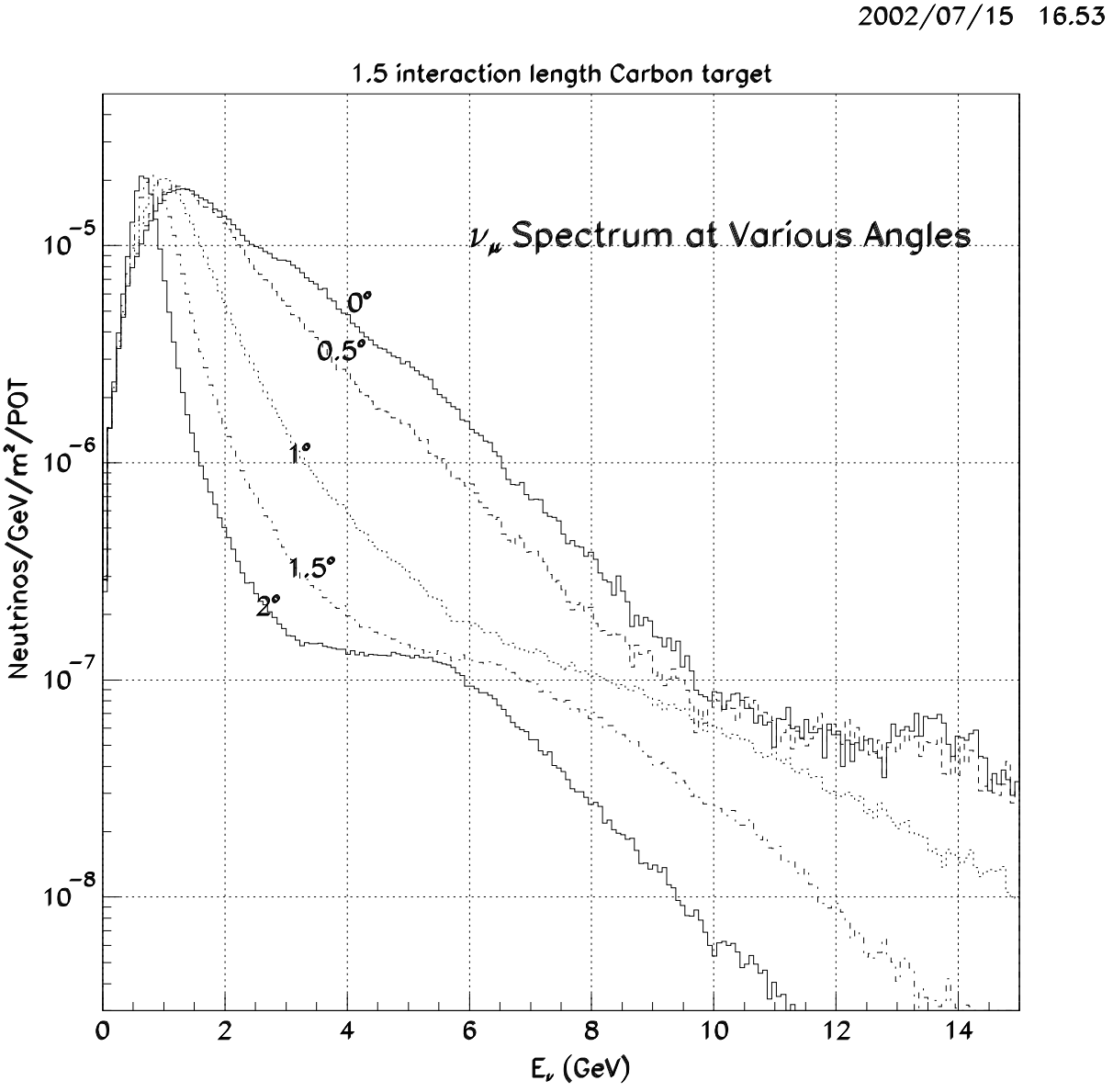

Figure 44: Wide band horn focussed muon neutrino spectrum for 28 GeV protons on a graphite target. The spectra of neutrinos are calculated at various angles with respect to the 200 m decay tunnel axis and at a distance of 1 km from the target.

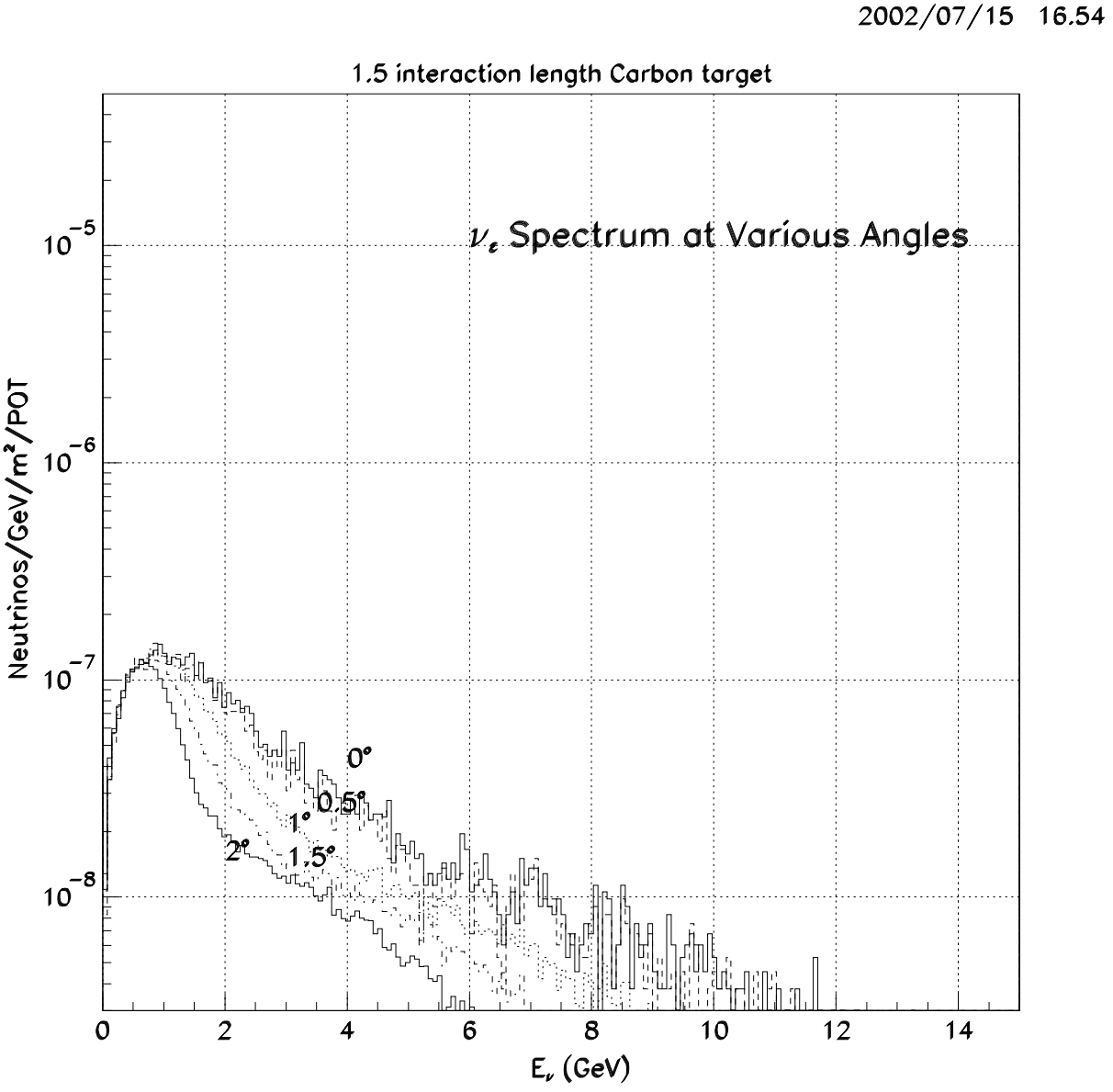

Figure 45: Wide band horn focussed electron neutrino spectrum for 28 GeV protons on a graphite target. Spectra of ν_e are calculated at various angles with respect to the 200 m decay tunnel axis and at a distance of 1 km from the target.

- Survivability of the target intercepting energetic, high intensity proton bunches.
- Irradiation issues
- Engineering integration issues
- Heat generation and removal from the horn
- Horn mechanical response

Findings of a number of recent studies [24], including experimental results from AGS Experiment E951 [34], on target issues for the muon collider/neutrino factory project are taken into consideration in this effort.

Figures 47 and 48 show the spectra of π^+ and π^- that are produced from a 2-interaction length target for various materials. For a conventional neutrino beam, the useful part of the pion spectrum is in the energy region above 2 GeV. For this reason, high-Z targets are no longer advantageous and low-Z targets are preferred.

In addition to maximizing the flux, the target/horn configuration must survive the thermal shock induced by the beam and the high current. Specifically, the target scheme must (a) ensure the removal of the deposited beam energy within the 400 ms period and (b) survive the thermally induced elastodynamic stresses that are expected to be comparable to the mechanical strength of most common materials. Similar concerns are valid for the horn, itself, which will be subjected to rapid heating and, as a result, high levels of thermal stress that will propagate in its volume. In order to satisfy the first requirement, several cooling scenarios are being investigated such as edge-cooling, forced helium cooling in the space between the target and the horn, and radiation cooling. All of these schemes present challenges stemming from integration with the horn in a limited space. To satisfy the second requirement, materials must be selected such that they can withstand and attenuate the thermal shock and be radiation resistant. To address this, low-Z carbon based materials such as graphite and carbon-carbon composites are being considered. These materials, while they have a lot of promise, present some challenges. Figure 46 shows the target mounted in the first horn. Also the helium cooling system for the target and the water cooling manifold for the horn are shown.

Two different forms of carbon, ATJ graphite and a carbon-carbon composite are considered as candidate target materials. These two types have been exposed to the AGS beam in the E951 experiment[34]. The carbon-carbon composite is a 3-D woven material that exhibits extremely low thermal expansion below 1000^oC and responds like graphite above that.

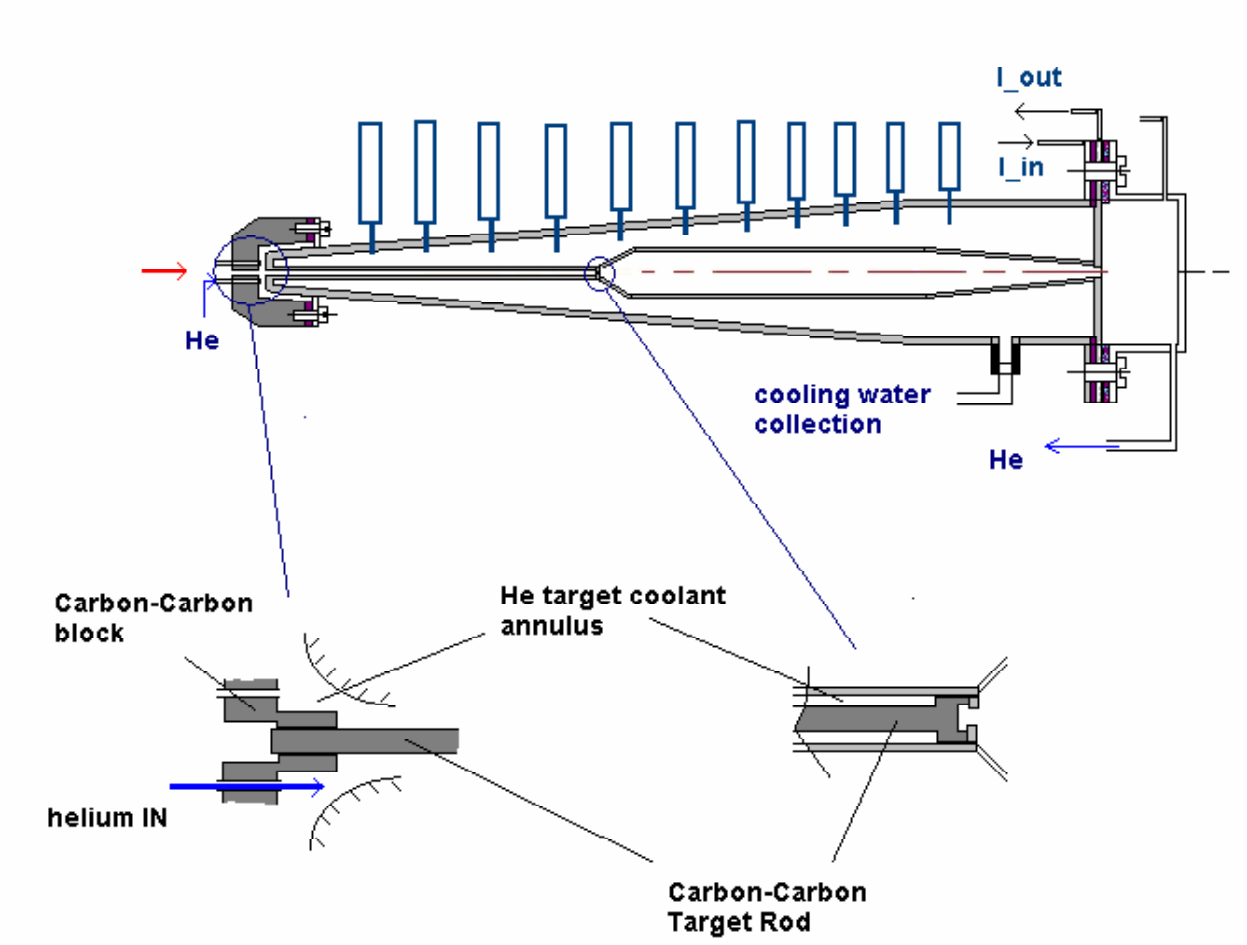

Figure 46: Sketch of the first horn with the graphite target mounted. The target is cooled by helium. The horn is cooled by spraying water on the conducting surface.

Preliminary studies on the feasibility of using carbon-based targets for this neutrino beam have been conducted. Specifically, utilizing the energy deposition estimates from MARS for 1 mm and 2 mm RMS beam spots (corresponding to 3 mm and 6 mm radii of target), the thermal shock response and the survivability potential of the target were studied. The total energy deposited on the target (and which needs to be removed between pulses) is 5.1 kJ for the 1mm spot and 7.3 kJ for the 2mm spot.

Since the 1 mm RMS beam spot is the most serious case, it is examined in detail. For the 100 TP beam the peak energy density is of the order of 720 J/gram. This is expected to lead to instantaneous temperature increases of $\sim$ 1000°C. A detailed finite-element analysis that involves both the horn and the target needs to be performed so the heat removal of the system can be optimized and, most importantly, so the thermal shock stresses can be computed. A material with a small thermal expansion should experience smaller thermal stresses. However, carbon-carbon composite materials exhibit an increasing thermal expansion at higher temperatures. This behavior of the material needs to be examined further. If the high temperature performance of this material is not satisfactory, a larger beam spot size could be used. From energy density considerations, a 2 mm rms beam spot would have a peak temperature rise per pulse that is less than a third of the 1 mm rms case. This would ensure that the material will be well within the safe zone. Cooling of the front-end is achieved by maintaining the temperature at the surface of the first 4 cm to 27^{o}C.

We examine the optimal geometry for high-energy pion production utilizing a carbon target. In Figure 49 we see the result of varying the radius of a 1.5 interaction length (60 cm) long carbon target as we varied the proton beam radius. For this analysis the target radius was constrained to 3 times the proton beam rms radius. We note that although the total secondary pion production increases with radius, the desired high-energy portion of the production spectra is enhanced with smaller beam spot sizes. In Figure 50 we fix the beam/target radius at (2mm/6mm) and find that the production of 7-9 GeV pions increases with target length up to about 80 cm (2 interaction lengths) and then remains essentially constant up to 2 m.

We now explore the impact of bringing 100 TP protons/spill onto a carbon target. For this analysis we utilize MARS to calculate the energy deposition due to the hadronic showering within the target. We examine the two cases of 3 mm and 6 mm radius targets in Figure 51. We note the peak energy deposition density occurs near the entrance of the target and has the respective values of 700 and 200 J/g. As a figure of merit, 300 J/g is considered the danger regime where metal targets suffer damage due to the propagation of thermal

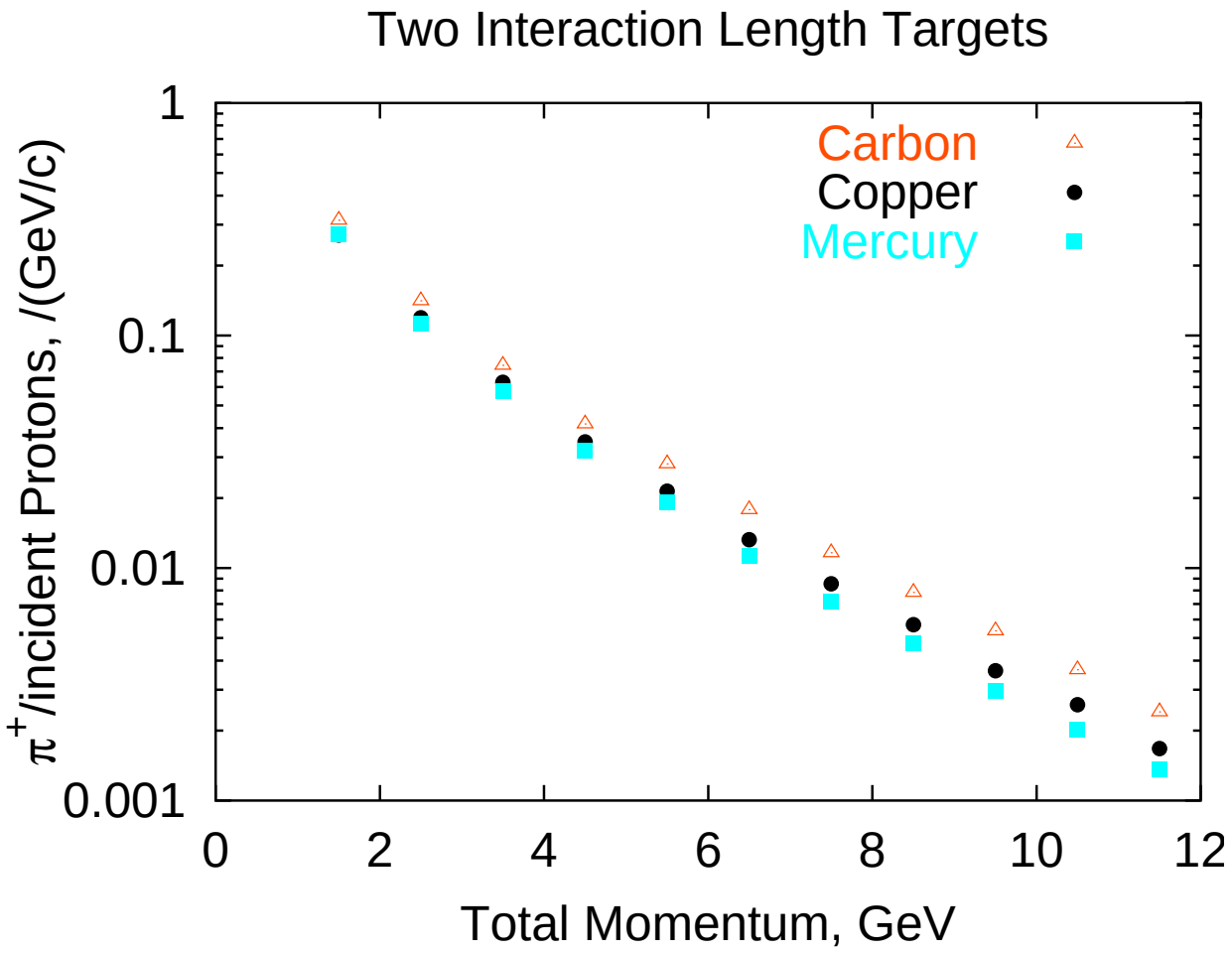

Figure 47: The number of π^+ per incident proton is shown as a function of its momentum for carbon, copper and mercury targets. The target is two interactions lengths long for each material.

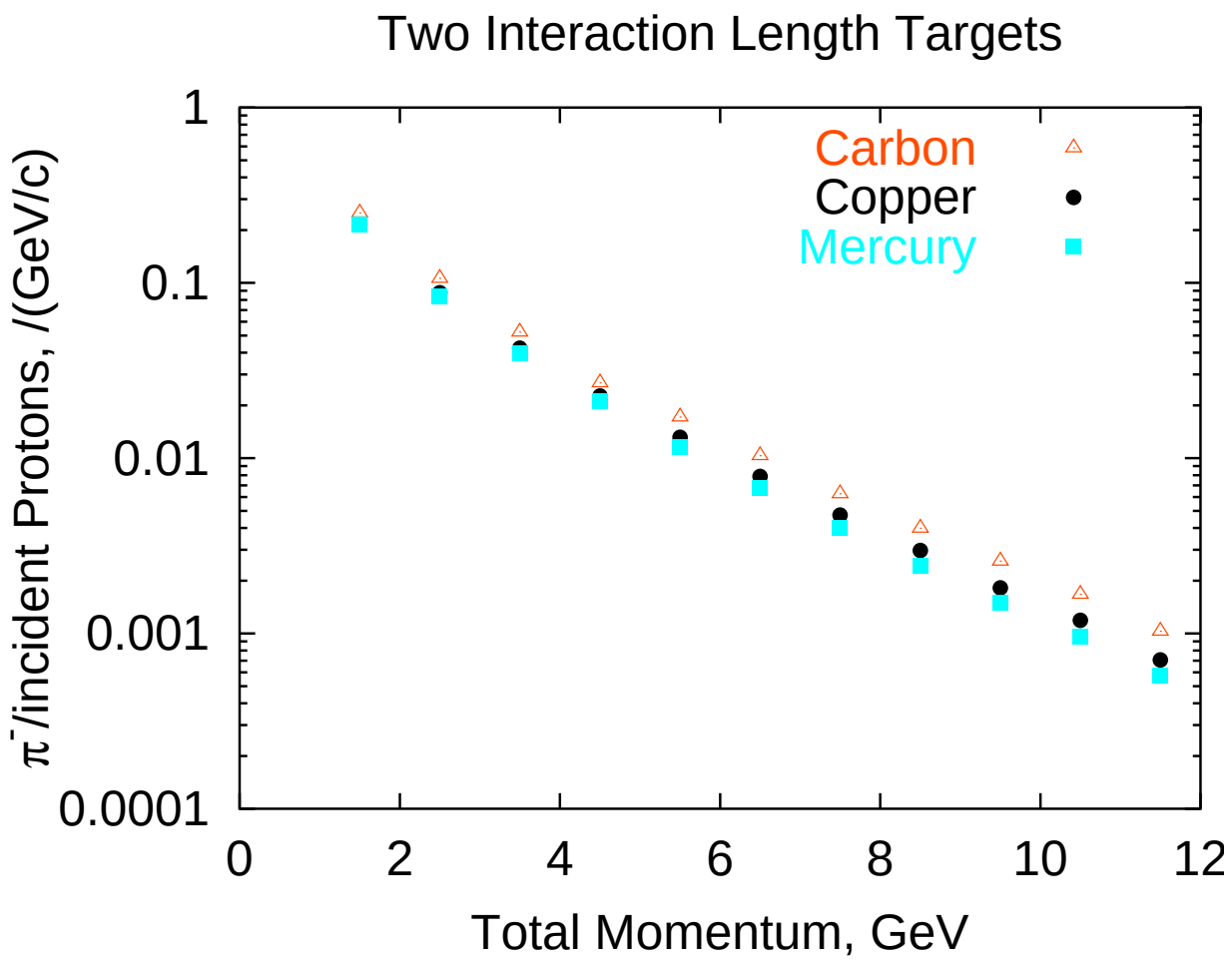

Figure 48: The number of π^- per incident proton is shown as a function of its momentum for carbon, copper and mercury targets. The target is two interactions lengths long for each material.

generated pressure waves through the material. There is, however, evidence that carbon can withstand energy depositions in this regime. The best evidence to date comes from experience in the NUMI target development program. The NUMI carbon target is designed to expect 390 J/g peak energy deposition. A NUMI target test, performed in 1999, utilized a specially focussed beam to produce energy depositions in the range of 400 to 1100 J/g without any external evidence of target breakup.

The secondary particle shower resulting from the interaction of primary protons with the low-Z target will add to the transient heat load of the horn. This shower will be less significant for low-Z targets than for high-Z targets. However, its effect will be examined, and added to the electric resistance heat load estimated above.

There will be activation of the target and horn structure due to secondary and primary particles. This activation will be primarily due to spallation products and neutrons generated in the secondary shower. The survival of the primary target in the radiation field needs to be examined. This can only be carried out experimentally using a prototypic proton beam on samples of the appropriate target material. The change in physical properties including, thermal expansion coefficient, elastic modulus, and yield strength, need to be examined as a function of proton fluence.

In the current option the target is an 80-cm long cylindrical rod with 12 mm diameter sizes. The 12 mm diameter target is chosen to intercept 100 TP, 2 mm rms proton beam. With this beam size, the total energy deposited as heat in the target is 7.3 kJ with peak temperature rise of about 280°C. Heat will be removed from the target through forced convection of helium through the outside surface. This is a good solution for the 1 MW beam power.

6.3 Cost of the neutrino beam

A preliminary estimate of the direct costs without burdens is shown in Table 5. The costs are based on the the RHIC injector work, as well as the E889 proposal and the neutrino factory study. The conventional construction costs are dominated by the size of the hill which is approximately proportional to the third power of the decay tunnel length. In our cost estimate we assume that we will bury the beam dump underground to reduce the height of the hill. It is assumed that the target station shielding can be retrieved from existing resources. We have also estimated the cost assuming a 200 m long decay tunnel. The spectra shown in Figure 42 are based on this 200 m tunnel filled with air.

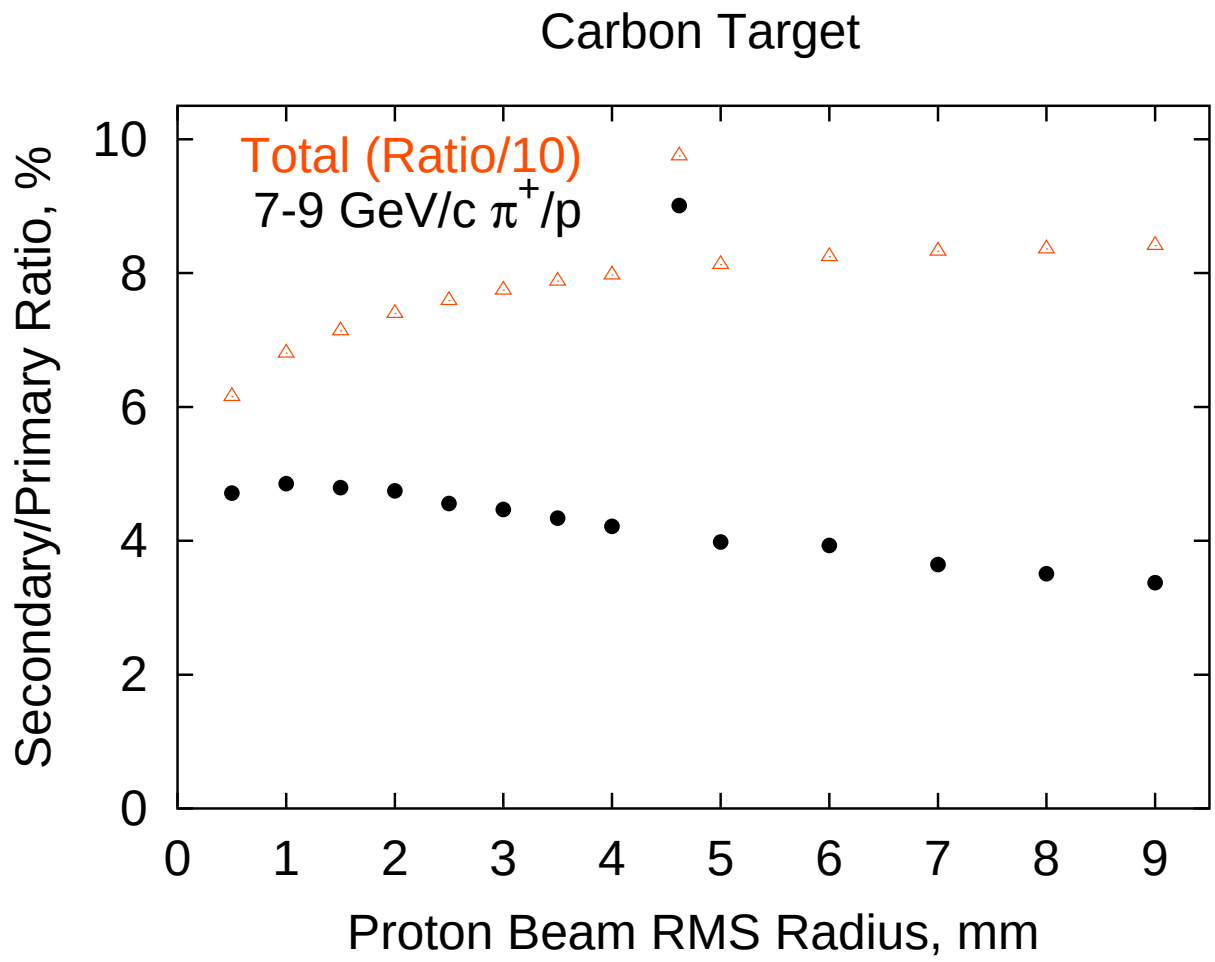

Figure 49: The ratio of the numbers secondaries to the number of primaries is shown as a function of RMS beam radius. The target radius is assumed to be three times the RMS beam radius and the target length is 1.5 interaction lengths.

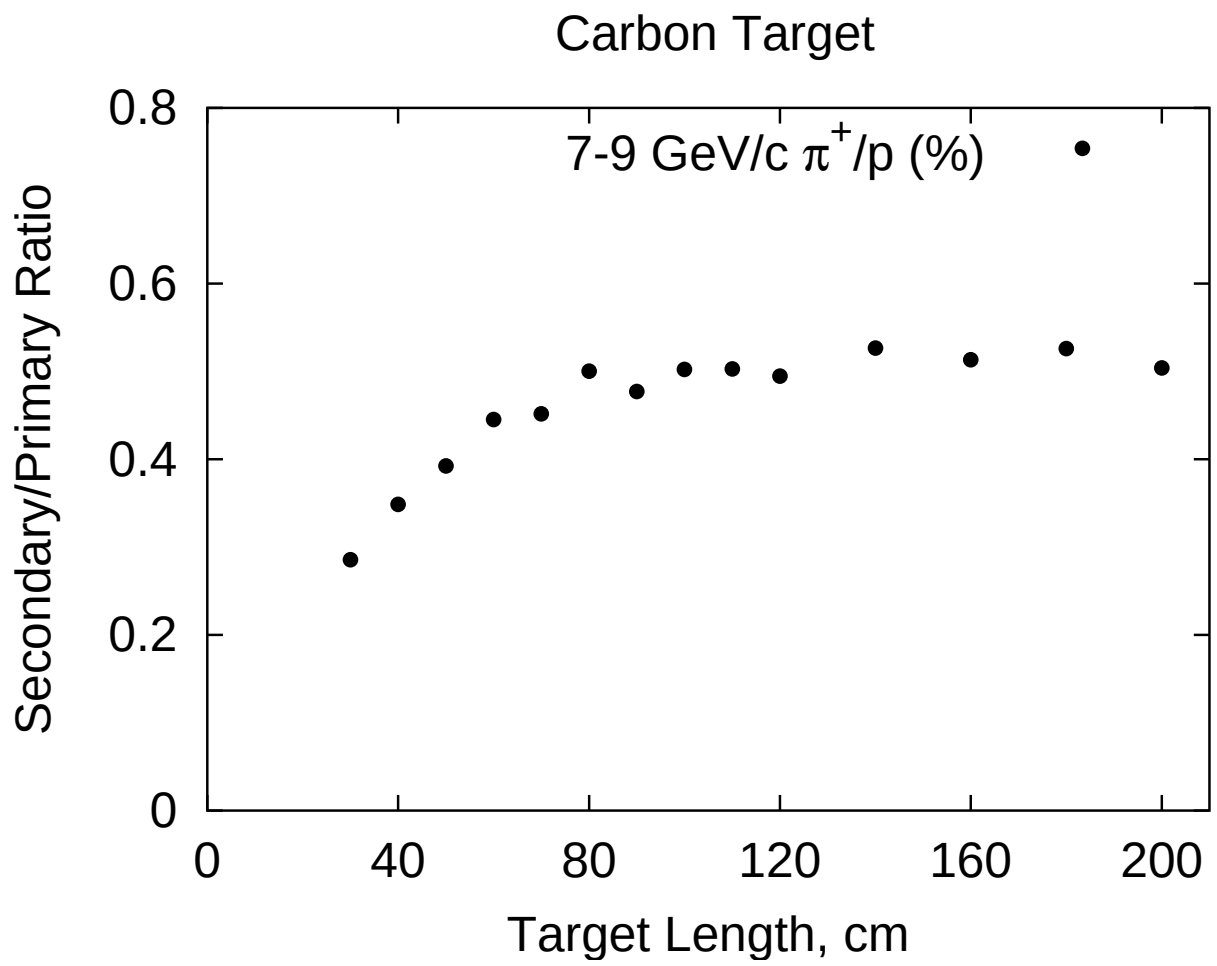

Figure 50: The ratio of the number of secondaries to the number of primaries is shown as a function of the target length for a target radius of 6 mm and a RMS beam size of 2 mm.

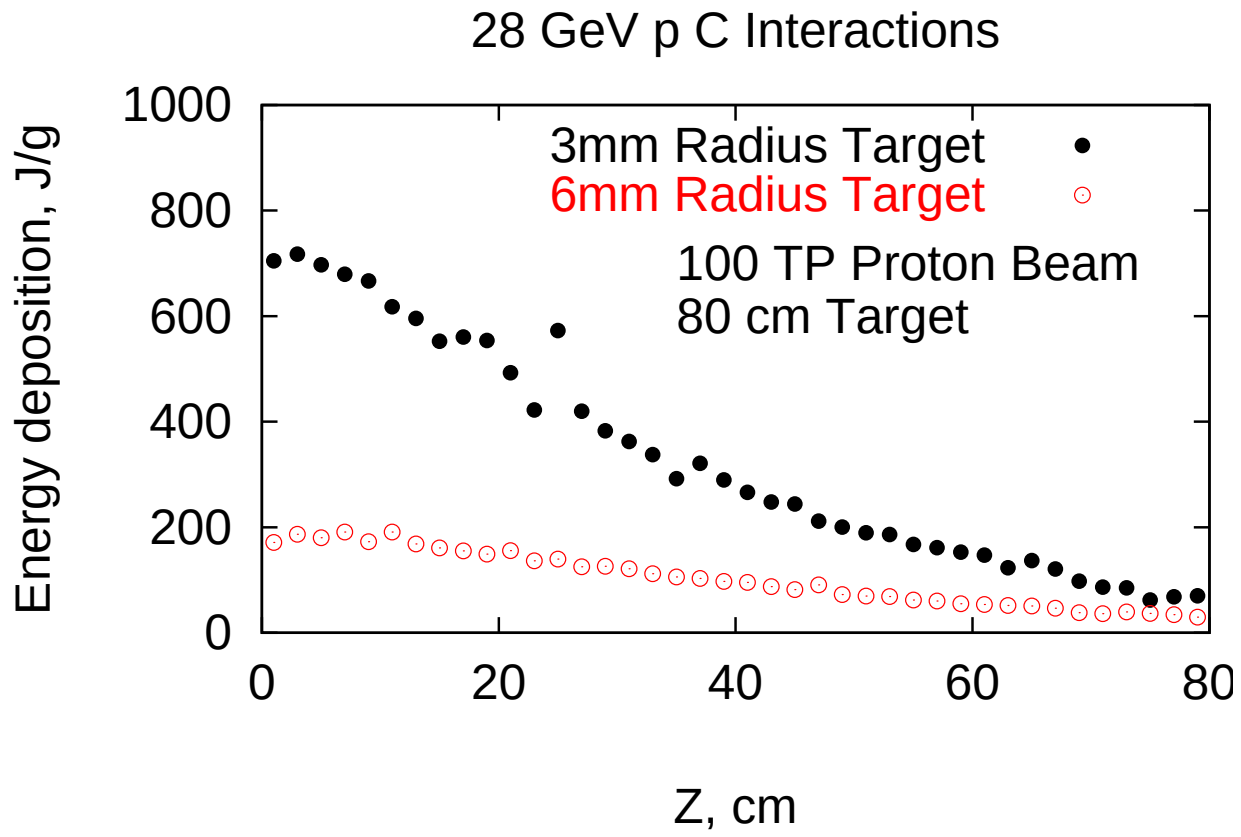

Figure 51: The energy deposition is shown as a function of target axial position for a 28 GeV 100 TP beam.

Table 5: Preliminary direct cost (FY02$M) of building the neutrino beam with 200 meter decay tunnel. These costs do not include EDIA contingency, and overhead.

Item	basis	cost
Proton transport	RHIC injector	$11.8 M
Target/horn	E889	$3 M
Installation/Beam Dump	New	$2.6 M
Decay Tunnel	E889	$0.4 M
Conventional const. (hill)	New	$8 M
Conventional const. (other)	E889	$9 M
Total		$35 M

7 Conclusion

The possibility of making a low cost, very intense high energy proton source at the Brookhaven Alternating Gradient Synchrotron (AGS) along with the forthcoming new large underground detectors at either the National Underground Science and Engineering Laboratory (NUSEL) in Homestake, South Dakota or at the Waste Isolation Pilot Plant (WIPP) in Carlsbad, New Mexico, allows us to propose a program of experiments that will address fundamental aspects of neutrino oscillations and CP-invariance violation. This program of experiments is unique because of the very long baseline of more than 2500 km from Brookhaven National Laboratory to the underground laboratories in the West, the high intensity of the proposed conventional neutrino beam, and the possibility of constructing a very large array of water Cherenkov detectors with total mass approaching 1 megaton. This report examined the design and construction of the necessary AGS upgrades and the new neutrino beam which will have a proton beam of power ∼1.0 MW. We have examined the potential physics reach of such an experiment. We used the running scenario of a 1 MW AGS, 500 kT of fiducial detector mass, and 5×10^7 secs of running time. With these conditions, we conclude that such an experiment is capable of precisely measuring Δm^2_{32} and $\sin^2 2\theta_{23}$; it has excellent sensitivity to $\sin^2 2\theta_{13}$ with a signal spectrum that is very distinctive. Moreover, if $\sin^2 2\theta_{13}$ is sufficiently large (> 0.01) the experiment is sensitive to the CP-violation parameter δ_{CP} with only neutrino running. With the additional option of running in anti-neutrino mode, the experiment will be able to distinguish between the cases $\Delta m^2_{31} > 0$ versus $\Delta m^2_{31} < 0$ using distinctive distortions to the observed electron or positron spectrum. Lastly, the very

long baseline will allow the measurement of Δm^2_{21} with approximately the same resolution as KAMLAND but in the $\nu_\mu \rightarrow \nu_e$ appearance channel if the LMA solution is correct for the solar neutrino deficit.

The AGS complex is unique because it can be upgraded simply by increasing the repetition rate of the machine. This ability allows us the flexibility to continuously upgrade the facility to as much as 4.0 MW [35]. In this proposal we have examined upgrades up to 1.0 MW. The direct costs of such an upgrade are estimated to be approximately \$140M. This compares well with the estimated costs for the detectors and the neutrino beam-line. Neither the duration of the construction period nor the anticipated cost of the improvements to the BNL AGS complex is large in relation to plans and expenditures now usual for major apparatus in high energy and elementary particle physics. Moreover, the improvements to the AGS and the new beam line will be available for carefully chosen other physics (for example, rare muon and kaon decays as well as muon EDM measurements)[51, 52], while advancing our understanding of the neutrino section.

8 Appendix I Working Group Charge and Assignments

Director's Office

Building 510F
P.O. Box 5000
Upton, NY 11973-5000
Phone 631 344-5414
Fax 631 344-5820
tkirk@bnl.gov

date: December 1, 2001

to: S. Aronson, M. Harrison, D. Lowenstein,
R. Palmer, V. Radeka W. Marciano, M. Diwan and W.T. Weng

from: T. Kirk
Associate Laboratory Director,

HENP subject: Neutrino R&D Working Group Charge and Assignments

Attached, please find the Charge to the Neutrino R&D Working Group that we have discussed. As agreed, Bill Marciano will be the Neutrino Team Leader, Milind Diwan will be the Physics Goals and Detector Team Leader and Bill Weng will be the Accelerator and Beam Systems Team Leader. The recruitment of working participants on the teams will be the responsibility of the team leaders, aided by the department heads and myself. The composition of the R&D teams will not be limited to BNL employees. In fact, the participation of outside physicists in the study will have obvious benefits for the next stage of the work which is expected to be the establishment of a formal collaboration and the creation of a formal proposal to the funding agency or agencies to build and operate a neutrino beam and detector system and carry out an experimental neutrino physics program. If the work gets off to a promising start and the physics prospects appear to be

sufficiently compelling, it is possible that the initiation of the collaboration and the start of a related proposal may overlap the R&D study in time. Such an outcome could also have benefits for the timely advance of neutrino physics.

We are initiating neutrino R&D work without explicit funding for this purpose. Accordingly, the R&D work should be regarded as part of the participants research activity, work that is generally supported by the Laboratory research mission in high energy and nuclear physics. I expect that the department heads will help and support the teams to carry out the work within their capabilities. This has already been discussed and agreed to. If conflicts arise about the allocation of internal resources and priorities between the needs of the R&D study and other activities of the departments that cannot be settled between the team leaders and the department heads, I will establish a forum for reconciliation of the conflict. I believe we are all aware of the importance to the Laboratory of a successful outcome for this work and we will expend our efforts accordingly.

Attachment (1)

Cc: P. Paul

Charge to the BNL Neutrino R&D Working Group

December 1, 2001

BNL intends to initiate an R&D study to refine the technical basis for a future proposal to employ the BNL AGS as the source of a 1MW (or possibly greater), ~1GeV neutrino beam for the continuing exploration of neutrino physics, including CP-violation in the neutrino sector. We also expect as the second element of this R&D study, to be key organizers of an experimental physics and detector design effort that will engage interested physicists in the U.S. and other countries in the preparation of the conceptual basis for a formal proposal to design and build a neutrino detector system to exploit the BNL neutrino beam and to carry out the associated neutrino physics program.

To this end, the Laboratory will designate three R&D leaders for these efforts: the Neutrino Team Leader; the Accelerator and Beam Systems Team Leader; and the Physics Goals and Detector Design Team Leader. These three leaders will, in turn, be responsible for organizing the technical work that will enable a good scientific proposal to be written to the funding agencies that are identified as potential sponsors of this new U.S. particle physics effort. The three team leaders will serve until this R&D study is complete and documented in a written report. It is intended that the written R&D report should be completed no later than June 1, 2002.

The specific roles of the three Team Leaders comprise:

Neutrino Team Leader: The Neutrino Team Leader (NTL) will have responsibility for ensuring that the overall goals of a successful neutrino physics program have been covered by appropriate R&D studies in each of the important contributing technical systems and that there is a coherent overall time evolution plan that is consistent with

preparing a compelling proposal that addresses the goals of neutrino physics in a timely manner. This role should be understood as primarily a guidance and oversight role rather than a detailed management role. The balance and completeness of the study is the primary responsibility of the NTL.

Accelerator and Beam Systems Team Leader: The Accelerator and Beam Systems Team Leader (ABSTL) is the person primarily responsible for planning, staffing, carrying out and reporting on the accelerator and neutrino beam forming systems that are relevant for the preparation of a credible proposal to construct and operate a 1MW or greater proton target and associated useful neutrino beam(s) using the AGS (suitably upgraded) as the proton driver. To accomplish this mission, the ABSTL will be helped by the relevant BNL department heads to identify sufficient and appropriate technical staff to carry out the needed studies. The ABSTL is also expected to create an appropriate discussion and reporting forum(s) where the ongoing progress in this R&D effort can be reported and discussed for the general benefit of interested parties and participants. The ABSTL role is understood to be the principal management role for accomplishing the desired R&D studies in the accelerator and beam forming elements of the overall R&D program.

Physics Goals and Detector Team Leader: The Physics Goals and Detector Team Leader (PGDTL) is the person primarily responsible for planning, staffing, carrying out and reporting on the physics goals and detector strategies that are relevant for the preparation of a credible proposal to construct and operate a detector array that can exploit the 1MW or greater neutrino beams from the AGS proton driver. To accomplish this mission, the PGDTL will be helped by the BNL Physics Department head and (hopefully) by neutrino community scientists and engineers in other institutions to find sufficient and appropriate scientific staff to carry out the needed studies. The PGDTL is also expected to create appropriate discussion and reporting forums where the ongoing progress in this R&D effort can be reported and discussed

for the general benefit of interested parties and participants. The PGDTL role is understood to be the principal management role for accomplishing the desired R&D physics and detector studies for the overall neutrino R&D program.

9 Appendix II Underground Detector Construction at Homestake

Plans for the construction of a multiple module megaton Cherenkov detector at the Homestake Mine have gone through a number of essential evaluation and design stages consisting of rock strength and stability evaluation, chamber design and layout, construction planning and sequencing and development of budget and timetable. Here is a summary of these steps.

9.1 Determination of Excavation Stability

The Rock Stability Group at the Spokane Research Laboratory of NIOSH (National Institute of Occupational Safety and Health) carried out an evaluation of the stability of large excavations as a function of depth in the Yates rock formation in the Homestake Mine. This involved a three-dimensional finite difference evaluation using the FLAC3D program. These results were compared with the empirical prediction charts of Barton and Grimstad and Barton. The conclusions were that 50 meter diameter by 50 meter high chambers could be safely excavated and would be stable for long term occupancy at 2150 meter depth and probably somewhat deeper.

The Yates rock quality was determined by direct measurement of samples taken from the accessible edges of this formation. Before excavation begins, it is essential that core samples from various internal sections of the proposed rock formation are measured and the excavation reevaluated.

9.2 Construction of Multiple 100 kiloton Modules in the Homestake Mine

Using the results of the stability evaluation a group of ex-Homestake mining engineers, (Mark Laurenti - former Chief Mine Engineer, Mike Stahl - former Mine Production Engineer and John Marks - former Chief Ventilation Engineer) designed an array of ten 100 kiloton water Cherenkov chambers. The chambers are located along the circumference of a 250 meter radius circle that is centered on the Winze 6 shaft. The top of each chamber is connected to the 6950 ft station of the shaft via a horizontal, radial tunnel. A similar tunnel connects the bottom of each chamber to the 7100 ft shaft station. Fresh air will be sent to each

chamber via the top tunnel and exhaust air removed via the bottom tunnel, thus providing independent air supplies to each chamber.

During chamber construction, waste rock will be removed via the bottom tunnel. This will prevent rock dust from one chamber contaminating the fresh air supply of another chamber. Once construction is completed, the bottom chamber to tunnel connection will be sealed. A spiral ramp that surrounds each chamber and is used for access during construction will then complete the ventilation loop between top and bottom tunnels.

Each chamber will have a concrete liner. The inner surface of the liner provides a smooth surface for the water tight plastic liner that will separate the Cherenkov counter fill from the chamber walls. The liner also provides additional mechanical stability for the excavation. If necessary, drainage can be provided between the concrete liner and the surrounding rock.

9.3 Construction Timetable and Cost

Marc Laurenti has worked out a detailed timetable and budget for the construction of these modules including initial rock evaluation coring, construction of both top and bottom access tunnels, removal of waste rock, maintenance of mining equipment, etc.

The excavation process consists of continuous repetition of three separate tasks, (1) drilling and blasting of rock, (2) removal of the rock rubble, and (3) installation of rock and cable bolts to stabilize the freshly exposed rock walls. Each excavation cycle is about 10 weeks with 3 weeks for each of the above three steps. There is a considerable cost savings in excavating three chambers at the same time, with a three week phase shift between steps in each module. This arrangement permits each of the three specialized crews to move from one excavation to the next every three weeks or so and continue using the same equipment and carry out their specialized tasks. In contrast, using one crew to sequentially do three different tasks will result in idle equipment for 2/3 of the time and inefficiency as they switch from one task to another.

For the three module mode, the cost of excavating each chamber is \$14.7M. This includes \$3.25M for the concrete liner and a 15% contingency. In contrast, the cost of excavating a single module is \$16.9M including liner and contingency. The total required equipment cost is the same for both of these construction modes.

Assuming three shifts/day and 5 days/week operation, it will take 208 weeks or 4 years to excavate each 3 module group. This time could be reduced by going to a 6 or 7 day week. The Homestake Company frequently operated on 6 or 7 day per week basis.

9.4 Rock Removal

Each 100 kiloton module (105 m3) involves the removal of about 416,000 tons of rock including access tunnels, domed roof, etc. For three chambers this results in 1,248,000 tons of rock in 4 years or 312,000 tons of rock per year. Since the hoisting capacity of the Winze 6 - Ross shaft system is 750,000 tons per year, the simultaneous construction of three modules utilizes only 40% of the capacity of this shaft system.

9.5 Equipment Cost

Since all mining equipment has now been removed, new mining equipment will have to be purchased or leased. The required equipment, one Face Drill, two LHD loaders, 2 Bolters, 2 Underground Support Vehicles, 2 Lift Trucks, 1 LH Drill and 2 ITH Drills, costs about $4.2M. It may be possible to arrange for leases instead of purchasing these items. Normal equipment maintenance has been included in the construction cost. It is unclear whether the cost of this equipment should be assigned to this specific task or should be part of the general facility budget.

9.6 Choice of Depth and Depth Dependent Cost

There has been considerable discussion of depth necessary for very large detectors and the costs associated with deep detector locations. It is clear that the deeper the detector, the lower the cosmic ray muon and associated particle background. It is always preferable to have lower background. We can quantify the background limit by specifying that there be less than one cosmic ray related event per year within the megaton detector during the time that the accelerator neutrino beam is on. If we assume the accelerator beam is on for one microsecond per second, this requirement specifies an upper limit of $1.6x10^{-6} mu/m^2/sec$, essentially the cosmic ray flux at about 7000 ft depth. The effect of this specification is that every event observed in the detector during the beam-on time is due to a neutrino from the accelerator without any cuts whatsoever.

The question then is one of access and rock strength, namely, does a specific facility have ready access to a deep location and is the local rock structure capable of supporting large chambers. For Homestake the answer to both of these questions is YES. The present mine extends to 8000 ft, about 1000 ft deeper than the proposed detector location, and the rock seems strong enough to readily permit the excavation of large chambers.

In the appendix we provide a comparison of costs of building the megaton Cherenkov detector at 6950 ft depth vs at the 4850 ft depth. As indicated there, the maximum additional cost for putting the megaton Cherenkov array at 6950 ft versus at 4850 ft is 5-6% of excavation cost or less than 2% of total detector cost.

9.7 What Lessons About Depth Can be Learned from Previous Experience?

Detectors are located underground to reduce background in the detector due to cosmic rays. The deeper the detector, the lower the cosmic ray background. We have yet to have a detector that claimed to be "too deep". The only issues are: (1) is there a substantial additional cost associated with depth, and (2) are there technical limits associated with rock strength, etc. that limit depth at a given location? For many existing laboratories, depth is specified by what is available at that facility. Only two locations, the Sudbury mine (SNO), and the Homestake Mine (chlorine), have multiple levels available. SNO chose to be at 6800 ft, essentially the same as the proposed megaton detector. Since chlorine was the first underground neutrino detector, there were no precedents and so it might be instructive to review the sequence of events that led to its location.

In 1962, Ray Davis tested a small perchloroethylene detector in a limestone mine in Barberton, Ohio at a depth of 2200 ft. The 37Ar production was completely dominated by cosmic rays. That started a search for a much deeper site. There were two possibilities in the U.S., with Homestake the preferable one. At that time, in 1965, 4850 ft was the deepest level that the Company would agree to. At the time the prediction for the solar neutrino signal was larger than now, there was no thought about signal depression because of neutrino flavor conversion and no one expected a final measurement with a 5% statistical precision. By the early to mid-1970's it was already clear to us that the cosmic ray induced background was too large, given the observed signal, and that we needed a larger and deeper detector. Unfortunately, at the time, the Company was not willing to consider a deeper and larger detector.

The final result was that the cosmic ray induced signal is 10% of the solar neutrino signal in the chlorine detector and the uncertainty in that signal is the largest contributor to the systematic uncertainty. The lesson is clear - locate detectors as deep as possible and be sure that there is a roadmap to detector enlargement.

A detailed construction plan for the construction of three 100 kiloton modules in four

years at the 7000 ft depth in the Homestake Mine has been developed. The total construction cost of these three modules is about $44 M or $11M/year. In addition, there must be a one time purchase of about $4.2 M worth of mechanized mining equipment. The lead time in delivery of the mining equipment can be used to carry out coring of the rock region in which the detector array is to be constructed.

9.8 Comparison of Costs at 4850 ft versus 6950 ft

There are two depth dependent costs, the cost of hoisting rock and the cost of rock and cable bolting. To estimate this effect, we determine the difference in costs between identical chambers built at the 4850 ft level (the bottom level of the Ross shaft, the upper hoist system, and the beginning of the Winze 6, the lower hoist system) and the 6950 ft level. The direct manpower costs for hoisting the extra 700 meters in the Winze 6 are about $0.30/ton. The power costs add another $0.20/ton for a total of $0.50/ton or $208,000 per 100 kiloton module, where shaft maintenance costs have not been included.

The incremental rock support costs are more difficult to determine. The cable bolting planned and budgeted for these modules is far greater than required. This was done to insure that the chambers would have a minimum 50 year occupancy. A similar approach to corresponding excavations at the 4850 ft level might result in exactly the same bolting pattern and thus the same cost. Another approach would scale the bolting cost by the difference in rock stress between the two levels. The rock stress in the Homestake and Poorman formations, the formations that have been extensively studied in mine, are rather surprising. The measured vertical stress $S_v = 28.3 \times DkPa$, where D is the depth in meters, is exactly what is expected for a fluid of density 2.9 (the rock density). The horizontal stress is very direction dependent. Along the high stress axis $S_{h1} = 14,328 + 12.4 \times DkPa$, while along the low stress axis, $S_{h2} = 834 + 12 \times DkPa$. Presumably, the high horizontal stress results from the rock folding that resulted in the upbringing of the gold ore deposit to the surface and thus its discovery.

We assume that the effective stress at 6950 ft is about 35% greater than the corresponding one at the 4850 ft level. Since the total cost of the cable and rock bolts is $910,000 and the related labor, including benefits, is about the same, we assign a depth dependent cost increase of $630,000 for rock support. Combining this with the increase in hoisting costs gives a total of $838,000 or 6% of the total construction cost. Note that this is less than 2% of the complete detector cost.

However, there are three offsetting costs that reduce the cost of constructing the Cherenkov detector array at 6950 ft vs. at 4850 ft. The first of these is the water fill. The total water fill for the megaton detector is 250 million gallons. Removing that much water from the local streams would be quite significant, especially given the present drought conditions in the area. Instead, we plan to use the water that is being pumped from the bottom of the mine at the 8000 ft level. This water will be purified to remove any light scattering or absorbing material and any radioactive contaminants. Since the mine now pumps out about 350 gallons per minute, we will require about 1.4 years worth of water distributed over the construction time of the entire detector. For a detector at the 6950 ft level, this water is only pumped up 1000 ft while for a detector at 4850 ft, the water must be pumped up about 3100 ft. The cost savings here is about 1/4 of the increase in rock hoist cost or about $50,000.

The second offsetting cost is that of cooling the Cherenkov detector. Operating the detector at 10^oC gives 1/4 the photomultiplier noise of operation at 20^oC. Since the rock temperature at the 4850 ft level is over 35^oC and still higher at 6950 ft, cooling will be necessary at either depth. The mine has an enormous refrigeration plant (2400 ton capacity) at the 6950 ft level, with a fairly short path for the coolant from the refrigeration plant to the detector. A detector at the 4850 ft level will either require a new refrigeration plant at that level or the installation of 2000 ft of vertical coolant piping in the mine shaft. We have not estimated the cost of either of these steps, but they are clearly very substantial.

The third offsetting cost is that the level structure at 4850 ft does not readily lend itself to the construction and ventilation system described above. If the upper detector access is at 4850 ft then the lower, rock removal tunnel is at 5000 ft. Unfortunately, there is no ventilation exhaust system at that level and waste rock would have to be raised in order to get it into the hoist system. The alternate approach, putting the top access at 4700 ft, would require additional excavation in order to provide the necessary tunnels for the upper access.

The material in this section was assembled and compiled by Kenneth Lande based on work done by a number of senior mining engineers who previously were in charge of mining operations at the Homestake Mine.

List of Figures

List of Tables

References

[1] "Neutrino Oscillation Experiments for Precise Measurements of Oscillation Parameters and Search for $\nu_\mu \rightarrow \nu_e$ Appearance and CP Violation. LETTER OF INTENT to Brookhaven National Laboratory.", D. Beavis, et al., hep-ex/0205040.

[2] National Underground Science Laboratory at Homestake, Lead, SD, http://mocha.phys.washington.edu/NUSL/

[3] Waste Isolation Pilot Plant, Carlsbad, NM, http://www.wipp.carlsbad.nm,us/

[4] Y. Fukuda et al., Phys. Rev. Lett. **81**, 1562 (1998) S. Fukuda et al., Phys. Rev. Lett. **86** 5656, 2001; E.W. Beier, Phys. Lett. **B283**, 446 (1992); T. Kajita and Y. Totsuka, Rev. Mod. Phys. **73**, 85 (2001).

[5] Q. R. Ahmad et al., Phys. Rev. Lett. **87** 071301 (2001). S. Fukuda et al., Phys. Rev. Lett., **86** 5651 (2001).

[6] C. Athanassopoulos et al., Phys. Rev. Lett. **77** 3082 (1996); C. Athanassopoulos et al., Phys. Rev. Lett. **81** 1774 (1998)

[7] Booster Neutrino Experiment, Fermi National Laboratory, http:/www-boone.fnal.gov/

[8] S. H. Ahn et al., Phys. Lett. **B 511** 178 (2001).

[9] The JHF-Kamioka neutrino project, Y. Itow et al., arXiv:hep-ex/0106019, June 2001.

[10] Letter of Intent to build an Off-axis Detector to study numu to nue oscillations with the NuMI Neutrino Beam, D. Ayres et.al, hep-ex/0210005

[11] Numi MINOS project at Fermi National Accelerator Laboratory, http:/www-numi.fnal.gov/

[12] CERN Neutrinos to Gran Sasso, http://proj-cngs.web.cern.ch/proj-cngs/

[13] L. A. Ahrens et al., Phys. Rev. **D 41**, 3297 (1990).

[14] S. Kasuga *et al.*, Phys Lett. **B374**, 238 (1996).

[15] Ph.D. thesis, Eric Sharkey, State University of New York at Stony Brook, May 2002.

[16] Jiro Arafune, Masafumi Koike and Joe Sato, Phys. Rev **D56**, 3093 (1997).

[17] William J. Marciano, arXiv: hep-phy/0108181, 22 Aug 2001.

[18] I. Mocioiu and R. Shrock, Phys. Rev. **D62**, 053017 (2000); I. Mocioiu and R. Shrock, Snowmass eConf C0106063 (June, 2001), JHEP **0111**, 050 (2001).

[19] M. Diwan, I. Mocioiu, R. Shrock, and B. Viren, BNL-Stony Brook report, in preparation

[20] By L. Wolfenstein (Carnegie Mellon U.). 1978. In *West Lafayette 1978, Proceedings, Neutrinos '78*, West Lafayette 1978, C3-C6 and *Washington 1978, Proceedings, Long-distance Neutrino Detection*, 108-112.

[21] E889 Collaboration, Physics Design Report, BNL No. 52459, April, 1995. http://minos.phy.bnl.gov/nwg/papers/E889/

[22] KAMLAND experiment, JAPAN. http://kamland.lbl.gov/

[23] 3M Collaboration: Proposal titled: Megaton Modular Multi-Purpose Neutrino Detector, Nov. 26, 2001.

[24] S. Ozaki et al., eds., *Feasibility Study-II of a Muon-Based Neutrino Source* (June 14, 2001), http://www.cap.bnl.gov/mumu/studyii/FS2-report.html M. Zisman, Status of Neutrino Factory and Muon Collider R&D, PAC2001, WOAB008

[25] Atmospheric Muon Flux at Sea Level, Underground, and Underwater. E.V. Bugaev et al., Phys. Rev. **D 58** (1998).

[26] Physics Potential and Feasibility of UNO, UNO collaboration, June 2001. SBHEP01-3.

[27] A. Ruggiero, *Design Considerations on a Proton Superconducting Linac*, BNL Internal Report 62312, 1995.

[28] Ruggiero, A.G., A Superconducting Linac as a New Injector to the BNL AGS, BNL Internal Report, C-A/AP/40, February 2001.

[29] L. A. Ahrens et al., Phys. Rev. **D 34**, 75 (1986).

[30] N.V. Mokhov, "The MARS Code System User Guide, Version 13 (95)", 1995

[31] "Proposal to Study Production for the Neutrino Factory and for the Atmospheric Neutrino Flux", CERN-SPSC/99-35

[32] "A Facility to Study Proton-Nucleus and Heavy Ion Collisions Using a Large Acceptance Detector with Particle Identification Capabilities", BNL.

[33] "Effects of beam plugs and hadronic hose", B. Viren, NUMI-0719, 2001-07-06. "Neutrino Fluxes, Hadron Production and the Hadronic Hose", M. Messier, et al., NUMI-070, 2000-12-01.

[34] H. Kirk et al., "Target Studies with BNL E951 at AGS," PAC2001, TPAH137

[35] M.J. Brennan et al., , *1 MW AGS proton driver*, presented by T. Roser at Snowmass'01 (June 2001),

[36] C. McGrew *et al.*, Phys. Rev. D **59**, 052004 (1999).

[37] F. Arneodo et al., Nucl. Instrum. Meth. **A471** 272-275 (2000)

[38] D.B. Cline, F. Sergiampietri, J.G. Learned, K.T. McDonald, *LANNDD, A Massive Liquid Argon Detector for Proton Decay, Supernova and Solar Neutrino Studies, and a Neutrino Factory Detector* (May 24, 2001), astro-ph/0105442

[39] Also see F. Sergiampietri, *On the Possibility to Extrapolate Liquid Argon Technology to a Supermassive Detector for a Future Neutrino Factory*, presented at NuFACT'01 (May 26, 2001),

[40] M. Diwan, S. Kahn, R.B. Palmer (Brookhaven). Mar 1999. Published in *New York 1999, Particle Accelerator, vol. 5* 3023-3025

[41] M.V. Diwan et al., *Proposal to Measure the Efficiency of Electron Charge Sign Determination up to 10 GeV in a Magnetized Liquid Argon Detector (μLANNDD)*, submitted to BNL (April 12, 2002),
http://www.hep.princeton.edu/m̃cdonald/nufact/bnl_loi/argonprop.pdf

[42] J. Wei et al. *Low-loss design for the high-intensity accumulator ring of the Spallation Neutron Source*, Phys. Rev. ST Accel. Beams 3, 080101 (2000).

[43] R. Garoby, *Bunch Merging and Splitting Techniques in the Injectors for High Energy Hadron Colliders*, CERN/PS 98-048.

[44] M. Bai et al., *Adiabatic excitation of longitudinal bunch shape oscillations*, Phys. Rev. ST Accel. Beams 3, 064001, 2000.

[45] K. Brown, et al., "First Beam Tests of the Muon Collider Target Test Beam Line at the AGS," PAC2001, TPAH129

[46] N. Simos, et al., "Thermal Shock Analysis of Windows Interacting with Energetic, Focused Beam of the BNL Muon Target Experiment," PAC2001, TPAH085

[47] R.B. Oswald, et al., " One-Dimensional Thermoelastic Response of Solids to Pulsed Energy Deposition," Journal of Applied Physics, Vol. 42, No. 9, pp. 3463-3473, 1971

[48] D. Burgreen, "Thermoelastic Dynamics of Rods, Thin Shells and Solid Spheres", Nucl. Sc. And Eng., 12, 203-217, 1962 P. Sievers, "Elastic Stress Waves in Matter due to Rapid Heating by Intense High-Energy Particle Beam," LAB.II/BT/74-2, CERN, 1974

[49] H. Conrad, "On Elastic Stress Waves in Targets", Institut fur Festkorperforschung, 1994

[50] ANSYS Engineering Analysis of Systems, Swanson Analysis Systems Inc.

[51] Muon Electric Dipole Moment experiment.
http://www.bnl.gov/edm/

[52] Rare Symmetry Violating Processes,
http://meco.ps.uci.edu/RSVP.html